DETERMINING THE THERMAL CONDUCTIVITY OF EARTH PLASTER SAMPLES WITH MORTAR MIXES SUITABLE FOR AFRICAN ARCHITECTURE

A THESIS SUBMITTED TO
THE GRADUATE SCHOOL OF NATURAL AND APPLIED SCIENCES
OF
MIDDLE EAST TECHNICAL UNIVERSITY

BY

BENARD ALUMA

IN PARTIAL FULFILLMENT OF THE REQUIREMENTS
FOR
THE DEGREE OF MASTER OF SCIENCE
IN
BUILDING SCIENCE IN ARCHITECTURE

APRIL 2023

Approval of the thesis:

DETERMINING THE THERMAL CONDUCTIVITY OF EARTH PLASTER SAMPLES WITH MORTAR MIXES SUITABLE FOR AFRICAN ARCHITECTURE

submitted by **BENARD ALUMA** in partial fulfillment of the requirements for the degree of **Master of Science** i**n Building Science in Architecture, Middle East Technical University** by,

Prof. Dr. Halil Kalıpçılar
Dean, Graduate School of **Natural and Applied Sciences** _____

Prof. Dr. F. Cana Bilsel
Head of Department, **Architecture**
_____

Prof. Dr. Soofia Tahira Elias-Ozkan
Supervisor, **Architecture, METU**
_____

Examining Committee Members:

Asst. Prof. Dr. Bekir Özer Ay
Architecture, METU _____

Prof. Dr. Soofia Tahira Elias-Ozkan
Architecture, METU _____

Assoc. Prof. Dr. Ayşegül Tereci
Architecture, NEU _____

Prof. Dr. Neşe Dikmen
Civil Engineering, ISUBU _____

Asst. Prof. Dr. Rukiye Çetin
Architecture, AYBU _____

Date: 25.04.2023

I hereby declare that all information in this document has been obtained and presented in accordance with academic rules and ethical conduct. I also declare that, as required by these rules and conduct, I have fully cited and referenced all material and results that are not original to this work.

Name Last name: Benard Aluma

Signature:

ABSTRACT

DETERMINING THE THERMAL CONDUCTIVITY OF EARTH PLASTER SAMPLES WITH MORTAR MIXES SUITABLE FOR AFRICAN ARCHITECTURE

Aluma, Benard
Master of Science, Building Science in Architecture
Supervisor: Prof. Dr. Soofia Tahira Elias-Ozkan

April 2023, 135 pages

Earth has been used as a building material in African architecture for millenniums. Building with earth in combination with other indigenous materials as additives has various benefits, including affordability, availability, and exceptional moisture-balancing and ventilation properties. However, they have certain limitations, such as their brittleness, lack of durability, and poor water resistance. Numerous studies, such as that of Pedergnana (2022), on mixes produced with ten types of sands, 11 types of fibers, and 13 types of biopolymers, have been conducted to improve these properties. On the other hand, more research was needed to determine the impact of the additives on the thermal properties of earth mixes, especially those that would be suitable for use in African architecture.

Therefore, 18 samples were selected from Pedergnana's research that contained three suitable additives (straw, sand, and cow dung) as well as two others (sheep wool and pine-needles) for comparison. Consequently, this study determined the effect of these additives on the thermal conductivity of the selected samples measured by a simplified method that is based on Fourier's heat transfer equation. The research

revealed that the thermal conductivity of mud plasters decreased with an increase in the fiber content as well as the amount of cow dung. On the other hand, an increase in the amount of sand increased the thermal conductivity of the earth mixes. The thermal conductivity of fiber-stabilized samples was determined to be between 0.39 and 0.58 W/mK; that for samples with sand and fiber was between 0.41 and 0.60 W/mK, while the cow dung-stabilized samples had values ranging from 0.43 to 1.19 W/mK.

Keywords: Mud plaster mixes, Natural additives, Natural fibers, Thermal conductivity, Adaptive material use in African architecture.

ÖZ

AFRİKA MİMARİSİNE UYGUN HARÇ KARIŞIMLARIYLA HAZIRLANMIŞ TOPRAK SIVA ÖRNEKLERİNİN ISIL İLETKENLİKLERİNİN BELİRLENMESİ

Aluma, Benard
Yüksek Lisans, Yapı Bilimleri, Mimarlık
Tez Yöneticisi: Prof. Dr. Soofia Tahira Elias-Ozkan

Nisan 2023, 135 sayfa

Toprak, Afrika mimarisinde binlerce yıldır bir yapı malzemesi olarak kullanılmaktadır. Yerel katkı maddeleriyle zenginleştirilmiş toprak ile yapı inşa etmenin çeşitli avantajları vardır. Bu avantajlar uygun maliyetli olması, bileşenlerin kolayca bulunabilmesi ve olağanüstü nem dengeleme ve havalandırma özelliklerine sahip olmasıdır. Ancak bu avantajlarının yanı sıra üretilen malzemenin kırılgan bir yapıya sahip olması, dayanıklılık eksikliği ve su direncinin zayıf olması bu malzemenin kullanımında birtakım sınırlamalar getirmektedir.

Pedergnana'nın (2022) on çeşit kum, on bir çeşit elyaf ve on üç çeşit biyopolimer ile üretilen karışımlar üzerine yaptığı çalışma gibi çok sayıda çalışma toprağın sahip olduğu olumsuz özellikleri iyileştirmek için yapılmıştır. Öte yandan, katkı maddelerinin toprak karışımların termal özellikleri üzerindeki etkisini, özellikle de Afrika mimarisinde kullanıma uygun olanları belirlemek için daha fazla araştırmaya ihtiyaç duyulmuştur.

Bu nedenle, Pedergnana'ın araştırmasından yola çıkılarak, üç uygun katkı maddesi (saman, kum ve tezek) ve karşılaştırma için diğer iki katkı maddesini (koyun yünü ve çam iğnesi) içeren toplam 18 örnek çalışılmak üzere seçilmiştir. Sonuç olarak, bu

çalışma bu katkı maddelerinin seçilen örneklerinin ısı iletkenliği üzerindeki etkisini Fourier'in ısı transferi denklemine dayanan basitleştirilmiş bir yöntemle ölçerek belirlemiştir. Araştırma, çamur sıvaların ısıl iletkenliğinin, lif içeriğinin yanı sıra tezek miktarındaki artışla azaldığını ortaya koymuştur. Öte yandan, kum miktarındaki artış toprak karışımlarının ısıl iletkenliğini artırmıştır. Lifle stabilize edilmiş numunelerin ısı iletkenliği 0,39 ile 0,58 W/mK arasında; kum ve lif içeren numunelerin 0,41 ile 0,60 W/mK arasında; tezekle stabilize edilmiş numunelerin ise 0,43 ile 1,19 W/mK arasında değişen değerlere sahip olduğu belirlenmiştir.

Anahtar Kelimeler: Çamur harç örnekleri, Doğal katkılar, Doğal lifler, Isı iletkenliği, Afrika mimarisinde adaptif malzeme kullanımı.

To God, the Giver of all Wisdom, who has sustained me throughout the process of writing my thesis.

ACKNOWLEDGMENTS

I would like to express my deepest gratitude to my supervisor Prof. Dr. Soofia Tahira Elias-Ozkan for her guidance and patience. This research was made possible by her invaluable and innovative contributions. She always believed in me and encouraged me to keep going. I would also like to thank Mr. Matthieu Pedergnana for allowing me to conduct experiments on his mud plaster samples for my thesis, and for his academic guidance. I also extend my gratitude to Azra for her significant role in the experimental setup used in this study.

I would like to express my heartfelt appreciation to Gülin, Dilara, Cozby, and Timothy for their timely support throughout my master's studies. Their assistance meant a great deal to me and facilitated my academic career.

I extend my sincerest gratitude to my mother for imparting in me the significance of education, despite not having had the opportunity to pursue it herself. Her teachings have instilled in me the values of diligence and perseverance, which have been instrumental in my personal and professional growth. I am grateful for her unwavering help and guidance, which have contributed to my success.

I would also like to extend my appreciation to my brother, Mr. Onzima Robert Boyle, for his consistent support and counsel. He's set the bar high, and I hope to continue following in his footsteps.

Lastly, I am thankful to the All-Powerful God, the source of wisdom, for sustaining me throughout the writing process. And to my religious community for their constant prayers and encouragement.

TABLE OF CONTENTS

LIST OF TABLES

TABLES

LIST OF FIGURES

FIGURES

CHAPTER 1

INTRODUCTION

Building with earth is still a common practice in many countries; approximately one-third of the world's population lives in earthen houses, with the figure rising to more than half in developing countries (Laborel-Préneron, Aubert, Magniont, Tribout, & Bertron, 2016). According to Montana, Randazzo, & Sabbadini. (2014), earthen materials are still the principal construction materials in many present-day Asian and African countries. Conversely, a decline in the use of earthen materials was observed in developed nations, where modern materials such as cement were preferred for decades after World war II due to their durability (Laborel-Préneron et al., 2016). Today there is a growing interest in earthen materials, and research is being carried out to improve their durability (Montana et al., 2014).

Numerous construction techniques employ earthen materials, including adobe, rammed earth, straw clay, wattle and daub, cob, super adobe, and compressed blocks. Earth is also used as plaster and mortar material. Earth plasters are building envelope components made of clay, water, and sometimes plant aggregates or fibers to prevent drying-induced linear shrinkage (Laborel-Préneron et al., 2016). Other additives, such as cow dung and ashes from agro-processing wastes, are included to reduce crack-related damages, a practice common in many African countries (Manu, 2013).

Earth plasters and mortars have many advantages; they can improve the building life cycle sustainability due to their low embodied energy and the fact that raw natural clay can be used as a binder without any processing and is widely available around the world (Lima, Correia & Faria, 2016). Earth plasters also have a high adsorption and desorption capacity due to their high hygroscopicity, acting like moisture buffers that help to balance the relative humidity of the indoor environment (Alexander Asal,

2018). This moisture buffering attribute of mud plasters promotes thermal comfort of interior spaces. Besides, it also helps to avoid health conditions related to high humidity (Soldatova, Larisa, Rocca-Serra, Dumontier, Shah & Nigam, 2014). According to Minke (2006), relative humidity of up to 70 percent can reduce the amount of fine dust in the air, activate the skin's protective mechanisms against microbes, and shorten the lifespan of numerous bacteria and viruses. In contrast, a value above 70% causes discomfort due to the reduction of oxygen intake by blood in a warm-humid environment.

Furthermore, mud plasters serve as passive removal materials (PRMs) that control indoor pollution without the production of significant chemical byproducts or high energy consumption (Lima et al., 2016). Besides, earth plasters improve the thermal insulation of a wall, thereby improving the energy efficiency of a building and potentially decreasing the reliance on mechanical ventilation and air conditioning systems (Montana et al., 2014). The dwellings rendered with mud plaster have excellent thermal properties; the walls in such houses function as a natural Trombe wall, slowly absorbing heat during the day and dissipating it at night (Bosman & Salzmann-McDonald, 2015). The process maintains the interior cool during the day and warm at night (Chen, 2020). This property of earth plasters is also crucial in African vernacular architecture because it maintains a cool interior temperature during a hot day (Fraser, 1962).

Despite the advantages mentioned above, earth plasters are susceptible to cracking caused by shrinkage after drying (Montana et al., 2014). Furthermore, mud plasters have low mechanical strength and water resistance (Ouedraogo, Moussa, Millogo, Aubert, Messan, Seynou, Zerbo & Gomina, 2019). The earth plasters have low tensile strength, are susceptible to mechanical damage, possess low wood adhesive strength, and become heavy after absorbing water. However, Beas (1991) noted that if the earth contains 10% to 20% clay, it will partially resist erosion from ambient rainfall. Otherwise, wind-driven precipitation can cause severe decay. Furthermore, earth plasters require periodic maintenance to repair cracks that develop over time

(Beas, 1991; Odeyale & Adekunle, 2008). According to Egenti, Khatib & Oloke. (2013) and Beas (1991), earth construction is typically labor-intensive.

1.1 Research problem

As previously stated, earthen materials that are being used in Africa have numerous benefits, including improving building life cycle sustainability due to their low embodied energy; they also help to balance the relative humidity of the indoor environment, which contributes to the thermal comfort of interior spaces; they act as passive materials that control indoor pollution; and they have good thermal properties. However, despite the advantages, the majority of African people prefer to use modern materials, which are also costly and mostly imported, and traditional building materials are regarded as primitive. Moreover, some of these materials are unsuitable for Africa's climate; for example, using corrugated iron sheets as roofing material causes homes to become unbearably hot during the day because they readily conduct heat energy. On the other hand, earthen materials are thermally appropriate for the region.

To address the durability problem, research is being conducted to improve the mechanical and physical properties of commonly used traditional materials, particularly mudbricks and plasters, bringing them up to construction industry standards while retaining their ease of use, low environmental impact, and comfort. However, the thermal properties should also be investigated.

This research focused on gathering information through a comprehensive literature review regarding different waste products from the agricultural and mining industries that can be used as additives in stabilizing mud samples and plasters in African architecture. Additionally, thermal conductivity was of particular interest because it affects the thermal comfort of interior spaces, which is a significant factor for houses constructed in the climate of the majority of African countries. It also

provided an overview of common techniques for measuring the thermal conductivity of insulation materials, as well as the factors that affect their accuracy.

1.2 Aims and Objectives

This research aimed to determine the thermal conductivity of various mud-mortar samples that had been tested earlier for their physical and hygric properties during a PhD study (Pedergnana, 2022). In the research, Pedergnana (2022) utilized ten types of sand, eleven types of fibers, and thirteen types of biopolymers. Furthermore, the author utilized food-grade substances such as egg white, mayonnaise and Linseed oil. However, for this study, samples stabilized with straw, sand, and cow dung were chosen due to the availability of the additives on the African continent. Besides, the practice of utilizing food-grade substances for the purpose of stabilizing mud samples is uncommon in African societies and may be deemed socially unacceptable. Furthermore, since thermal conductivity measuring equipment are not easily affordable by researchers in African or Asian countries, the objective was to use a simplified experimental setup based on the equation of Fourier's Law of heat transfer.

With regards to the aims, the research tried to answer the following questions;

- Which organic and inorganic additive are available and used in traditional mud buildings in Africa?
- What were the thermal conductivity values of the mud plasters samples prepared by Pedergnana (2022) by using fibers, sand and cow dung as additives?
- Can a simple experimental set up using the equation of Fourier's Law of thermal conductivity provide acceptable results that are comparable to those reported by other researchers?

To fulfill the aims, the following were the main objectives of this study:

- To carry out a literature review in order to determine the organic and inorganic additives readily available in Africa and traditionally used in mud architecture.
- To determine the thermal conductivity of mud plaster samples using a simple setup and to compare the results with the ones obtained by other researchers.

1.3 Disposition

In the first chapter of this study, the advantages and disadvantages of earthen plasters were discussed. The second chapter focused on the literature review of earthen materials and possible organic and inorganic materials that can be used in stabilizing earthen plasters. The research, however, focused on natural fibers that are predominantly derived as byproducts of agricultural practices, owing to their easy availability and eco-friendliness. Given that agriculture is the most prevalent economic activity in the African continent, the waste generated from agricultural activities can be utilized to stabilize mud samples. The subsequent section examined the effects of incorporating fiber, sand and cow dung into earthen plasters.

In the conclusion of this chapter, the methods for measuring thermal conductivity were categorized into three groups: steady-state, transient or unsteady, and calculation. Furthermore, the experimental procedure and conditions of some experimental designs for measuring thermal conductivity were analyzed. Finally, the grain size distribution of the clay used to produce samples of mud plaster was described. Similarly, information was provided about the additives used to stabilize the earthen plaster samples, including the type of sand, plant fibers, and cow dung.

In the third chapter, the sample experimental design based on the Fourier's law of thermal conductivity equation was discussed in depth providing information regarding the setup and procedure. Furthermore, details regarding the utilized samples, including size, density, thickness, and nomenclature by mix code and sample number, as well as the percentage of additives by volume and weight, were

provided. Besides, the samples in this study were divided into three categories: fibers, sand and fiber, and cow dung.

In the subsequent chapter, the results of the experimental design were compared to those reported in the literature review. It should be noted that the mud plaster samples used in this study were prepared and tested by Matthieu Pedergnana for his doctoral research (Pedergnana, 2022) and some of his work was reported in (Pedergnana & Elias-Ozkan, 2021b); while some of his samples were also tested for their thermal properties and presented in (Pedergnana & Elias-Ozkan, 2021a). In this study, 18 samples were chosen; five stabilized by fiber, eight by a combination of fiber and sand, and five by cow dung. Their thermal properties were tested, and the results were subsequently compared to his research. Since only a small number of samples were tested for their thermal properties by Matthieu Pedergnana, who primarily focused on the physical, mechanical, durability, hydric, and hygric properties of earth plasters, this investigation therefore adds details about the thermal behaviors of the other samples.

CHAPTER 2

LITERATURE REVIEW ON EARTHEN MATERIALS AND MEASUREMENT OF THERMAL CONDUCTIVITY

In this chapter, a literature review on earthen plasters is presented. The chapter also explored agricultural and industrial wastes that can be used to improve the thermal conductivity of mud samples. Stabilization of earthen plasters with fiber, sand and cow dung was also discussed. Finally, the study also looked into various methods used to measure mud samples' thermal conductivity and the factors that affected their accuracy.

2.1 Earth as a construction material

Earth has been used as a building material in different ways for a long time (Taallah, Guettala, Guettala & Kriker, 2014). Hunter-gatherers erected small shelters, camps, and huts made of clay throw as early as 12000 years ago; the origin of the first settlement built using soil was primarily in the Near East and the Middle East (Alexander Asal, 2018). Earth was used as a building material during the Ubaid period in ancient Mesopotamia around 5000 – 4000 B.C. (Pollock, 1999). From pyramids in Egypt to the Great Wall of China, a number of renowned architectural marvels were constructed also using earth (Odeyale & Adekunle, 2008).

Earth is composed of clay, silt, sand, and occasionally larger aggregates such as gravel and stone; it can be categorized into clayey, silty or sandy loam according to the most dominant component (Alexander Asal, 2018). According to Minke (2006), clay acts as a binder while silt, sand and other aggregates act as fillers. Earth is readily available and it varies depending on the geographic location (Oshike, 2015).

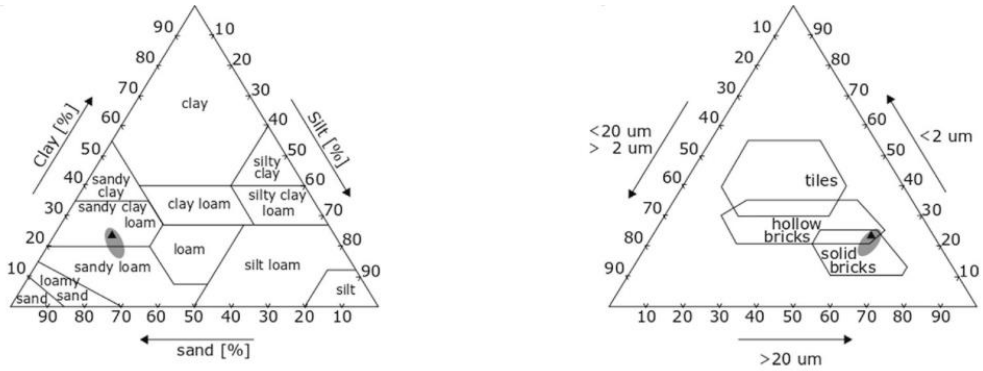

Figure 2.1 The Winkler diagram classification of soil (left), products of soil depending on soil composition (right) (Muñoz et al., 2021)

Earth is the most commonly used traditional material in Africa as seen in Figure 2.2. It is also used for construction in South and North America, Asia, and some parts of Europe. According to Laborel-Préneron et al. (2016), at least a third of the world's population lives in houses built with earthen materials. Earth is utilized with techniques that vary based on local climate, environment, traditions, and customs of the area in question (Aghimien, Mukanjuola & Taiwo, 2016).

Figure 2.2 World map showing earth architecture and construction techniques (Houben & Hubert, 1994)

2.1.1 Agricultural and industrial wastes that can be used in stabilization of earthen materials

This section of the research looked at agricultural and industrial wastes in Africa that can be used to stabilize earthen materials. These materials are not durable and are vulnerable to damage from torrential rains; stabilizing helps to reinforce physical properties such as compressive and tensile strength while also improving thermal properties. Furthermore, valorizing these agricultural and industrial byproducts can help reduce their environmental impact.

2.1.1.1 Agricultural waste

Most of the countries in the African continent depend on agriculture as the primary source of income. While the continent is home to 60% of the world's arable land, only 9% of the land in Sub-Saharan Africa is arable land (OECD-FAO, 2021). According to a report by the Food and Agriculture Organization (FAO), agriculture accounts for 14% of the overall gross domestic product (GDP) in the continent. However, on a country-by-country basis, it accounts for three percent of the gross domestic product in more developed nations like South Africa (OECD-FAO, 2021).

a. Waste and residues

Figure 2.3 depicts the total amount of ash produced from cassava peel, maize cob, rice, and groundnut shells in certain African nations. Mozambique has the lowest percentage of ash at 5.5%, followed by Guinea at 5.9%. Tanzania comes in third place with 4.1%. Senegal, on the other hand, produces the least amount of ash at 0.4%. Such agricultural wastes can be used to strengthen mud samples by incorporating them into the soil matrix. Byproducts with pozzolanic properties, such as ashes of rice husks, bagasse, bamboo leaves, cassava peels, maize cobs, palm kernels shells, groundnut shells, and coconut shells, can be used as supplementary

cementitious materials (SCM) in the production of cement instead of industrial SCM, such as fly ash (FA) and ground granulated blast furnace slag (GGBS) (Schmidt, Commeh, Olonade & Leno, 2021). However, it should be noted that such ashes occur in low amounts, and there is no organized system to collect them.

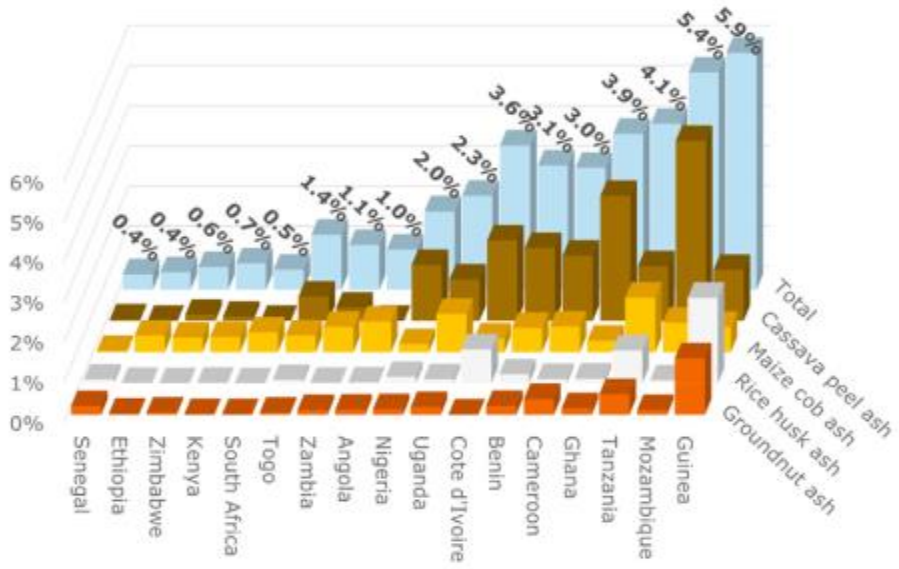

Figure 2.3 Agricultural wastes from selected African countries (Schmidt et al., 2021)

b. Natural plant fibers

Since ancient times, fibers have been used as reinforcement in earthen materials (Almusaed & Almssad, 2015; Babé et al., 2020). The cellulose content of fibers ranges from 60 to 80 % by weight, while the lignin content ranges from 5 to 20 % by weight depending on the type of fiber; furthermore, their moisture content is up to 20% by weight. (Mallick, 2007). Plant fibers are divided into five groups: seed fibers, leaf fibers, bast fibers, fruit fibers, and stalk fibers (Bhattacharyya, Subasinghe & Kim, 2015).

Fibers reduce linear shrinkage and crack formation; they also influence the mechanical and thermal characteristics of composite materials depending on the physical and chemical properties of fibers (Taallah et al., 2014). Minke (2006) observed that the addition of fibers reduces shrinkage because the clay content is diminished, and a certain amount of water is absorbed by the fibers' pores. Using natural fibers is also beneficial for the population because they are abundant locally, have economic benefits, require little energy, and allow for the reduction of environmental impact (Alawar, Hamed & Al-Kaabi, 2009; Taallah & Guettala, 2016). However, fibers are hydrophilic and can degrade during processing (Taallah et al., 2014). Some fibers may not adhere properly to the soil matrix (Jové-Sandoval et al., 2018). Incompatibility between the soil and the fiber in composite materials may result in high moisture absorption and poor mechanical properties, leading to the weakening of the soil-fiber bonds over time (Alawar et al., 2009).

This section of the research focused on the chemical and physical properties of some fibers produced as a byproduct of agricultural activities. Alawar et al. (2009) reported that crystal structure, degree of crystallinity, spiral angle of fibrils, degree of polymerization, porosity content, lumen size, and chemical composition impacted the mechanical properties of fibers. Consequently, these properties affect the behavior of composite materials.

I. Cereal straws

Straw as a construction material has good thermal properties; it is an excellent insulator due to its natural properties. According to Almusaed & Almssad (2015), houses made of straw provide comfortable interior spaces regardless of the hot weather because they have a tendency to keep the internal temperature cool. This is true even in regions that experience extreme heat. However, straw has a low resistance to fire, is vulnerable to infestation by insects, and deteriorates rapidly when exposed to high moisture levels.

Compared to other conventional materials, straw is said to have a better R-value (Almusaed & Almssad, 2015). However, this value can shift significantly depending on the type of straw that is being considered. According to Nunes, (2017), nearly 90 percent of the cereal crop straws, such as wheat, barley, oats, rye, and rice, contain water-soluble elements, ash, and silica. These elements are found in cereal grains. Additionally, cereal plants typically contain cellulose, hemicellulose, and lignin in their cell walls. Straw is also used to fortify earthen materials, in addition to being incorporated into masonry walls (Hadji, Ihaddadene, Ihaddadene, Betga, Charick, & Logerais, 2020).

II. Bamboo fibers

Bamboo is a construction material that belongs to the grass subfamily Bambusoideae (Nunes, 2017). It is considered one of the fastest growing plants. According to Abdul Khalil, Bhat, Jawaid, Zaidon, Hermawan & Hadi, (2012), bamboo matures in only three years, whereas it can take over twenty years for wood. According to Ben (2016), it can grow to a height of 100 centimeters in a single day. Abdul Khalil et al. (2012) revealed that bamboo has tensile strength comparable to mild steel in their study. Furthermore, they noted that bamboo has a microfibrillar angle that ranges from 2-10º, making it resistant to fire. Moreover, bamboo contains 60% cellulose and a high lignin content. Additionally, it is resistant to both insect and fungal attacks. It is also regarded as a practicable alternative to the use of wood.

Bamboo fibers can also be used to reinforce composite materials; they are extracted mechanically, chemically, and even treated with enzymes (Mallick, 2007). It is important to note that the properties of bamboo fibers derived from different regions and ages, as well as different parts of the bamboo and extraction conditions, vary considerably (Mallick, 2007). It is also worth noting that bamboo fibers have a high water absorption capacity, resulting in poor interfacial bonding between hydrophilic materials and the fibers (Hao, Sapuan, Hassan & Sheltami, 2018).

Figure 2.4 Bamboo (left) and bamboo fiber (right) (Nunes, 2017)

III. Palm trees

Palm trees are native to tropical, subtropical, and warm temperate climates (Laborel-Préneron et al., 2016). Palm tree byproducts include fronds (leaves) and empty fruit bunches, which have multiple applications. The empty fruit bunch of oil palm (OPEFB) is a palm oil industry waste that is produced during the oil extraction process (Faizi, Shahriman, Majid, Shamsul, Ng, Basah, Cheng, Afendi, Zuradzman, Wan & Hazry, 2016). It is composed of 63% cellulose, 18% hemicellulose, and 18% lignin (Reddy & Yang, 2015). The OPERB fibers have abundant potential that has not been effectively utilized (Rame, 2018). The fibers have high tensile strength which can be chemically treated to reduce hydrophilicity (Reddy & Yang, 2015).

Figure 2.5 Empty fruit bunch OPERB (Faizi et al., 2016)

Borassus flabellifer is a member of the Aceraceae family and primarily grows in tropical regions (Reddy & Yang, 2015). This palm tree produces fibers with a maximum length of 45 cm and high tensile strength; husks also produce coarse and fine fibers with good dry and wet strength (Reddy & Yang, 2015). Date palm trees, on the other hand, are members of the phoenix dactylifera genus and are found in the Middle East, Northern Africa, the Canary Islands, Pakistan, India, and California (Alawar et al., 2009). The fibers around the stem of date palm tree can be used to reinforce earthen materials.

Figure 2.6 Date palm tree (left), the fibers around the stem (right) (Alawar et al., 2009)

IV. Banana fibers

Bananas are widely available worldwide; annually, between 120 and 150 million tons are produced (Mallick, 2007). Banana fiber is a bast fiber with comparatively good mechanical properties that is obtained from the pseudo-stem of the banana plant (Musa sepientum) (Mukhopadhyay, Fangueiro, Arpaç & Şentürk, 2008). The fibers are eco-friendly and have important properties such as low density, low weight, low cost, high tensile strength, and resistance to water and fire (Mostafa & Uddin, 2015). They are mechanically extracted and typically contain 50% cellulose, 17% lignin, and 4% ash. However, the percentages of content vary by region (Mallick, 2007).

Mostafa & Uddin (2015) stated that cellulose is responsible for the mechanical properties of the fiber, whereas lignin and hemicellulose provide natural decay resistance.

Similar to other lignocellulosic fibers, fibers have a variable tensile property; however, their elongation is considerably low due to a low microfibrillar angle of 11º and a relatively high percentage of crystallinity (Mallick, 2007).

Figure 2.7 Banana fiber immersed into Sodium Hydroxide solution (left) (Mostafa & Uddin, 2015), SEM showing the cross-section of banana fiber (Mukhopadhyay et al., 2008)

V. Sisal fibers

The Sisal plant is a member of the Agavaceae family and grows in arid and tropical climates (Silva, Filho, Filho, & Fairbairn, 2010; Mishra, Mohanty, Drzal, Misra, & Hinrichsen, 2004). Sisal fibers are extracted using a number of distinct techniques (Ouakarrouch, El Azhary, Mansour, Laaroussi & Garoum, 2020). The fiber is composed of 54- 66% cellulose, 17% hemicellulose, 7-14% lignin, 1% pectin, and 1-7% ash; the physical properties of the fibers are determined by these chemical compositions (Mishra et al., 2004). Furthermore, the microstructure is made up of individual fibrous cells that are linked together by the central lamellae (Silva et al., 2010).

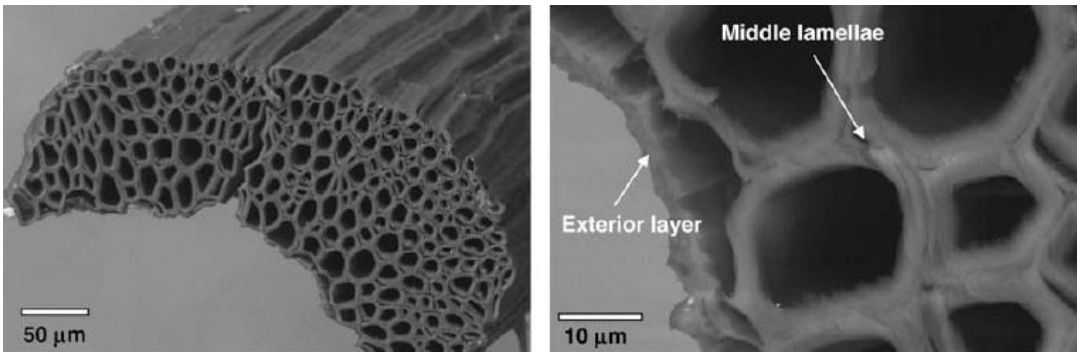

Figure 2.8 Microstructure of sisal fiber showing individual cells connected by the central lamellae (Silva et al., 2010)

VI. Kenaf

Kenaf is indigenous to east and central Africa and grows in the continent's tropical and subtropical forests (Mansingh, Binoj, Manikandan, Sai, Siengchin, Mavinkere, Bharath & Indran, 2022). Nonetheless, more than 70% of the world's kenaf is produced by India and China (Abbas, Aziz, Abdan, Nasir & Norizan, 2022). Kenaf plant belongs to the Mavaceae family and can reach a height of 1.5 to 4m in 4 to 5 months growing at a rate of 10cm per day (Abbas et al., 2022; Bhattacharyya et al., 2015). The plant's cortex accounts for 30 to 40% of its dry weight, while the core is responsible for 60 to 70 % (Mansingh et al., 2022). The fibers extracted from the bast and core of the plant through the process of retting contain 31% to 72% cellulose and a microfibrillar angle of 9º to 15º (Da Silva et al., 2021). This attribute gives fibers high tensile strength as compared to other fiber types. Consequently providing a substitute for reinforcement in the construction industry (Abbas et al., 2022). Furthermore, the fibers contain 5 to 20% by weight of lignin and 20% by weight of moisture (Mansingh et al., 2022). However, just like other natural fibers, kenaf fiber has a high water moisture capacity, affecting interfacial bonding when incorporated into composite materials (Abbas et al., 2022).

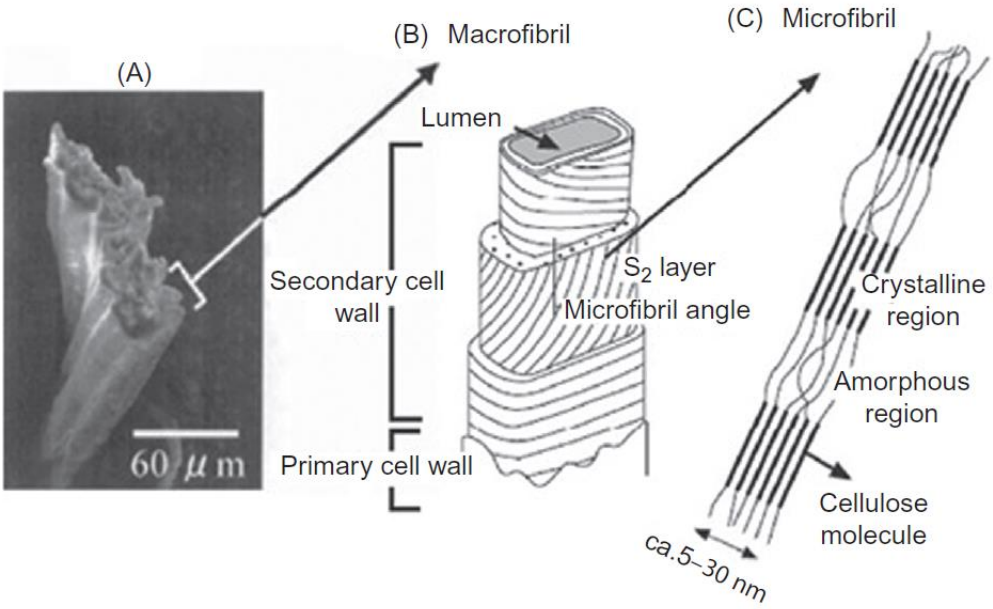

Figure 2.9 Microstructure showing the macrofibril and microfibril of Kenaf fiber (Hao et al., 2018)

VII. Hemp fibers

Hemp has been grown for diverse purposes for thousands of years (Nunes, 2017; Charai et al., 2021). It is a member of the Cannabaceae family (Suwansaard, Kongpun, & Khemkhao, 2022). According to Singh, Mamania & Shinde,(2018), most climates are suitable for growing hemp. The plant yields three primary byproducts: fiber, shaves, and seeds (Nunes, 2017).

Hemp fibers are divided into two sections: the bast and the core section (Hao et al., 2018). Bast hemp fiber is composed of 55–77% cellulose, 2–22% hemicellulose, 0.8–18% pectin, and 2.9–13% lignin (Nunes, 2017). These attributes, along with the microfibril angle, influence mechanical properties such as tensile strength and modulus of the fibers (Charai, Sghiouri, Mezrhab & Karkri, 2021). Hemp can be used in construction due to their insulation capacity (Nunes, 2017). Furthermore, the

fibers also have high mechanical resistance and low density (Suwansaard et al., 2022).

Figure 2.10 Hemp plant (left), hemp stem cut longitudinally (right) (Nunes, 2017)

VIII. Flax

Flax is a type of annual plant that is rich in cellulose and can grow to a height of 90 centimeters in moderate climates (Kouta, Saliba & Saiyouri, 2020; Nunes, 2017). Cellulose accounts for 65–75% of the fibers, pectin, hemicellulose, and lignin account for 20%–25%, and water makes up 8–10% of the fibers (Khelifi, Lecompte, Perrot & Ausias, 2016). The physical properties of fiber are influenced by cellulose, hemicellulose, and lignin.

Table 2.1 Physical properties of fibers used in stabilization of earthen materials, adapted (Mallick, 2007)

Property	**Hemp**	**Flax**	**Sisal**	**Jute**
Density *(g/cm^3)*	1.48	1.4	1.33	1.46
Modulus *(GPa)*	70	60-80	38	10-30
Tensile strength *(MPa)*	550-900	800-1500	600-700	400-800
Elongation to failure *(%)*	1.6	1.2-1.6	2-3	1.8

The physical properties of hemp, flax, sisal, and jute fibers are displayed in Table 2.1. The density of hemp fiber is 1.48 g/cm^3. While the densities of flax, sisal, and jute fibers are 1.40, 1.33, and 1.46 g/cm^3, respectively. In contrast, the modulus of fibers ranges between 30 and 80 GPa. The tensile strength of hemp fiber ranges between 550 and 900 MPa. However, flax has a tensile strength between 800 and 1500 MPa, which is greater than that of other fibers. Sisal and jute fibers have a value that is between 600 to 700 and 400 to 800 MPa, respectively. The elongation failure ranges from 1.2 to 3%, with Sisal fibers reporting the highest value.

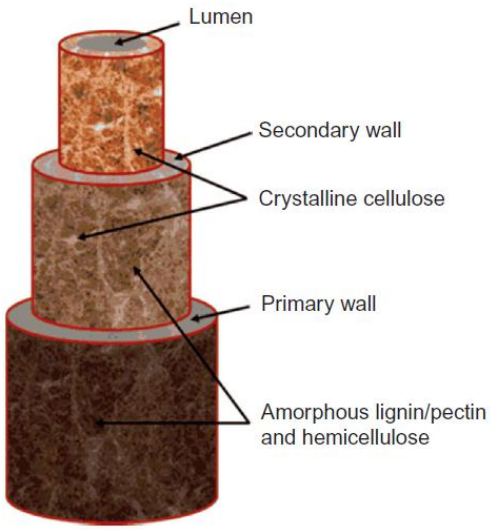

Figure 2.11 Structural elements of natural plant fiber (Bhattacharyya et al., 2015)

2.1.1.2 Mining and Industrial Waste

Mining in Africa is a prominent industry, and 30% of the world's reserves are found in the continent. According to a Nordic Africa Institute (NAI) report, Africa has a considerable portion of the world's most essential minerals and metals such as gold, diamond, cobalt, chromium, and manganese. This means that a significant amount of waste is produced due to mining activities. Approximately 20-25 billion tons of solid waste are generated on an annual basis (Almeida, Ribeiro & Silva, 2020). In

South Africa, the mining industry accounts for about 87% of the total waste produced per annum (Haywood, 2021). According to the UN Environment Program, only 4% of the waste in Africa is recycled; most of it is not correctly disposed of, causing severe environmental concerns. However, this byproduct can be used in the production of building materials.

Several studies have been carried out to valorize waste products from mining activities. For example, it can be used in Alkali activated products (geopolymers) produced by a combination of alumino-silicate powder with an alkaline solution. Mining waste can also be used in compact composites, especially from marble or quartz residue. The waste can also be incorporated into bricks to increase their mechanical strength and thermal conductivity. Iron ore waste is used in adobe, extruded, or compacted soil blocks to improve on their physio-thermal properties. In addition, it can also be used in the production of mortar. However, mining waste may be hazardous, necessitating energy-intensive and expensive purification processes such as electro mediation and desulfurization.

2.1.2 The effect of fiber, sand, and cow dung stabilization on the thermal conductivity and physical properties of mud samples

Earthen plasters have been utilized in dwellings since Neolithic times, and stabilizing clay plasters with natural fibers such as grass and straw and biowaste such as cow dung is common (Maheri, Maheri, Pourfallah, Azarm & Hadjipour, 2011). However, according to Obonyo, Tate, Sika & Tia, (2010), construction using these materials has not been adequately documented, particularly in Africa; as a result, their benefits have been diminished. This part of the study discusses the effects of inclusion of fibers, sand and cow dung on the thermal conductivity and the physical properties of mud plaster samples. Although thermal conductivity is the primary focus of this

research, physical properties such as density and porosity have also been included because they affect the thermal conductivity of the composite material.

2.1.2.1 Fiber and sand

Including fibers into clay matrix generally decreases the thermal conductivity of mud samples due to various factors; it promotes the formation of homogenous composite materials with closed porosity for mud samples stabilized by short fiber, thereby reducing bulk density (Millogo, Morel, Aubert & Ghavami, 2014). The other reason may be due to incorporation of lightweight fibers with good thermal insulation properties (Laborel-Préneron et al., 2016). Furthermore physical properties such as density, diameter, length shape and size of the fibers also influence thermal conductivity of composite materials (Maheri et al., 2011; Nasla, Gueraoui, Cherraj, Samaouali, Nchiti, Jamil, Arab, & Bougtaib, 2021). On the other hand incorporating sand increases the composite's thermal conductivity (Omer, 2018).

Lima et al., (2016) evaluated the effect of varying clay-earth-to-sand ratios and fiber inclusion on the properties of mud plaster samples. The research revealed that samples with higher clayish earth ratios had a higher thermal conductivity due to the increase in bulk density. Ashour, Wieland, Georg, Bockisch, & Wu (2010) incorporated wheat and barley straw into earth plaster samples. The study revealed that the thermal conductivity of barley straw-reinforced plaster decreased as fiber content increased but increased as sand content increased. Furthermore, the same trend was observed for mud plasters stabilized by wheat straw. However, samples with barley straw inclusion had better thermal insulation than samples stabilized by wheat straw. Moreover, straw fibers significantly reduced the thermal conductivity of the samples compared to sand.

Ouedraogo et al. (2019) investigated the effects of fiber incorporation on the physical, thermal, and mechanical properties of mud samples by incorporating 0.2, 0.4, 0.6, and 0.8% by weight of fonio straw into the soil matrix. The thermal

conductivity decreased with an increase in fiber content due to high porosity and partly due to cellulose in the fonio straw which has good thermal insulating properties. Millogo et al. (2014) included Hibiscus cannabinus fibers of 30 mm and 60 mm long into the soil matrix in varying proportions of 0.2, 0.4, 0.6 and 0.8 % by weight. As fiber content increased, thermal conductivity decreased. Furthermore, longer fibers had greater thermal insulation properties than shorter fibers. However, they had a negative effect on the compressive strength of composite.

Babé, Kidmo, Tom, Mvondo, Boum, & Djongyang (2020) examined the viability of using millet waste to improve thermal conductivity and compressive strength. For this experiment, 0, 1, 2, 3, and 4% millet waste contents were used. The incorporation of millet waste increased the mechanical properties of the earthen materials. This behavior was attributed to the cellulose in the millet waste, which contributed to improved flexural strength. However, the compressive strength of specimens without millet waste was higher than that of 1,3 and 4% fiber content. Furthermore, the thermal conductivity of the mud samples decreased as the fiber content increased due to a decrease in bulk density and an increase in fiber length.

Araya-Letelier, Antico, Burbano-Garcia, Concha-Riedel, Norambuena-Contreras, Concha & Saavedra (2021) studied the effect of incorporating jute fibers on physical and mechanical performance of mud samples. The authors included 0.5 and 2.0% by weight of jute fibers with varying lengths of 7, 15, and 30mm. The experiment showed that thermal conductivity decreased with an increase in the curing time. This reduction was attributed to the decline in the moisture content as the curing time increased. Thermal conductivity was also affected by the length of fibers; longer fibers reduced the thermal conductivity but increased the thermal insulation of composite material. Calatan, Hegyi, Dico & Mircea (2016) included 3-15% by volume hemp fiber and 10- 60% by volume straw contents in the soil matrix and reported a decrease in thermal conductivity with the increase in fiber content.

Dieye, Sambou, Faye, Thiam, Adj & Azilinon, (2017) conducted experiments to determine the effect of binders on the mechanical and thermal properties of earthen

materials. The authors incorporated Typha Australis fibers of varying lengths (1mm to 42mm) into the soil matrix. The experimental data showed a direct relationship between the binder content and mechanical strength; an increase in binder percentage increased the mechanical strength. The binder content consisted of clay and water, which formed a viscous mixture of percentage mass greater than 75% (>75%). The same relationship was observed between thermal conductivity and binder percentage; an increase in binder percentage increased the specimen's dry density, thereby increasing the thermal conductivity. Ajouguim, Talibi, Djelal-Dantec, Hajjou, Waqif, Stefanidou & Saadi, (2019) incorporated alkali-treated Alfa fibers into soil matrix. The fibers had varying lengths (2-2.5 cm). Adding the fibers decreased the density of specimens. However, alkali-treated fibers exhibited a lower density due to the reduction of pores in the clay matrix. Thus, the thermal conductivity also decreased with the addition of fibers.

Santos, Nunes & Faria, (2017) examined the impact of partial replacement of fine sand with a phase change material (PCM) and the addition of low quantities of oat fibers and hydrated air lime. The addition of PCM, fibers, and lime to the soil matrix reduced thermal conductivity due to a decrease in bulk density, which increased the porosity of the composite. Lima & Faria (2016) studied the effect of oat straw and Typha fiber wool incorporation. Six mortars containing the same clayish earth and siliceous sand volumetric ratio of 1:3 were prepared with varying proportions by weight of 10, 20, 40, and 80%. The addition of oat fiber led to a decrease in thermal conductivity due to the reduction of bulk density of the composite. The same trend was observed for samples stabilized with Typha fiber. However, the mortar with the lowest Typha fiber content by weight had a slightly higher thermal conductivity value than the reference sample. The authors attributed this to the densification of matrix pores caused by the addition of a small amount of fiber.

Bamogo, Ouedraogo, Sanou, Aubert & Millogo, (2022) investigated the effect of dolomite lime and fiber addition on the physical, hydric, thermal, and mechanical properties of earth render. Clay powder was combined with 2.4% and 6% dolomite lime by weight. The study revealed that the addition of dolomite lime reduces the

thermal conductivity of the composite due to an increase in closed porosity caused by the formation of calcium silicate (CSH) and magnesium silicate (MSH) hydrates. Palumbo, McGregor, Heath & Walker, (2016) investigated the hygrothermal properties of earth plasters stabilized with 1% and 2% by weight of barley straw and corn pith. The incorporation of fibers into the matrix of the soil decreased linear shrinkage, increased compressive strength, and enhanced the thermal insulation properties of earth plasters. Furthermore, it affected the equilibrium moisture content and the dynamic moisture buffering properties. Thermal conductivity was significantly reduced by about 60% and 78% when corn pith was added, and by about 36% when barley straw reinforcement was used. However, there was no significant difference when barley with different fiber lengths was included.

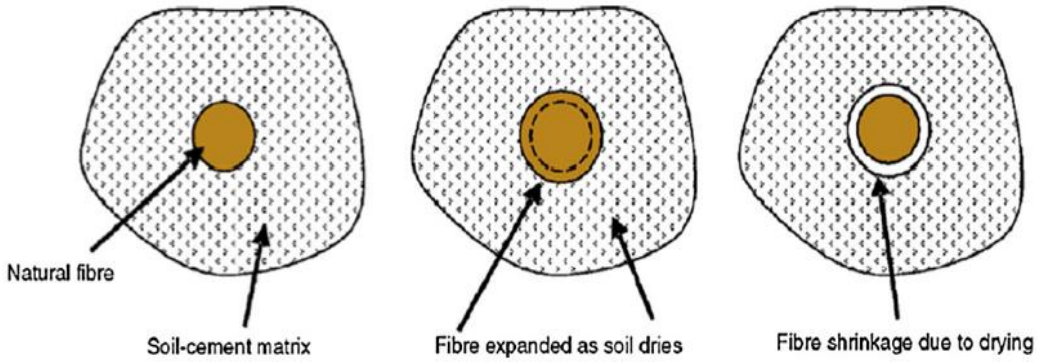

Figure 2.12 Fiber deformation due to variation in moisture content (Segetin et al., 2007)

Randazzo, Montana, Hein, Castiglia, Rodonò & Donato, (2016) evaluated the mineralogical and textural impact of pre-mixed clay-based plasters and a Terra Rossa sample. The research revealed that thermal conductivity decreased as porosity increased. The lowest thermal conductivity was observed in samples of Terra Rossa with the highest porosity. Singh et al. (2019) investigated the influence of clay soil mixed with quartz on the thermal conductivity of mud samples. In this study, the

thermal conductivity values of 90:10, 85:15, and 80:20 ratios of earth to sand were determined. The experiment revealed that 80:20 and 85:15 ratios increased thermal conductivity, while 90:10 decreased it.

Ngaram (2020) investigated the influence of moisture content on the thermal conductivity of mud samples. The investigation revealed that thermal conductivity increased as soil moisture content increased. The behavior was attributed to the replacement of pure air, which has a thermal conductivity of approximately 0.0272 W/mK at 38°C, with water, whose thermal conductivity ranges from 0.6106-0.6327 W/mK at 26.5 to 45°C.

Bassoud, Khelafi, Mokhtari, & Bada, (2021) assessed the influence of salty sand on thermomechanical properties of mud samples. The thermal conductivity of samples stabilized with 50, 60, 70, and 80% sand increased to 0.73, 0.75, 0.95, and 1.05 W/mK, respectively. The sample containing 90% normal sand had the highest thermal conductivity, whereas samples with 10% and 20% salty sand had the lowest thermal conductivity. The proportion of clay decreased the thermal conductivity, while the proportion of sand increased the value.

Singh, et al. (2019) investigated the effect of different quartz proportions on the thermal conductivity of mud samples. The samples were created with ratios of 100:0, 95:5, and 80:20 Earth to sand. The sample containing a ratio of 95:5 earth to sand had the highest thermal conductivity, measuring 0.9173 W/mK, while the sample containing a ratio of 90:10 earth to sand had the lowest thermal conductivity, measuring 0.60846 W/mK. Omer (2018) studied the effect of density, moisture, salt concentration and organic matter on the thermal conductivity of different soil types. The thermal conductivity value increased with the increase in soil bulk density due to increase in porosity. Sand had a thermal conductivity of 0.58 to 1.94 W/mK, sandy loam had a value of 0.19 to 1.12 W/mK, loam had a value of 0.29 W/mK to 0.76 W/mK, and clay loam had a value of 0.36 to 0.69 W/mK at densities of 1.23 to 1.59 g/cm^3 and water contents of 1.4 to 21.2%.

Ekwue, Stone, & Bhagwat, (2006) investigated the effect of moisture on thermal conductivity and reported that thermal conductivity and bulk density increased with increasing moisture content up to the point beyond which the bulk density decreased with further increase in moisture content. This behavior was attributed to the size and geometric configuration of the water layers surrounding the particles. Brouard, Belayachi, Hoxha, Ranganathan & Méo, (2018) evaluated the effect of moisture content on clay plasters stabilized with sunflower and Rape straw at 66, 86, and 98% humidity and concluded that water content had greater impact on the thermal conductivity of clay aggregate plaster than fiber incorporation.

Rivera-Gómez, Galán-Marín, López-Cabeza & Diz-Mellado (2021) studied the influence of soil characteristics on the thermophysical and acoustic properties of earth samples stabilized with natural polymers and wool fibers. Experimental data showed that the red soil (SR: liquid limit 25.6%, plastic limit 14.1%, and plastic limit 11.5%) had better thermal and mechanical properties. Hadji et al. (2020) studied the effect of mixing two types of soil (agricultural soil, liquid limit 54.78% and plasticity index 7.88%, and Hamada soil liquid limit 21.93% and plasticity index 6.88%) on samples stabilized with wheat straw. The study showed a reduction in thermal conductivity when straw was incorporated into the soil matrix. Hamada soil produced better thermal properties than agricultural soil.

Nasla et al. (2021) examined the influence of pine needles and straw fiber on the mechanical behavior and thermal conductivity of mud samples containing 1, 2, 3, and 4% by weight of pine needles and straw fiber and revealed that thermal conductivity decreased as the percent content of fibers increased. Incorporating fibers created more voids between the particles in the samples. The study revealed that straw fibers had better thermal performance than pine needles; the lowest thermal conductivity of 0.589 W/mK was reported for straw-reinforced samples, while the lowest value for pine needles stabilized samples was 0.682 W/mK. Ul Abdin & Khitab (2021) incorporated Pine needles of 13, 25, and 50 cm lengths. Their research showed that including the fiber decreased the density while increasing fiber length also increased the density.

Pedergnana & Elias-Ozkan (2021a) studied the hygro-thermal, hydric, and mechanical properties of earth plasters stabilized with chaff, flax, straw, pine needles, siliceous sand, and coarse siliceous sand. The sample reinforced with siliceous sand and chaff exhibited the lowest thermal conductivity, 0.44 W/mK, whereas the sample reinforced with flax exhibited the highest thermal conductivity, 0.80 W/mK. The research revealed that samples reinforced by thin fibers had a higher conductivity due to increased bulk density and reduced porosity.

Table 2.2 Physical properties of fibers used in stabilization, adapted (Laborel-Préneron et al., 2016; Pedergnana & Elias-Ozkan, 2022)

Fiber type	Fiber length	Fiber amount	λ/ W/mK	References
Hemp fiber		10 – 60 % by volume	0.35	Calatan et al. (2016)
Flax fiber	30 mm	20% by volume	0.80	Pedergnana & Elias-Ozkan, (2021a)
Jute fiber	7, 15 & 30 mm	0.5 & 2.0% wt	1.00	Araya-Letelier et al. (2021)
Barley straw				Ashour et al. (2010)
Kenaf	30 & 60 mm	0.2, 0.4, 0.6 & 0.8% wt	1.30 – 1.70	Millogo et al., (2014)
Wheat straw				Ashour et al. (2010)
Millet fiber		0, 1, 2, 3 & 4 % wt	0.74 – 0.96	Babé et al. (2020)
Alfa fibers	2- 2.5 cm	1 & 1.5% wt	1.17 – 1.51	Ajouguim et al., (2019)
Pine needle		1, 2, 3 & 4 %wt 20% by volume	0. 68 – 0.77 0.55	Nasla et al., (2021) Pedergnana & Elias-Ozkan, (2021a)
Oat fibers				Santos et al. (2017)

Table 2.2 cont'd

Fonio straw		0.2, 0.4, 0,6 & 0.8 % wt	0.30 – 1.10	Ouedraogo et al. (2019)
Chaff		20% by volume	0.44, 0.56	Pedergnana & Elias-Ozkan, (2021a)
Straw		1, 2, 3 & 4 % wt, 20% by volume	0.59 – 0.68	Nasla et al., (2021)
	40 mm		0.70	Pedergnana & Elias-Ozkan, (2021a)

2.1.2.2 Cow dung and processed cow dung

Cow dung is the undigested food residue consumed by herbivores such as cows; It contains plant fibers, microorganisms, amine compounds, potassium, fragments of intestinal tissues, and trace amounts of sulfur, calcium, iron, magnesium, and manganese (Kulshreshtha, Vardon, Meesters, van Loosdrecht, Mota, & Jonkers, 2022). Cow dung is used as a floor coating material and to stabilize adobe bricks and plasters in African vernacular architecture (Millogo et al., 2016).

Cow dung influences the properties of earthen materials when it is mixed into the soil matrix. Mahamat, Hamid, Soultan, Khayal, Elhamdouni, Garoum & Gaye (2015) investigated the effect of cow dung incorporation on the thermophysical properties of mud samples and concluded that cow dung inclusion significantly decreased the thermal conductivity of the composite materials. This behavior was attributed to the increase in closed porosity of mud samples. Millogo et al. (2016) included 1 to 3% by weight of cow dung into soil containing 43, 17.5, and 36% by weight of sand, silt, and clay, respectively, to determine the influence of cow dung incorporation. The authors concluded that inclusion of cow dung improved the physical and mechanical properties of earthen samples. The author also noted that the water-resistant capacity was due to the reaction of cow dung with kaolinite and

quartz, which produced insoluble silicate amine responsible for gluing isolated particles together.

Kulshreshtha et al. (2022) studied the water-resistant capacity of cow dung when included into the soil matrix. The fresh cow dung used contained 42% fibers by weight and 58% microbial aggregate by weight. The authors concluded that microbial aggregates were responsible for the water-resistant behavior of cow dung due to the hydrophobicity of negatively charged particles rich in fatty acids. Gunvant et al. (2022) incorporated 70, 80, and 90% by weight cow dung ash and 10 to 30% lime into the soil matrix and observed a decrease in strength as cow dung content increased. On the other hand, Pachamama, Marco, Penido & Faria, (2020) included 5 to 20% by weight cow dung and 5% by weight air lime in a clay-to-sand ratio of 1:1, 1:2, 1:3 and 1:4 and observed a decrease of bulk density as the percentage of cow dung increased. Furthermore, 10% of cow dung increased compressive strength by 45%, flexural strength by 60%, and adhesive strength by 133%.

Bamogo et al. (2020) conducted an experiment to enhance the physical, mechanical, hydric, and thermal properties of cow dung-stabilized earthen renders. The utilized clay consisted of 62% by weight of Kaolinite, 31% by weight of quartz, 2% by weight of goethite, and stabilized with up to 6% by weight of cow dung. The authors observed that cow dung inhibits the spread of cracks because it adheres well to the clay matrix. The cow dung reacts with the kaolinite and quartz in a base medium to form insoluble amine silicate which connects isolated particles through free electronic doublets on the oxygen and nitrogen atoms thereby influencing the mineralogy of composite material. Furthermore, the authors observed a decrease in the thermal conductivity of mud samples due to the cellulose found in the undigested fibers of cow dung, which has excellent thermal insulating properties.

Ngowi, (1997) examined methods for enhancing earth construction in two Botswana villages by conducting an experiment with mud samples stabilized with 10 and 20 % by weight of cow dung. The author observed that adding wet or flocculant cow dung results in the formation of an inert matrix. Furthermore, cow dung envelops and

binds soil particles as they dry; thereby reducing the formation of cracks. However, the incorporation of cow dung did not influence the strength of the mud samples. Manu (2013) on the other hand, stabilized mud samples with 15, 20, 25, and 30% cow dung and observed an increase in density and compressive strength of 25% with 20% cow dung reinforcement.

Bahobail, (2012a) added 5, 10, and 15% by mass of cow dung, soap, palm oil, and ash to a soil containing 40% clay and 60% sand and observed an increase in thermal conductivity as the percentage of cow dung increased. However, the addition of ash resulted in a decrease in thermal conductivity. Mbereyaho, Irafasha, Habumugisha, & Musabirema (2020) incorporated 10, 20, 30, and 40% by weight of cow dung in a cow dung to cohesive soil ratio of 1:10, 1:5, 3:30, and 2:5 to determine water absorption, shrinkage, and the Atterberg limit. They concluded that 20% by weight cow dung had good properties and a high durability. On the other hand, Lekshmi, Vishnudas & Nair (2020) included 5, 10, 15 and 20% by weight and noted a decrease in compressive strength and linear shrinkage.

2.2 Analysis of methodologies and instruments used for measuring thermal conductivity of earthen materials

The thermal conductivity of a material is a measure of its capacity to conduct heat (Fay, 1967). Several techniques exist for determining the thermal conductivities of earthen materials (Fabbri, Morel & Gallipoli, 2018). For proper analysis, methods are divided into three categories: steady-state technique, non-steady-state or transient technique, and calculation using a mathematical model (Chen, 2020). Thermal conductivity measurement methods are founded on the fundamental laws of heat conduction and electrical analogy (ISO 8302:1991, 2019). The measurement systems are divided into three categories: room temperature operation (20 to 25^0C), below

room temperature operation (up to -180^0C), and high-temperature operation (up to 600^0C) (Yüksel, 2013).

The steady-state method determines a material's thermal conductivity when its thermal state is in equilibrium (Yang, Kim & Lee, 2018). According to Yüksel (2013), a steady state is reached when there is no temperature change with time and the temperature at opposite sides of the materials is constant. However, it should be noted that it takes a long time to reach the thermal equilibrium state hence one of the downsides of this method (Yüksel, 2013). Another problem is related to the expensive apparatus needed for this method (Robert, Etuk, Agbasi, Okorie, Ekpenyong & Anonaba, 2022). Furthermore, steady-state heat transfer cannot be easily determined due to other forms of heat loss, such as radiation, conduction and convection, inhomogeneity, and anisotropy (ASTM C 177, 2010). Nonetheless, this method gives the most accurate thermal conductivity values (Yüksel, 2013).

The method relies on Fourier's law of heat conduction to determine a material's thermal conductivity (Sánchez-Calderón, Merillas, Bernardo & Rodríguez-Pérez, 2022). Furthermore, the solutions are transformed into one-dimensional problems, simplifying the calculation; however, the calculations differ for models of an infinite slab, an infinite cylinder, and a sphere (Yüksel, 2013). To differentiate between types of thermal conductivity measurements, typical specimen geometry, measurement system configuration, and thermal conductivity magnitude are used (Yüksel, 2013). The thermal magnitude is calculated by employing a measuring technique that makes use of the direction of the heat flow, heat flow conservation, and an auxiliary layer with a known thermal property (ASTM C 177, 2010; Fay, 1967; ISO 8302:1991, 2019).

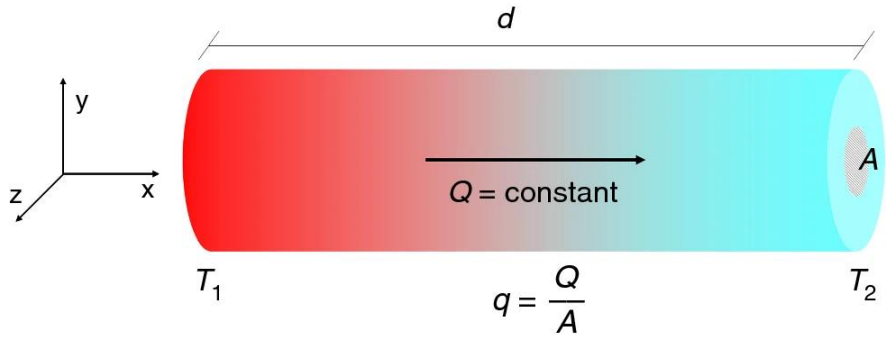

Figure 2.13 Illustration of steady-state heat transfer from T_1 to T_2 across distance d (Sánchez-Calderón et al., 2022)

The transient state method measures thermal conductivity in the course of heating with the help of transient sensors (Yüksel, 2013). Unlike the steady-state method, the values of thermal conductivity are quickly determined. The transient methods rely on a signal measurement by evaluating the feedback response following the transmission of a signal to the specimen in order to determine the heat generation in the specimen (Fabbri et al., 2018). The method generally utilizes needle probes or wires (Pekdoğan & Tahsin, 2016).

There are four major methods for measuring thermal conductivity: the guarded hot plate method, the hot-flow meter method, the hot wire method, and the laser flash diffusivity method (Yüksel, 2013). The guarded hot plate, or a heat flow meter is preferred to measure thermal conductivity of insulated material; laser flash methods are utilized for highly conductive ceramics, metals, and certain composites (Fabbri et al., 2018). The hot-wire method is used to measure the thermal conductivity of large specimen of refractory materials (Yüksel, 2013).

On the other hand, a mathematical model can also be used to determine thermal conductivity. For example, Chen (2020) measured the thermal conductivity of CSEBs using a mathematical model with a national invention patent. The measurement principle was only linked to the thermal properties of the material. The values of thermal conductivity were obtained during the heating, similar to the

transient method. The temperature difference between the two opposite sides had to be determined before calculations. The author noted that the method gives a solution to the surface thermal resistance error, which is a significant problem for the steady-state method.

Table 2.3 Methods for measuring thermal conductivity adapted from (ASTM C 177, 2010; Chen, 2020; Yüksel, 2013)

Method of measuring thermal conductivity	Type of measurement
KD2 pro thermal analyzer	
Hot disk method	
Transient hot plate	Transient or unsteady state
Transient hot bridge	
Asymmetric hot plane	
Guarded hot plat	
Heat flow method	Steady state
Calculation from thermocouple	
Calculation from mathematical model	Calculation

Figure 2.14 depicts the number of papers per method of measuring thermal conductivity. According to collected data, the KD2 pro thermal analyzer is the most popular method. The apparatus measures thermal conductivity, resistance, volumetric specific heat capacity, and diffusivity (Decagon Devices, 2016). As mentioned previously, the instrument measures thermal conductivity in a transient state. A heated needle is inserted into the sample. During heating, the temperature is then read from the display. The device is user-friendly and employs a high heating rate strategy to reduce temperature drift error susceptibility. On the other hand, the findings revealed that guarded hot plate was the most popular steady-state method. This method works best with dry, homogeneous samples (ASTM C 177, 2010; ISO 8302:1991, 2019). The Guarded hot plate method comprises of thermal insulation, cold plates, a hot plate, and a guard heater system (Yüksel, 2013). The thermal conductivity of a material can only be measured after it has reached thermal

equilibrium, which occurs when both the heating and cooling plates have reached a constant temperature (ISO 8302:1991, 2019).

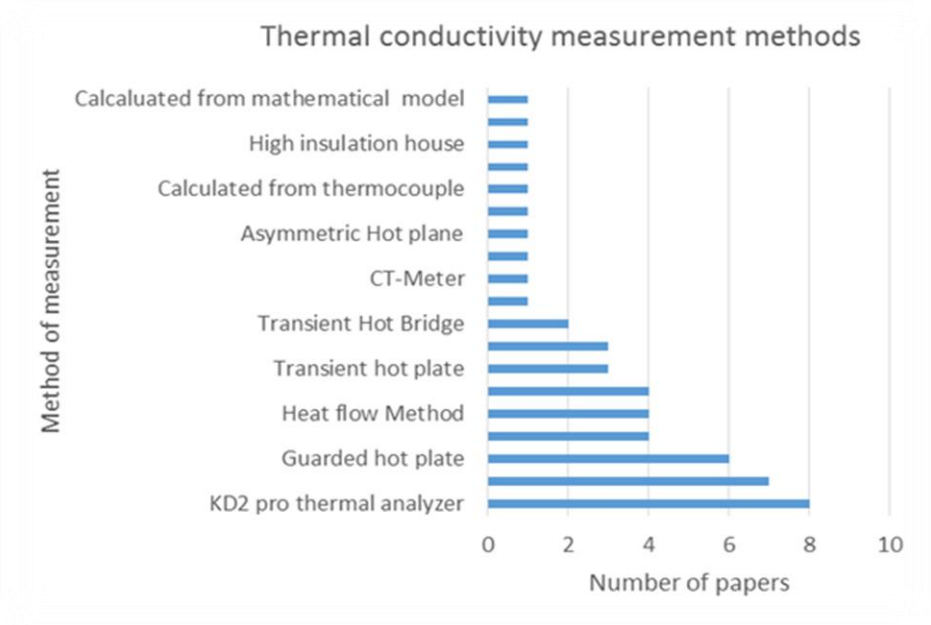

Figure 2.14 Methods of thermal conductivity measurements used in the papers studied from literature (Chen, 2020; Yüksel, 2013)

2.2.1 Experimental design and procedure for some methods of measuring thermal conductivity of mud samples

This section of the research will examine the experimental methodology of four methods used to measure the thermal conductivity of mud samples: the guarded hot plate, the KEM QTM 500 hotwire method, the centered hot plate method, and Lee's disk setup.

2.2.1.1 The guarded hot plate

The guarded hot plate (GHP) measures the thermal conductivity of a material when there is a steady state heat transfer between the hot plate and the cold plate (Yüksel, 2013). It is regarded as the most precise technique for measuring the thermal conductivity of thermal insulators, with a 1.5% margin of error over a limited temperature range close to ambient temperature (Salmon, 2001). The GHP is used to measure heat flux through low thermal conductivity materials (ASTM C 177, 2010). The GHP also utilizes Fourier's law of heat conduction (Ashour et al., 2010b).

The experimental setup includes a hot surface assembly comprising the metered section and primary guard, two cold surface assemblies, a secondary guard serving as edge insulation, a temperature-controlled secondary guard, and an environmental chamber (ASTM C 177, 2010; ISO 8302:1991, 2019; Ispir et al., 2016). The hot plate is electrically heated, whereas the cold plates are either Peltier coolers or liquid-cooled heat sinks (Ispir, Dikeç & Onbaşioğlu, 2016). The symmetrical experimental design consists of a guarded hot plate placed on the sides, with the heating element positioned between the two specimens (for double sided GHP) or between a single specimen and an auxiliary layer (ASTM C 177, 2010; ISO 8302:1991, 2019). The temperature on the hot side for the double sided GHP can be adjusted on the heating plate and the guarded plate (Yang et al., 2018). The electrical current is supplied independently to the metered area and the guarded plates (Yang et al., 2018). Furthermore, the heat flow from the metered area of the heating plate through the specimen to the cold plates is maintained at a stable lower temperature (Salmon, 2001).

The double-sided GHP simultaneously measures the thermal conductivity of two similar specimens (ASTM C 177, 2010). Conversely, for the single-sided GHP, heat flow passes through one specimen while the main heater's top serves as an insulating barrier (ISO 8302:1991, 2019).

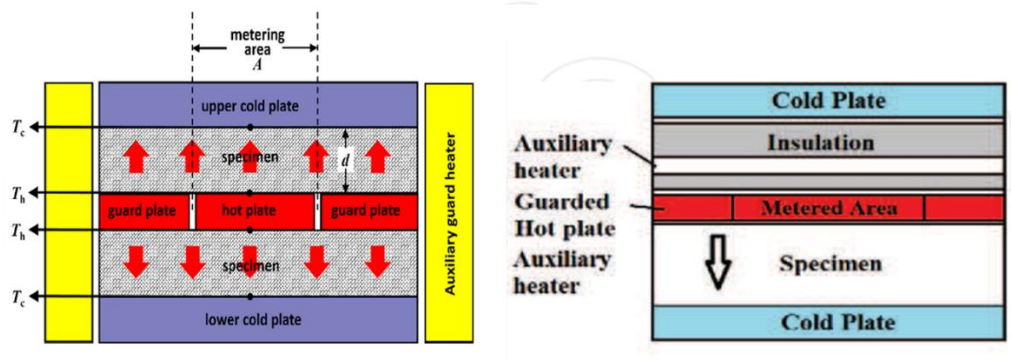

Figure 2.15 Double sided GHP with two specimen (left) (Yang et al., 2018), double sided GHP with one specimen (right) (Yüksel, 2013)

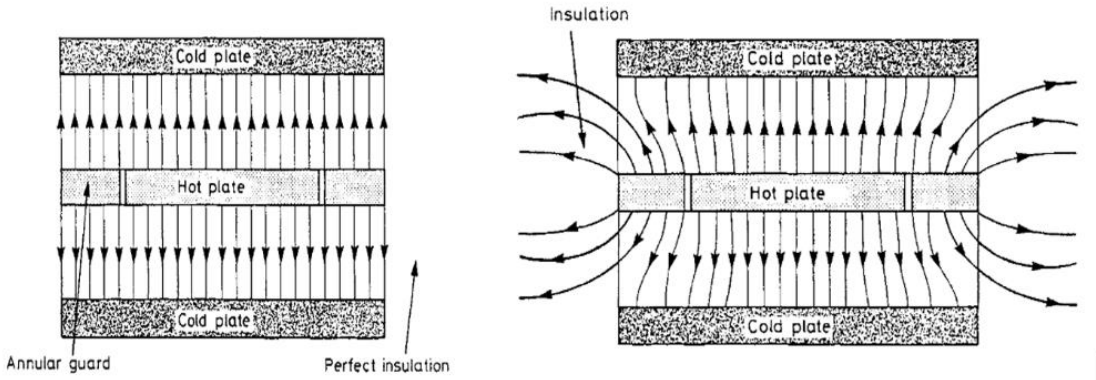

Figure 2.16 Ideal case (left) and practical case (right) illustration of heat flux distribution double sided GHP (Salmon, 2001)

Electrical heat is introduced into the plates in a square or circular form, and it must be applied at a constant heat rate (Yüksel, 2013). Furthermore, the heat flows unidirectionally towards the cold plates cooled by a Peltier or a liquid cooling system in both configurations (Yang et al., 2018). It is essential for the heat to flow in one direction to avoid erroneous thermal conductivity results (Yüksel, 2013). Differential thermocouples then record the temperature (Ispir et al., 2016). A predetermined heat rate is also supplied to the central heater (metered area), and the temperature of the guard heater is kept at the same temperature as the metered section by a controlled system (Yüksel, 2013). Furthermore, the temperatures of the plates and the adjoining thermal guard surfaces are kept within the same temperature range (ASTM C 177,

2010). The temperature sensors and the electrical power supply devices are connected to a system that records the information (Yüksel, 2013).

For accurate results, it is necessary to consider the steady-state condition, unidirectional heat flow, temperature of the hot plate and cold surfaces, specimen thickness, and specimen homogeneity (ASTM C 177, 2010; ISO 8302:1991, 2019). Furthermore, the GHP has edge loss errors that can be reduced by using wide guards and the proper selection of the ambient temperature; it also has gap errors due to the temperature difference, gap geometry, the structural support system, and the gap fill material (ASTM C 177, 2010). The Guarded hotplate (GHP) has international standards and guidelines for measuring the thermal conductivity of various materials, such as ASTM C 177-63 in the US, BS 874: 1965 in Great Britain, and DIN 52612 in Germany (Salmon, 2001; Yang et al., 2018).

I. Experimental design and procedure for Double and Single sided GHP

The Guarded hot plate (GHP) measures thermal conductivity of samples at a steady state (Salmon, 2001). A temperature gradient is created between the hot and cold plates, and the power rate in the hot plate with the metered area A is measured at the steady state (Yüksel, 2013). The heating and the cold plate are maintained at a steady temperature when the thermal equilibrium is attained; at this point, the thermal conductivity is measured considering the measurable parameters in the equation below;

$$K_{eff} = \frac{Q\Delta x}{A\Delta T} \quad \textbf{(1.1)}$$

Where;

K_{eff} is the effective thermal conductivity

Q is the heat power

ΔT is the temperature difference across the specimen

Δx is the specimen thickness

A is the heat transfer area (centered metered area)

For double sided GHP, the heat power Q is divided by 2 (Q/2).

II. Experimental design and procedure for λ-Meter EP 500 Guarded hot plate apparatus

The procedures are based from experimental research that was conducted by Ashour et al., (2010), who measured the thermal conductivity of natural plaster materials. The samples are placed in the device with their borders insulated with Polystyrene. Thermal conductivity measurements can be performed at the desired temperature, and the heat control does not turn off when the thermal conditions within the specimen are nearly stationary, allowing for temperature adjustment. The device has the capacity to automatically carry out three subsequent tests at different temperatures between 10 and 40ºC. Furthermore, the average temperature is computed from the cold and hot plates. The thermal conductivity is then calculated by software using data collected by a data logger.

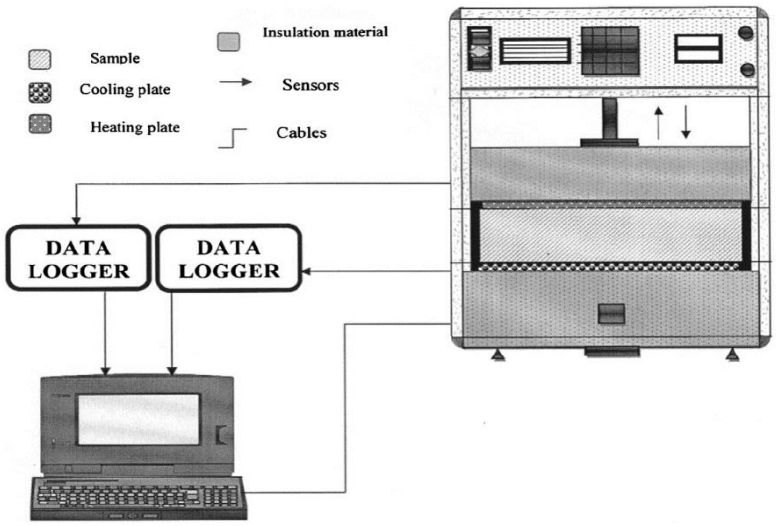

Figure 2.17 Experimental setup for λ-Meter EP 500 guarded hotplate (Ashour et al., 2010a)

2.2.1.2 KEM QTM 500 hotwire method

The device measures the thermal conductivity of samples in the process of heating with the help of transient sensors based on the ASTM C 1113-99 hot wire method (Dündar, Kurt, As & Uysal, 2012). The hot wire method operates on the principle of an ideal, constant heat generation source, an infinitely long and thin continuous line dissipating heat into an infinite medium (Kostic & Simham, 2009). The method is composed of a single heater wire and a thermocouple as seen in figure 2.14 (Kostic & Simham, 2009). The wire is electrically heated, and the change in resistance, and hence temperature, is measured as a function of time using Wheatstone bridge circuitry and a computerized data collection system (Pekdoğan & Tahsin, 2016). The heating power and the slope of temperature change in logarithmic time are used to calculate the thermal conductivity (Kostic & Simham, 2009). The hot wire method assumes that heat transfer to an infinite medium of thermal conductivity k_f and thermal diffusivity $\alpha_f = k_f / p_f C_s$ occurs solely via conduction, thereby increasing the temperature of both the heat source and the test medium over time; furthermore, the line heat source has a constant instantaneous temperature but is transient in time (Kostic & Simham, 2009).

The KEM QTM 500 hot wire method has a 5% precision and a measuring range of 0.023 W/mK to 12 W/mK (Qiu et al., 2022). The device also has a temperature range of -10 to 200ºC and can measure the thermal conductivity of samples with a minimum size of 100 x 50 x 20 mm^3 under laboratory conditions of 5 to 35ºC and relative humidity of less than 85% (Kyoto Electronics, 2009). Furthermore, the KEM QTM 500 hot wire has a 5% margin of error (Qiu et al., 2022).

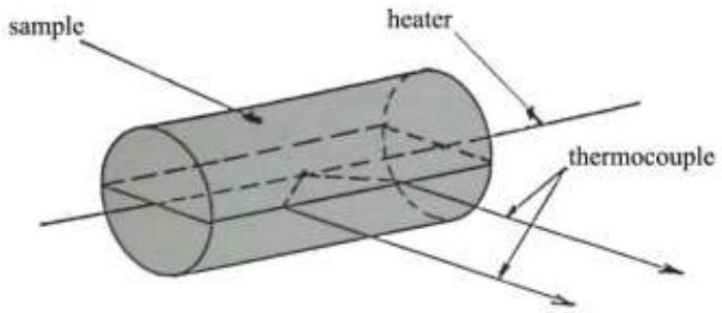

Figure 2.18 Illustration showing the hotwire method (Pekdoğan & Tahsin, 2016)

The experimental procedure is based on official user manual (Kyoto Electronics, 2009). The device is connected to a constant heat supply which causes the temperature in the heater to increase exponentially. The temperature curve is then plotted with the logarithm function of time on the x-axis as seen in Figure 2.19. The angle of the line is inversely proportional to the thermal conductivity; a higher angle indicates a low thermal conductivity and a lower angle indicates a high thermal conductivity.

The thermal conductivity is then calculated from the following equation;

$$\lambda = \frac{q.In(\frac{t_2}{t_1})}{4\pi(T_2 - T_1)} \quad \textbf{(1.2)}$$

Where;

λ is the thermal conductivity in W/mK

q is the generated heat per unit length of sample/ time

In is the natural logarithm

t1 and *t2* are the measured time length

T1 and *T2* are the temperature at *t1* and *t2*.

The thermal conductivity is calculated by a software which utilizes data collected from the sensor probe.

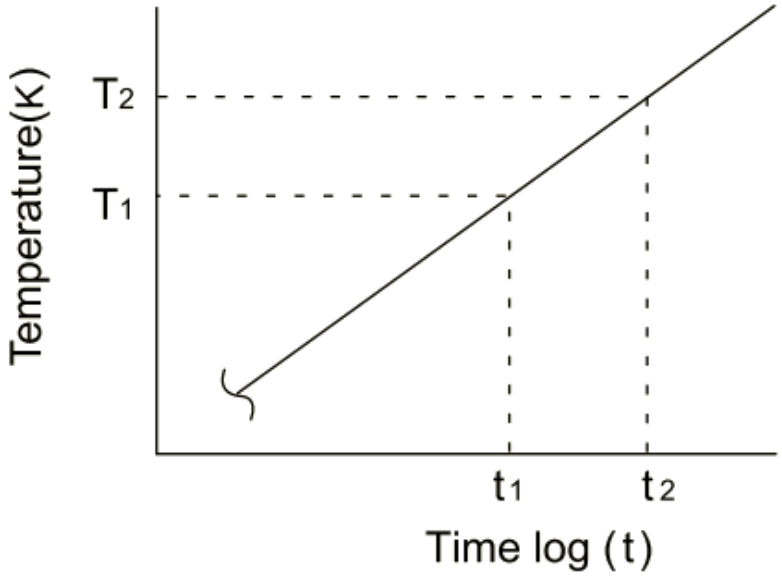

Figure 2.19 Temperature curve for a sample measured by QTM 500 (Kyoto Electronics, 2009)

2.2.1.3 The centered hot plate method

The centered hot plate method measures the thermal conductivity in steady-state. (Jannot, Felix & Degiovanni, 2010). The technique is based on taking a temperature reading at the center of the heating element (Laaroussi, Lauriat, Garoum, Cherki & Jannot, 2014). The sample to be tested for thermal conductivity is placed in the center of the heating plate; the plate is then sandwiched between the sample and 20 mm thick polyethylene foam (Lamrani, Laaroussi, Khabbazi, Khalfaoui, Garoum & Feiz, 2017a). It is essential to note that the cross-sectional area of the heating element, foam, and sample are all the same (Laaroussi et al., 2014). Using an aluminum block with a higher thermal conductivity, the top surface temperature is maintained at a

predetermined level so that the heat flux is primarily directed through the sample (Laaroussi et al., 2014). The second aluminum block is then positioned so that thermal equilibrium is reached within a reasonable amount of time (Lamrani et al., 2017a). The thermocouples T_o, T_1 and T_2 indicating the upper sample surface, lower sample surface and lower insulating form face temperatures respectively are positioned as depicted in Figure 2.20 (Laaroussi et al., 2014).

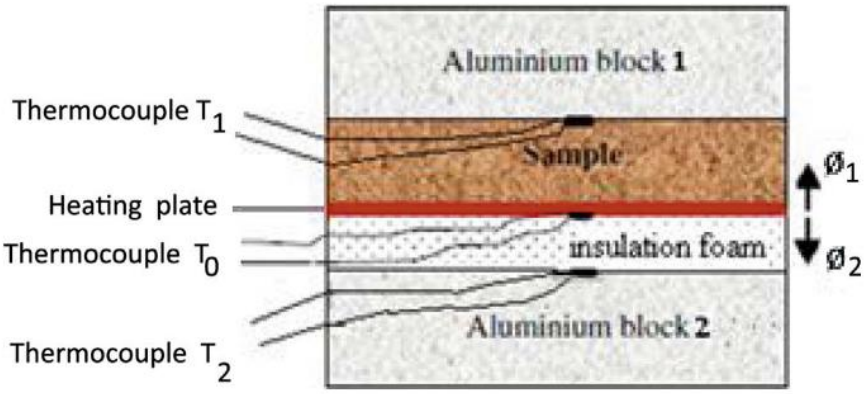

Figure 2.20 Experimental setup for centered heating plate (Lamrani et al., 2017b)

The thermal conductivity of the sample is then calculated from;

$$\lambda_{HPS} = \frac{e_1}{T_0 - T_1}\left[\frac{U^2}{RS} - \frac{\lambda_2}{e_2}(T_0 - T_2\right] \quad \textbf{(1.3)}$$

Where;

λ_{HPS} is the thermal conductivity in W/m^{2}K

e_1 is the sample thickness in mm

e_2 is a known thickness of the insulating foam in mm

λ_2 is a known thermal conductivity value of insulating foam.

U is the voltage in Volts.

R is a known resistance

S is the area of the heating element in m^2

The experimental setup is first calibrated using a sample of a known thermal conductivity (Lamrani et al., 2017a).

2.2.1.4 Modified Lee's disk method

The modified Lee's disk method measures the thermal conductivity of mud samples in thermal equilibrium (Robert et al., 2022). The sample is placed on a first brass disc with a diameter of 30mm that serves as a stable heat source and is controlled by a heating plate with a thermostat (Randazzo et al., 2016). It is essential to note that the sample being tested for thermal conductivity should have the same uniform thickness and cross-sectional area or diameter as the brass disc (Robert et al., 2022). A thermocouple is placed to measure the temperature variation of the first brass disk. Furthermore, a second brass disc is placed on top of the sample, and its temperature is monitored by a second thermocouple (Randazzo et al., 2016). The second brass disc has a predetermined heat loss $q_{loss}\,(T)$ in relation to its temperature or to the temperature difference with the ambient temperature (Randazzo et al., 2016). A specific temperature is determined, and the system is allowed to reach thermal equilibrium while a data logger records the temperature variation of the two brass discs and the ambient air temperature.

At steady state, the loss in heat energy is theorized to be the predetermined heat loss in the second brass disc; therefore, considering the temperature difference in the two brass discs *dT*, the thermal conductivity of the sample is calculated from the equation;

$$K(T) = q_{loss}(T)\frac{X}{AdT} \qquad \textbf{(1.4)}$$

Where;

$K(T)$ is the thermal conductivity in W/m^{2}K

$q_{loss}(T)$ is the estimated heat loss in first brass disc

dT is the difference in temperature between the first and the second brass disc

X and A is the thickness and area respectively of the circular sample.

2.2.2 Factors affecting the accuracy of the values of thermal conductivity

Before analyzing the factors influencing the effectiveness of thermal conductivity methods, it is essential to understand the principle of heat transfer. Heat energy can be transferred through three modes: conduction, radiation, and convection (ISO 8302:1991, 2019). There should be a temperature difference before heat is transferred from a hot region to a cold region (Fay, 1967). Different methods of measuring thermal conductivities were developed, considering these principles (Yüksel, 2013). Modes of heat transfer such as conduction depend on Fourier's law and usually occur in materials with high thermal conductivities (Fay, 1967). According to ISO 8302: EN, heat transfer property obtained from heat flow rate, temperature difference, and dimension may not depict the actual thermal conductivity values, especially in moist materials (ISO 8302:1991, 2019). For such cases, thermal resistance is considered an appropriate parameter. Generally, heat transfer is influenced by type and thickness of material, moisture content, and change in time and temperature (ISO 8302:1991, 2019).

As previously stated, thermal conductivity methods are classified into three types. Transient methods are considered destructive because the material has to be prepared according to a specific dimension (Fabbri et al., 2018). Furthermore, the material may be melted or a hole drilled into the sample for some methods, such is the case for Hotwire (Fabbri et al., 2018). However, modified versions have been developed. In transient methods, heat is applied to the specimen, and temperature change over

time are observed (ASTM C 177, 2010). Steady-state methods use unidirectional heat flow, power input, and temperature change to determine thermal conductivity when the material has attained thermal equilibrium (Yüksel, 2013). It employs the principle of Fourier's law to determine thermal conductivity (ASTM C 177, 2010). Many factors influence the accuracy of thermal conductivity values; sample surfaces, external data, boundary effects, sample homogeneity, and environmental conditions should all be taken into account when measuring thermal conductivity (Yüksel, 2013). Furthermore, for the guarded hot plate (GHP), edge loss error and gap imbalance errors should be considered (ASTM C 177, 2010).

The literature review shows a discrepancy in the values of thermal conductivity of earth-based materials. Fabbri, Morel & Gallipoli (2018) noted variations in thermal conductivity values ranging from 0.2 W m^{-1} K^{-1} to 2 W m^{-1} K^{-1}. The authors attributed this variation to various methods available in the market, and they suggested a study be done on the impact of these methods. Furthermore, various methods can produce different values under the same conditions. For example, Zhao, Qian, Gu, Jajja, & Yang (2016) compared thermal conductivity values obtained by the Laser flash method and Transient plane sources. The authors reported a 20% difference between the values obtained by the two methods, with the Laser flash method showing the highest value. However, it should be noted that while the Laser flash method has a standard protocol ASTM E 1461-92, the Transient plane source did not have a standard protocol at the time of reporting. Another interesting factor to consider is the principle of measuring thermal conductivity; although the two methods are interfacial methods, there is a difference in measuring protocol. The transient plane source method relies on the surface contact and requires measuring thermal diffusivity and volumetric heat capacity before determining the thermal conductivity (Zhao et al., 2016). This may cause further errors in measurement if the apparatus is not calibrated correctly. On the other hand, the Laser flash method is affected by light scattering that occurs when the laser beam hits the sample surface. Like the transient plane source, the laser flash method also depends on external parameters such as density, heat capacity, and thermal diffusivity to

determine thermal conductivity. Variation in thermal conductivity values is expected due to the use of different materials and conditions. However, as seen in an experiment by Fabbri et al., (2018), a significant difference was reported for the same material under the same condition using different methods. ISO 8302: EN recommends a ± 5% difference between the guarded hot plate and other similar methods. There should also be an internationally standardized protocol for the available methods. Currently, not all methods for measuring thermal conductivity have an internationally recognized protocol.

To reduce errors in the GHP, Salmon (2001) recommended that the plates be flat and made of a material with high thermal conductivity and emissivity. The author also suggests that the contact resistance between the plates and the specimen be uniform. Furthermore, the thermocouple placed on the plate should have a good thermal contact in order to read the required temperature effectively. The author also recommended placing thermocouples on the specimen surface for materials with thermal conductivities greater than 0.15 W/mK. Furthermore, to prevent lateral heat exchange, the temperature balance between the guard and the metered area should be kept within close limits.

2.3 Information about the mud plaster samples used in the investigation

As previously stated, the mud plaster samples used in this study were prepared and tested by Matthieu Pedergnana as part of his doctoral research (Pedergnana, 2022). Some of his work was reported in (Pedergnana & Elias-Ozkan, 2021b), and some of his samples were also tested for their thermal properties and presented in (Pedergnana & Elias-Ozkan, 2021a). A few of his samples were evaluated for their thermal properties in this study, and the results were compared to those of his study.

2.3.1 Earth

The earth used to prepare the mud samples came from Sorgun, a rural location in central Anatolia. It was made up of 34.5% sand, 21% silt, and 33.5% clay. According to the UCS earth classification, it is categorized as Sandy Clay (Figure 2.21). Figure 2.22 depicts the earth's particle size distribution (PSD) as determined by ASTM D422 and ASTM D7928 for particles larger than 75µm and smaller than 75µm. The PSD of soil particles bigger than 75µm was determined on a 2 kg sample of soil in accordance with ASTM D422 by passing oven-dried soil through a series of sieves and measuring the mass of soil retained in each sieve. In contrast, the PSD of particles finer than 75µm was determined in accordance with ASTM D7928; a 50g soil sample was weighed and sieved through a 75m mesh. A hydrometer was used to determine the amount of silt and clay in the soil using particles finer than 75µm. The time it took for the particle to settle was measured over a 24-hour period.

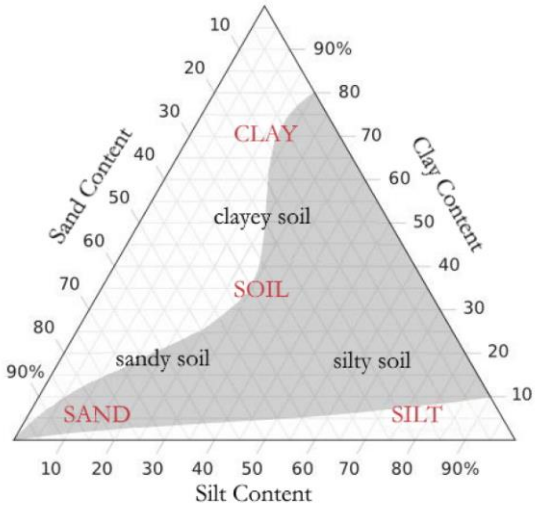

Figure 2.21 Soil classification in ternary plot (Drexel & Aigner, 2018)

A sample of soil passed through a 425µm sieve was used to determine the liquid limit LL, plastic limit PL, and plasticity index PI in accordance with ASTM D4318. The LL was determined by allowing a sample containing a specific amount of water to flow under shocks produced by a standard device; the LL was calculated based on at least three experiments conducted with varying amounts of water in the soil. The PL, on the other hand, was determined by rolling soil into a 3.2mm thread until it crumbed; the amount of water in the soil at this point determined its plastic limit. The PI is calculated as the difference between the PL and the LL. The liquid and plastic limits are recorded as 42.8 and 20.6 respectively.

The earth that was used to make the samples was prepared in three steps: first, it was allowed to dry in the air; second, the large particles, such as stones, were taken out. In order to prepare the earth mortar, the last stage included breaking the earth and sifting it through a 2mm sieve.

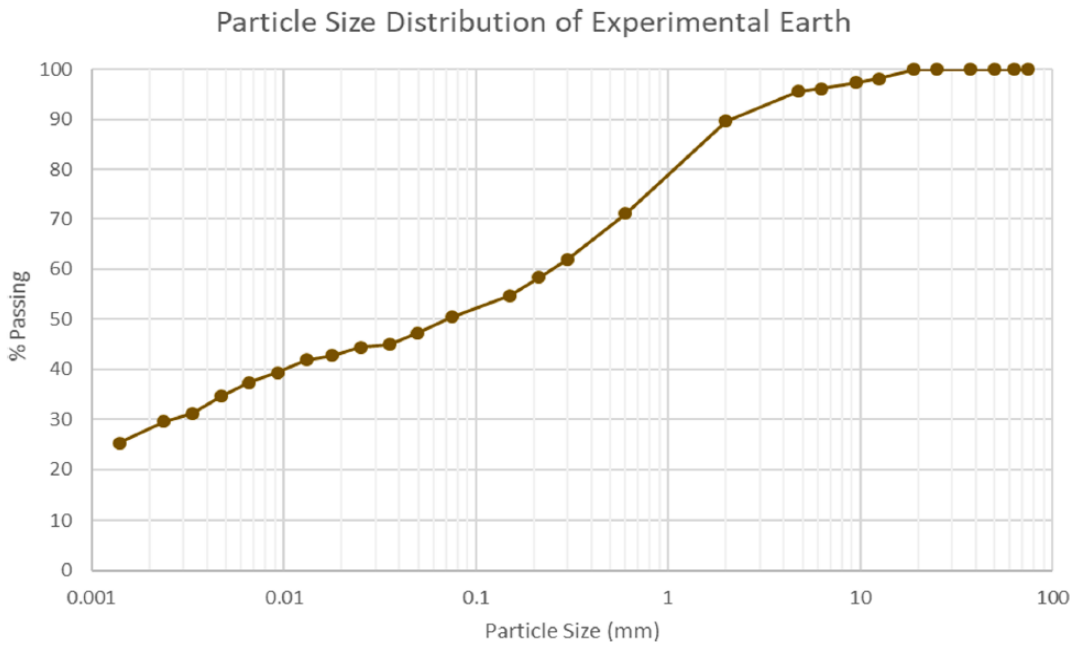

Figure 2.22 Particle size distribution of the earth used in the experiment adapted from (Pedergnana & Elias-Ozkan, 2021b)

2.3.2 Sand

The sand to be mixed with the earth was obtained locally. The commercial sand used as a reference was also acquired from Sorgun. It was sieved through 4.5 mm, and the resultant was a course grey sand (GGS). Yellowish sand obtained from Ankara was sieved through a 2 mm sieve to acquire yellow sand and then a 4.5mm sieve to obtain coarse yellow sand. Furthermore, the yellow sand was passed through a 0.8 mm sieve to get fine yellow sand. In addition to the sand, white sand, light graded siliceous river sand, and coarse siliceous river sand were used.

Table 2.4 Details of the physical properties of sand used adapted from (Pedergnana & Elias-Ozkan, 2021b)

Name	**Code**	**Color**	**Grain Shape**	**Washed**	**Max. Grain size** *(mm)*	**Loose Bulk density** *(kg/m2)*
Yellow sand	YS	Dark yellow	Angular	no	2.0	1440
Siliceous river sand	Si	Light yellow	Well Rounded	Yes	2.0	1520
Coarse Siliceous river sand	CSi	Light yellow	Well rounded	yes	2.0	1570

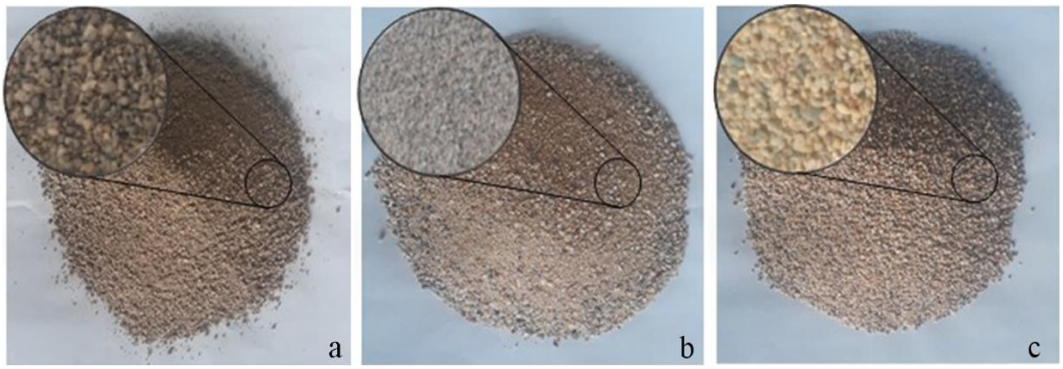

Figure 2.23 Sand used in the production of mud plaster samples adapted from (Pedergnana & Elias-Ozkan, 2022) (a: yellow sand, b: siliceous sand, c: coarse siliceous sand)

2.3.3 Plant fibers and cow dung

The fibers were obtained from agricultural by-products such as wheat threshing. The straw and Chaff were obtained from Sorgun, with the latter being used as reference material. The wheat straw was manually cut into small pieces from a thick part of the stalk; the length of the short straw ranged from 30 to 40 mm. Fresh cow dung, on the other hand, was used shortly after being collected on the farm where the animals were fed dry hay and straw. Finally, the Scott pine needles were obtained from the surrounding forests.

Figure 2.24 Chaff and straw used in stabilization of mud plaster samples adapted (Pedergnana & Elias-Ozkan, 2021b) (a: chaff, b: straw, c: pine needle)

Table 2.5 Plant and animals fibers used in stabilizing the mud samples adapted from (Pedergnana & Elias-Ozkan, 2021b)

Name	**Code**	**Max. Thickness** *(mm)*	**Fibre length** *(mm)*
Short Straw	SS	5	30 - 40
Pine needles	PN	2	10 - 40
Short wool	SSW	1	10 - 40

CHAPTER 3

MATERIALS AND METHODS

This chapter describes an experiment for measuring the thermal conductivity of mud plaster samples using a simplified experimental setup based on an equation from Fourier's law of heat transfer. The equation was modified to account for the parameters that could be measured under the existing laboratory conditions.

3.1 Materials

As previously stated, the mud plaster samples used in the experiments were prepared by Matthieu Pedergnana for his doctoral research. There was a total of 208 samples with different mixes but only 18 samples with appropriate mixes suitable for African architecture were selected. These samples were divided into three groups: fiber-stabilized samples, fibers and sand-stabilized samples, and cow dung-stabilized samples. The values of thermal conductivity obtained from this study were compared with those obtained from literature review.

3.1.1 Samples

Tables 3.1, 3.2, and 3.3 show the sizes, additives, percentage content by volume and weight, and densities of the mud samples used in this experiment. The samples were divided into three categories depending on their composition; Table 3.1 shows specimens stabilized with fibers. In Tables 3.2 and 3.3, samples were stabilized with sand and fiber, and cow dung, respectively. The sizes of the samples ranged from 8.0 x 8.0 x 3.5 cm^3 for small samples to 20.7 x 17.0 x 4.0 cm^3 for large samples. Samples were stabilized with short straw alone or a combination of straw, river sand, siliceous

sand and cow dung. The densities of the sample vary from 1,310 kg/m^3 to 2,200 kg/m^3.

Figures 3.1, 3.2, and 3.3 depict the classification of mixes of mud plaster samples. The samples that were only reinforced with short straw were coded as shown in Figure 3.1; the letter K stands for Kerkenes earth and the letter S stands for the short straw that was used to reinforce the mud plaster samples. The XX represents the percentage by volume of straw. Sample no.7, 6, 19, 139 and 134 were denoted as KS05, KS10, KS20, KS30, and KS40 respectively. Sample no.124 containing river sand, siliceous sand and short straw was assigned the code KRSiSXXXX, where K, R, Si, and S stand for Kerkenes earth, river sand, siliceous sand, and straw, respectively. The XX XX shows the volumetric percentages of siliceous sand and straw, respectively.

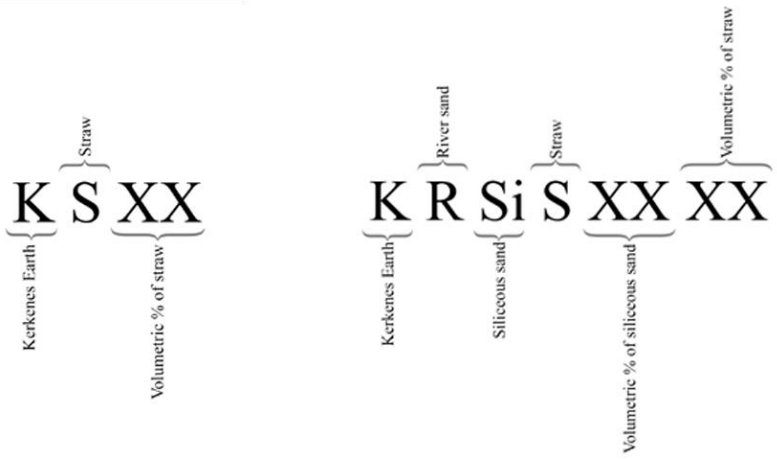

Figure 3.1 Mud plaster mix code for samples stabilized with straw (left), plaster mix code of samples stabilized with river sand, siliceous sand and fiber (right)

Figure 3.2 displays the mix code for mud plaster samples stabilized with river sand and straw, as well as the code for samples strengthened with straw and cow dung. K, R, S, and XX represent Kerkenes earth, river sand, short straw, and the volumetric percentage of straw, respectively, for the first code (on the left). Sample no.174, 121,166 and 122 were coded in this manner; sample no.174 of mix KRS00 was

utilized as a control sample since it had no straw; sample no.121 of mix KRS25 contained 25% by volume of straw; sample no.166 of mix KRS33 contained 33% by volume of straw; and sample no.122 of mix KRS40 contained 40% straw by volume. On the other hand, in the second code, K, S, C, and XX XX represent Kerkenes earth, short straw, cow dung, and the volumetric percentage of straw and cow dung, respectively. This was only applied to sample 44 (KSC2010), which was stabilized with 20% and 10% straw and cow dung by volume, respectively.

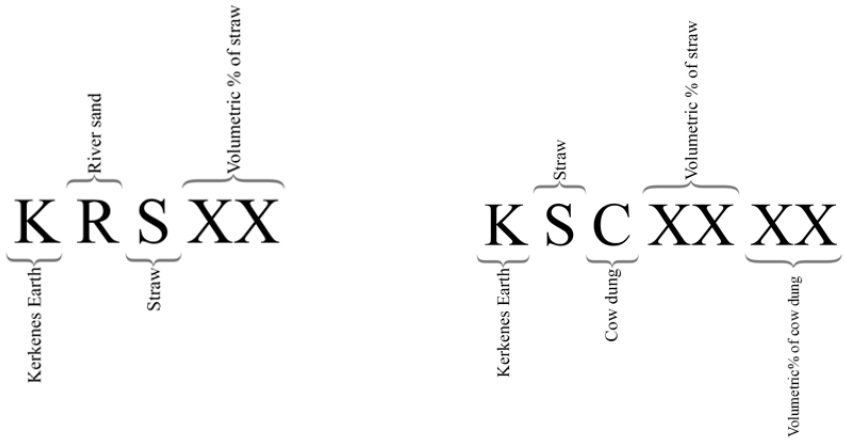

Figure 3.2 Samples stabilized with sand and fibers (left), Samples stabilized with Straw and cow dung (right)

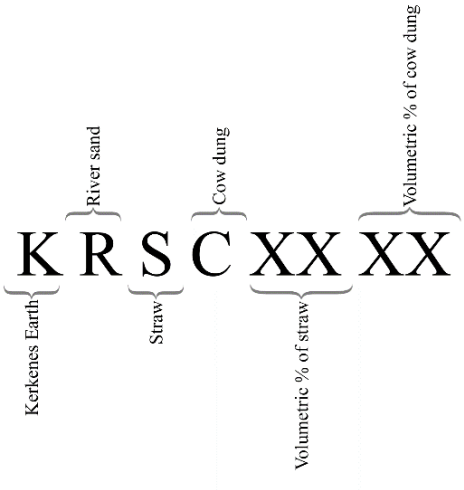

Figure 3.3 Mud plaster samples stabilized with river sand, straw and cow dung

Figure 3.3 shows the mix code utilized for samples stabilized with river sand, straw, and cow dung. The letters K, R, S, C, and XX XX stand for Kerkenes earth, river sand, short straw, cow dung and volumetric percentage of short straw and cow dung, respectively. This was done for four samples: no.47 of mix KRSC1511, which contained 15% straw and 11% cow dung by volume; no.198 of mix KRSC2015, which contained 20% straw and 15% cow dung by volume; no.17 of mix KRSC2010, which contained 20% straw and 10% cow dung by volume; and sample no.18 of mix KRSC2020, which contained 20% straw and cow dung by volume.

Table 3.1 and Figure 3.4 shows the samples stabilized with straw. The sizes range from 21.5 x 16.5 x 3.5 cm^3 for the biggest sample to 8.0 x 8.0 x 3.5 cm^3 for the smallest sample. The area of the earth samples significantly affected the thermal conductivity values obtained using the simple experimental setup. On the other hand, the densities varied from 971.2 kgm^{-3} to 2028.4 kgm^{-3}. Sample no.139 of mix KS30 had the lowest density but the second highest short straw incorporation percentage by volume and weight. Sample no.7 of mix KS05 had the highest density, with 5 and 0.3% by volume and weight of straw, respectively. It is also important to note the thickness of the samples because it affected their thermal conductivity values; thus, the thickness of the samples ranged from 3.8 cm for sample no.7 to 3.5 cm for sample no.19, 139, and 134.

Table 3.1 Mud plaster samples stabilized with straw

Sample Number	**Mix Code**	**Size** *(cm^3)*	**Amount of earth** *(% weight)*	**Amount of earth** *(% volume)*	**Amount of straw** *(% Volume)*	**Amount of straw** *(% weight)*	**Density** *(kg/m3)*
7	KS05	17.0 x 14.5 x 3.8	99	95	5	0.3	2028.40
6	KS10	16.5 x 16.0 x 3.7	99	90	10	0.6	1760.85
19	KS20	21.5 x 16.5 x 3.5	98	80	20	1.7	1634.95
139	KS30	8.0 x 8.0 x 3.5	98	70	30	2.2	971.21
134	KS40	8.4 x 8.3 x 3.5	96	60	40	3.8	1383.69

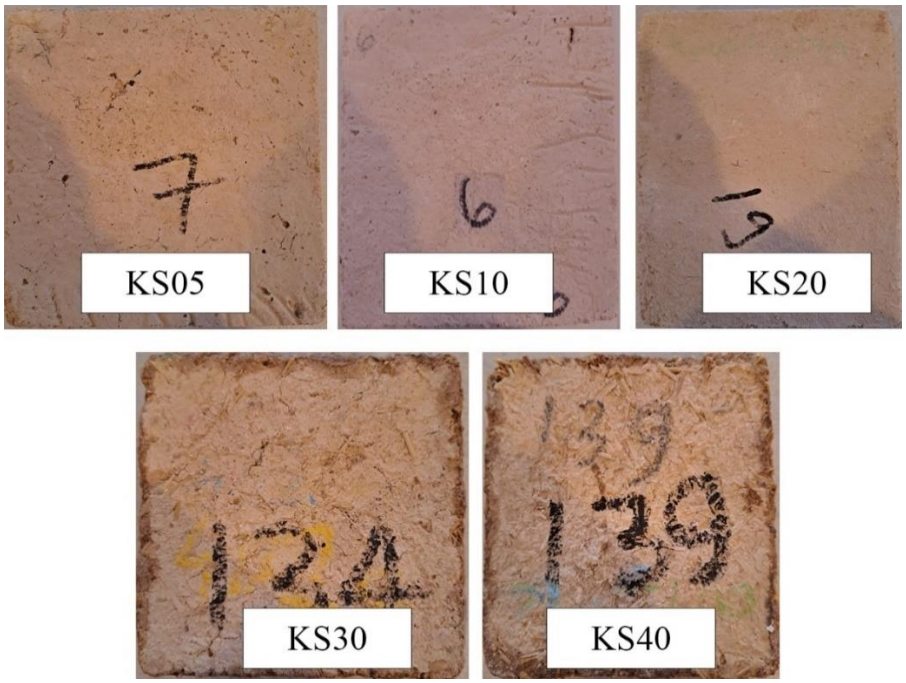

Figure 3.4 Samples stabilized with short straw; sample no. 7 of mix KS05 with 5% straw (upper left), sample no. 6 of mix KS10 with 10% straw (middle), sample no.19 of mix KS20 with 20% straw (upper right), sample no.134 of mix KS30 with 30% straw (lower left) and sample no. 139 of mix KS40 with 40% straw by volume (lower right)

Table 3.2 and Figure 3.5 show samples stabilized by fiber and sand. Sample no. 174 of mix KRS00, which consisted of 25% Kerkenes earth and 75% River sand by volume, was used as a reference since it has 0% short straw. The samples in this category were stabilized with straw, river sand (RS), and a graded commercial silicate sand (Si) with yellow grains that measured a maximum of 2 mm in diameter. Sample no. 124 of mix KRSiS4020 contains 40% Kerkenes white earth, 40% River sand, 40% Siliceous sand, and 20% short straw by volume. The latter sample is distinctly different in that it contains an additional Silicate sand aggregate compared to the other specimens in the category. On the other hand, samples no. 121, 166 and 122 contain 25, 33 and 40% short straw by volume respectively. As shown in Table 3.2, these samples contained varying percentages of earth and river sand by volume and weight.

Table 3.2 Mud samples containing different sand types and fibers

Sample number	Mix code	Size (cm)	Amount of earth (% weight)	Amount of earth (% volume)	Amount of River sand (% weight)	Amount of River sand (% Volume)	Amount of Silicate sand (% weight)	Amount of Silicate sand (% Volume)	Amount of straw (% weight)	Amount of straw (% volume)	Density (kg/m3)
174	KRS00	17.2 x 16.4 x 4.0	20	25	80	75			0	0	1748.2
124	KRSiS4020	20.4 x 16.5 x 4.0	40	40	59	40	59	40	1.1	20	1637.1
121	KRS25	20.5 x 17.0 x 4.0	58	50	41	25			1.4	25	1312.8
166	KRS33	19.9 x 16.0 x 3.8	41	33	56	33			2.4	33	1604.6
122	KRS40	20.5 x 17.0 x 3.8	41	30	56	30			3.1	40	1556.7

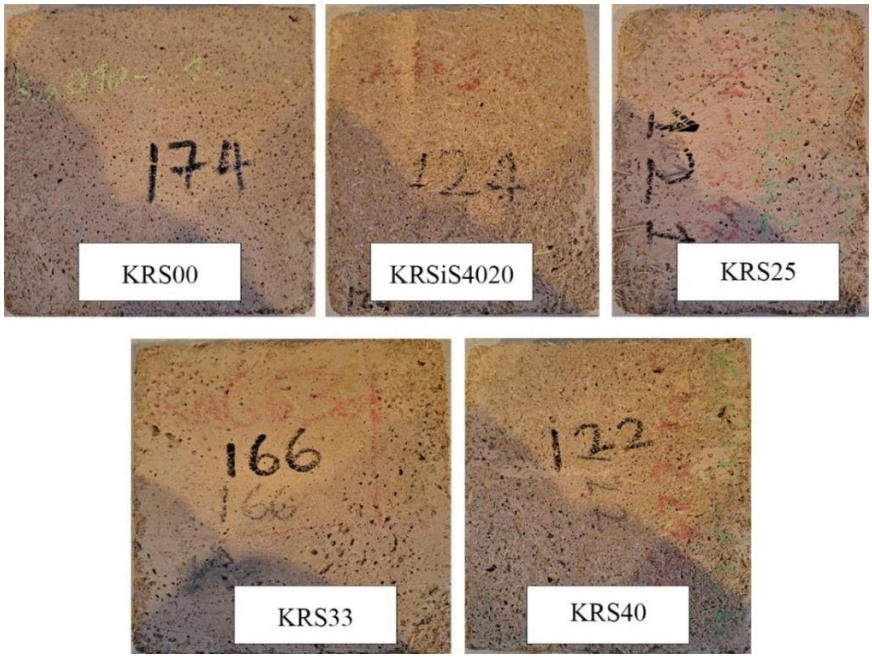

Figure 3.5 Samples stabilized with river sand, siliceous sand and straw; sample no. 174 of mix KRS00 reference sample (upper left), no. 124 of KRSiS4020 with 40% siliceous sand and 20% straw (middle), 121 of KRS25 with 25% straw, no. 166 of KRS33 with 33% straw (lower left) and no. 122 of KRS40 with 40% straw by volume (lower right)

Table 3.3 shows five samples containing cow dung as the main additive in addition to short straws and river sand. Some specimens, however, only have cow dung and short straw. This was the case with sample no. 44 of mix KSC2010, which consists of 80% Kerkenes white earth by volume, 20% straw by volume, and 10% cow dung by volume.

The sample size varies considerably; the biggest specimen, sample no. 18 of mix KRSC2020, has a volume of 20.0 x 16.2 x 3.8 cm^3 with a density of 1396.0 kgm^{-3}, while the smallest one, no. 44 of mix KSC2010, has a volume of 11.0 x 9.8 x 3.6 cm^3 with 1443.0 kgm^{-3}. Furthermore, the samples have a thickness ranging from 3.6 cm for sample no. 44 to 4.0 cm for sample no. 47 of mix KRSC1511 and 17 of mix KRSC2010.

Table 3.3 Mud plaster samples containing Cow dung

Sample number	**Mix code**	**Size (cm)**	**Amount of earth** (% weight)	**Amount of earth** (% volume)	**Amount of River sand** (% weight)	**Amount of River sand** (% Volume)	**Amount of Straw** (% weight)	**Amount of Straw** (% Volume)	**Amount of cow dung** (% weight)	**Amount of cow dung** (% volume)	**Density** (kg/m3)
47	KRSC1511	12.0 x 11.0 x 4.0	45	44	54	44	0.7	15	6	11	1571.9
198	KRSC2015	12.6 x 12.0 x 3.6	45	40	54	40	0.9	20	6	15	1471.6
17	KRSC2010	15.5 x 15.5 x 4.0	45	40	54	40	1.6	20	6	10	1488.0
44	KSC2010	11.0 x 9.8 x 3.6	98	80			1.6	20	8	10	1443.0
18	KRSC2020	20.0 x 16.2 x 3.8	45	40	54	40	0.9	20	11	20	1396.0

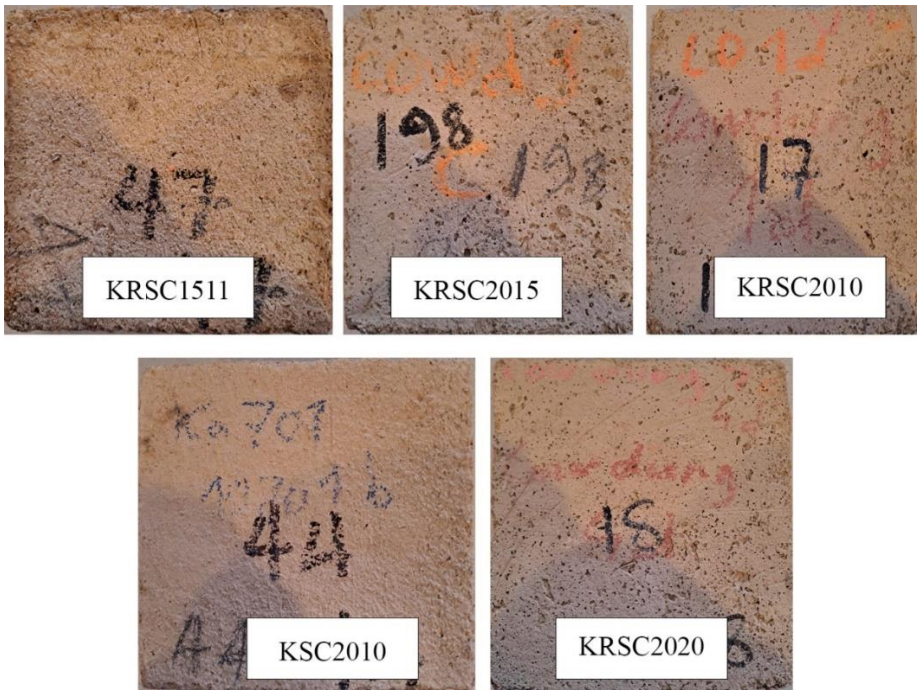

Figure 3.6 Samples stabilized with cow dung; sample no. 47 of mix KRSC1511 with 15% straw and 11% cow dung (upper left), sample no. 198 of mix KRSC2015 with 20% straw and 15% cow dung (middle), sample no. 17 of mix KRSC2010 with 20% straw and 10% cow dung (upper right), sample no. 44 of mix KSC2010 with 20% straw and 10% cow dung (lower left) and sample no. 18 of mix KRSC2020 with 20% straw and 20% cow dung by volume.

Sample no. 27 of mix KRPn20 stabilized with 20% pine needle, 50% Kerkenes earth and 50% river sand by volume, no. 162 of mix KRS40 stabilized with 40% short straw, 40% Kerkenes earth and 40% river sand by volume and no. 194 of mix KRSw20 reinforced with 20% short sheep wool, 50% Kerkenes white earth and 50% river sand by volume are shown in Table 3.4 and Figure 3.7. Sample no. 194 of mix KRSw20 is the smallest of the three specimens, but it has the highest density. Sample no. 27 of KRPn20, on the other hand, is the larger of the three specimens, with the lowest density of 1533.6 kgm^{-3}. It is imperative to note that although these specimens are not included within the three categories, they are used to compare the results obtained using the simplified method utilized in this study and the KEM QTM 500

hotwire method used by Pedergnana & Elias-Ozkan (2021a) and also to determine the effect of relative humidity and ambient temperature on thermal conductivity.

Table 3.4 Samples stabilized with river sand and pine needles, straw or sheep wool, respectively; for comparison with results reported in Pedergnana and Elias-Ozkan (2021)

Sample No.	Mix code	Size (cm)	Amount of Earth		Amount of River sand		Amount of fibers		ρ kg/m^3
			% weight	% volume	% weight	% volume	% weight	% volume	
27	KRPn20	21.0 x 17.0 x 4.0	50	50	54	50	2.0% pine needle	20% pine needle	1533.6
162	KRS40	20.5 x 17.0 x 3.8	45	40	53	40	1.1% straw	40% straw	1751.0
194	KRSw20	11.6 x 11.5 x 4.0	45	50	55	50	0.2% sheep wool	20% sheep wool	1657.2

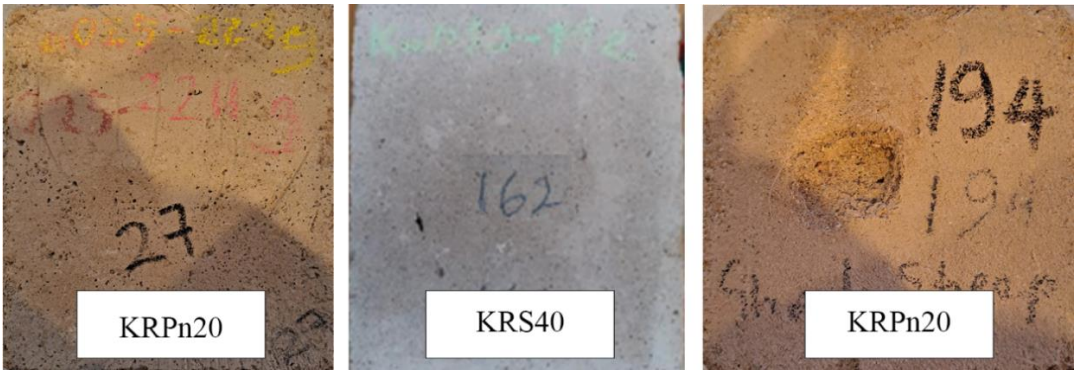

Figure 3.7 river sand and Pine needles, Straw or Sheep wool, respectively; sample no.27 of mix KRPn20 stabilized with 20% pine needle by volume (right), sample no.162 of mix KRS40 stabilized by 40% short straw by volume (middle) and sample no.194 of mix KRSw20 stabilized with 20% short sheep wool by volume (left).

3.1.2 Materials used for the experimental setup

This study measures the thermal conductivity of earthen samples using a steady-state customized experimental setup consisting of a power meter, a 500 W and 250 W Van der Heyden laboratory stove, Extruded Polystyrene Foamboard (XPS), and thermocouple surface sensors. Power meter UT230B with Voltage range AC 100V-

260V, maximum current capacity of 16 A, and +/- 1% accuracy is used to measure the power used by the hot plate, which serves as a heat source. Thermocouples with a temperature range of -40ºF to 212ºF are used to measure the temperature on the different surfaces of the samples. The thermocouples are connected to two *HOBO* data loggers with temperature- relative humidity external channels.

This method is an adaptation of thermal conductivity measurement using the steady-state, so an average time of one hour is allowed for the heat transfer to reach equilibrium. The power meter measures the energy used in the experiment in Kilowatt-hours (KWh), and the total time required for the sample's top surface to reach its maximum temperature (peak temperature) is recorded. The approximate energy passing through the specimen is calculated by converting the energy to watts and dividing by 2. The reason behind division by two will be further explained in the calibration process. The temperature difference between the top and the bottom sample surfaces can be determined from the information collected by the data logger. Then the thermal conductivity is calculated using the equation $k=Qd/(A*dt*dT)$.

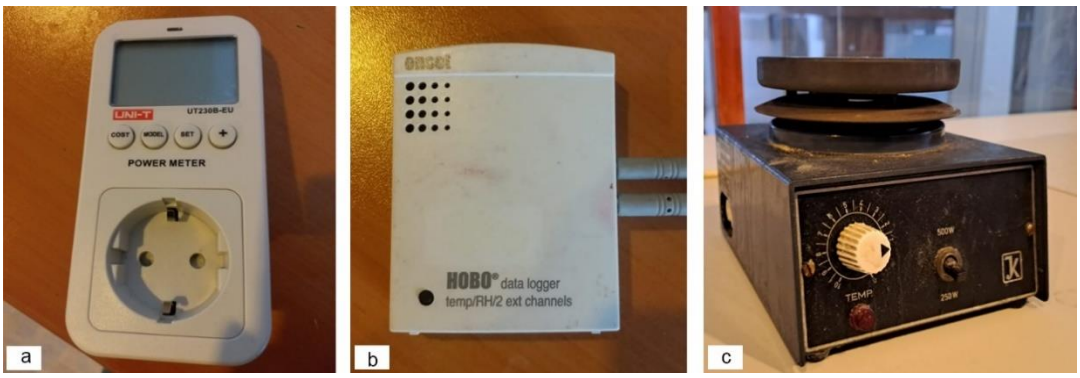

Figure 3.8 Materials used for experimental setup; a: power meter, b: HOBO data logger with temperature- relative humidity external channels and c: 500 W and 250 W Van der Heyden laboratory stove.

3.2 Methodology

As earlier stated, the methodology used in this research is based on the equation from Fourier's law of of heat transfer

$$q" = -k\frac{dT}{dX} \quad \textbf{(3.1)}$$

where;

k is the thermal conductivity in W/mK

q" is the heat flux

k is the thermal conductivity,

dT is the temperature change and

dX is the heat transfer distance.

The equation above is adapted to form the equation

$$k = \frac{Qd}{A * dt * dT} \quad \textbf{(3.2)}$$

where;

k is the thermal conductivity in W/mK

Q is the energy in Watts/hour (Wh)

d is the thickness of the earth sample in metres (m)

A is the area of the sample in m^2

dt is the time taken to reach equilibrium (hours)

dT is the temperature difference in Celsius (°C)

This customized thermal conductivity measurement method employs the same principles as the other steady-state methods, including the absolute technique and the guarded hot plate instrument. The heat is transferred unidirectionally in the system by conduction. The methods involve measuring the temperature difference ΔT and the surface area of the sample. The thermal conductivity is then determined using Equation 3.2. An error in ΔT of less than *1%* is acceptable in the absolute technique. However, since the study employed a simplified methodology to measure thermal conductivity, a considerable error margin is expected in this study. Moreover, the experiments were carried out in the laboratory, whose internal temperature was affected by the climatic conditions of the seasons; in summer, the ambient temperature was as high as 31.0ºC, and as low as 15.8ºC in fall. This in turn affected the thermal conductivity values. Further details on the effects of ambient temperature on thermal conductivity will be discussed later.

In order to use the measured data on Q (kWh) for the thermal conductivity measurements, it was divided by 2 to account for the heat travelling upwards through the sample and then going downwards. Hence if measured Q was 0.003 kwh, then the amount of energy used to heat the sample was Q/2= 1.5wh.

3.2.1 Experimental setup

The experimental setup consists of six layers of XPS; the first three layers are 34cm x 45cm x 3cm with a rectangular hole measuring 19.5cm x 26cm x 3cm to accommodate the laboratory stove (Figure 3.9). XPS was used in this experiment because it is a good heat insulator; it reduces the heat loss to the environment. The thermocouple T3 is placed through the hole on the third layer to measure the temperature under the circular hot plate (Figure 3.9). The fourth layer, with the same dimension as the other three layers, is placed right on top. This layer has a circle whose diameter is 18.5cm in which the circular hot plate is fitted. A 3cm thick ring made of glasswool and covered with baking paper is placed around the hot plate to prevent XPS from burning (Figure 3.10). The second thermocouple T2 is placed on

the hot plate to measure the variation in temperature as the experiment is being carried out. The specimen whose thermal conductivity is to be measured is located precisely in the middle of the hot plate. The thermocouple provides a point of contact between the hot plate and the sample. The fifth layer, with the varying dimensions has a rectangular hole slightly bigger than the sample; the layer is fitted in place so that it completely surrounds the specimen. This layer acts as a barrier to prevent heat loss from the sides. However, since the layer is only 3cm thick, the sixth layer with a rectangular hole of the same dimension is required to close off the sides of the sample completely. The third final thermocouple T1 is placed on top of the specimen (Figure 3.9).

Figure 3.11 depicts the complete experimental setup. The three thermocouples are connected to two data loggers, which are then connected to the computer via two USB cables. At the same time, the laboratory stove is plugged into a power meter which has been configured to measure the energy used to heat the hot plate in kilowatts per hour (kWh).

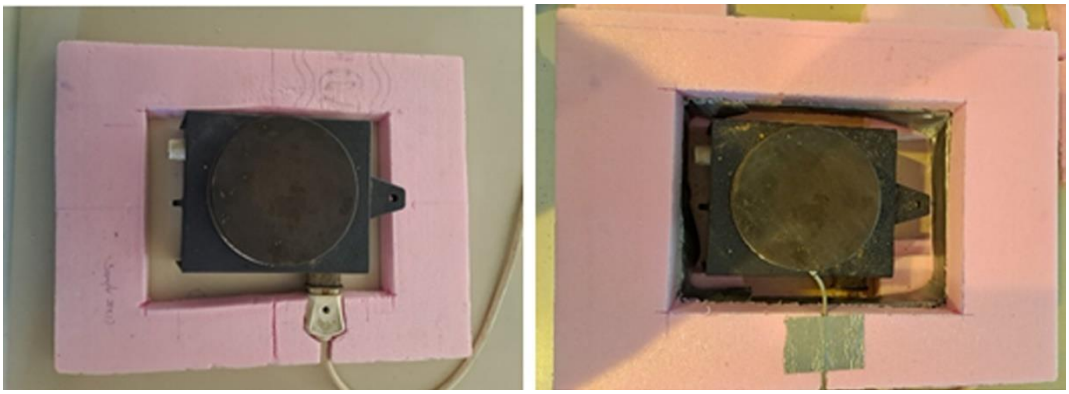

Figure 3.9 First layer with laboratory stove (left), a thermocouple placed under the hot plate

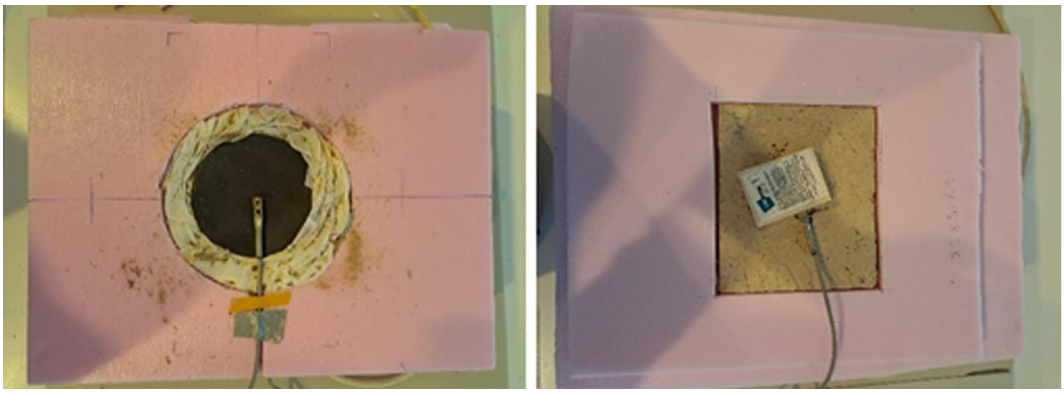

Figure 3.10 A ring of glass wool is placed between the hot plate and the fourth layer (left), a thermocouple placed on top of the earth sample

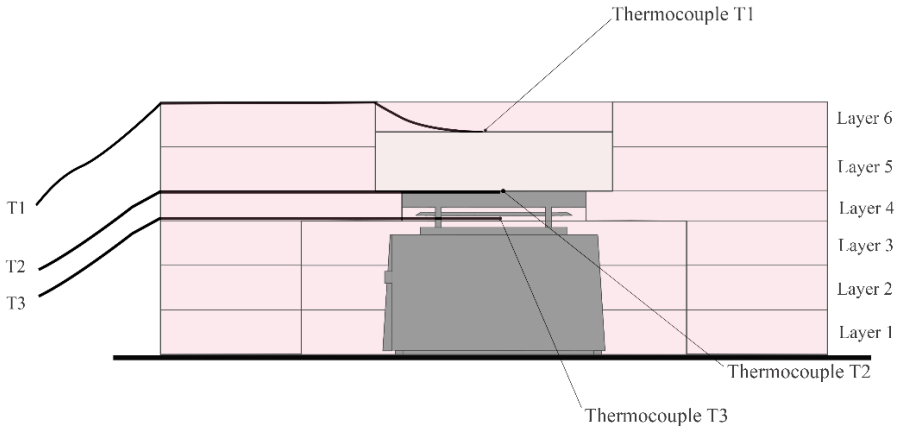

Figure 3.11 Illustration showing the section of experimental setup

3.2.2 Experimental procedure and calibration

The thermal conductivity results obtained by Pedergnana & Elias-Ozkan (2021a) were used to calibrate the experimental design since the samples used in this experiment were prepared, and some were tested in their study. The authors used the KEM QTM500 hot wire method to measure the thermal conductivity of samples measuring 10x10x4cm^3 with flat surfaces under 25ºC and 50% relative humidity (RH) laboratory conditions. The measurements on each sample were carried out

three times and the average thermal conductivity value was considered to prevent errors due to surface differences.

The calibration of setup used in this study was conducted when the ambient temperature was 15ºC, and the relative humidity (RH) was 42.8%. The total duration of the experiment was one hour (60 minutes). A steady-state is reached when there is no change in temperature or when thermal equilibrium is attained. The steady-state in this experiment was determined by analyzing the temperature of the two surfaces recorded by the data logger over an hour. Unlike in Pedergnana's study, most of the thermal conductivity measurements in this study were only performed once due to the length of the experiments. However, some experiments had to be repeated owing to procedural experimental errors.

Figure 3.12 shows the temperature variation between the top surface T_1 and the bottom surface T_2 of mud sample no. 124 of mix KRSiS4020. The specimen contains 40% Kerkenes white earth by volume, 40% river sand, 40% silicate sand, and 20% short straw. T_1 is the temperature of the unheated surface (the surface on top), while T_2 is the temperature of the area directly in contact with the heat source. A *500 W* and *250 W* Van der Heyden laboratory stove with adjustable temperature and power setting was used to heat the sample. Two different configurations were experimented with to determine the most appropriate setup. The first one involved heating the specimen faster, reaching the preset 40ºC mark in less than 2 minutes. The temperature dial was set to its maximum while the power dial was maintained at 250 watts. This arrangement produced a thermal conductivity value inconsistent with the one obtained by Pedergnana & Elias-Ozkan (2021). The second alternative consisted of gradually heating the bottom surface area of the specimen for an average period of three minutes. To achieve the desired configuration, the temperature dial was set to its lowest setting (one) and the power dial was set to 250 watts. A thermal conductivity value close to that declared by the authors was obtained. Thus, the second option was chosen.

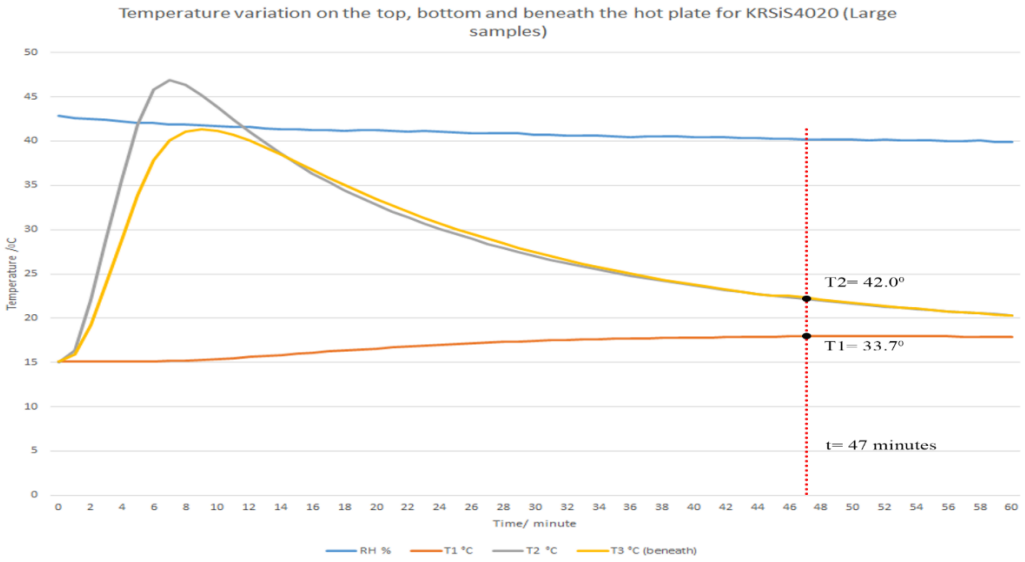

Figure 3.12 Temperature variation between the top and bottom surfaces of sample no. 124 of mix KRSiS4020 (Example of large samples)

The stove was connected to the power meter and plugged into an outlet. Temperature T_2 was left to increase gradually to 40ºC, at which point the power supply to the stove was cut off, which caused the bottom temperature T_2 to increase slightly and then decrease exponentially while the top surface temperature T_1 increased steadily. The energy needed to heat the hot plate and the heating time were noted. A steady state was attained when T_1 reached a peak temperature of 18.0ºC beyond which the temperature gradually reduced. The experiment was allowed to run for the remaining time, and the final results were tabulated into an Excel file with the equation $k=Qd/(A*dt*dT)$ preset as seen in Table 3.5. A temperature-time graph was also plotted to determine the bottom surface temperature T_2 attained when the top surface reached the peak temperature T_1= 18.0ºC. It can be seen from the graph in Figure 3.12 that bottom temperature T_2 was 22.0ºC. The temperature difference at that point was calculated by subtracting T_1 from T_2 $(\Delta T=T_2-T_1)$.

Table 3.5 Calculation of thermal conductivity of sample no. 124 of mix KRSiS4020 (large samples)

Sample number	**Measured data**						**Derived data**		
124	Size *(cm^2)*	Energy q_{total} *(wh)*	Energy q_{top} *(wh)*	Thickness *(m)*	dT *(ºC)*	dt *(hrs)*	Area sample *(m^2)*	Area hot plate *(m^2)*	λ *(W/mK)*
	20.4x16.5x 4.0	3.0	1.5	0.04	4.0	0.80	0.034	0.012	**0.56**

The final thermocouple was placed at the bottom of the hot plate to show the variation in temperature as the experiment proceeded. Figure 3.12 (yellow curve/T3) depicts the temperature changes over the course of 60 minutes. The temperature increased gradually for an average time of 3 minutes to a maximum temperature of T_3=41.3ºC compared to T_2= 46.9ºC attained by the second thermocouple at ambient temperature of 15.3 to 16.4ºC. This finding revealed that almost the same energy was heating the hot plate's top and bottom surfaces. Moreover, the two peak temperatures were approximately the same in some experiments. Thus, the same energy was required to heat both sides of the hot plate. The power meter measures the total energy used in heating both surfaces, thus the energy recorded by the power meter is divided by two to get the amount of energy required to heat the hot plate's top surface area $q_{top}=q_{total}/2$. For samples with a surface area less than the area of the hot plate (8.5 x 8.0 cm^2 specimens), the energy q_{top} is further multiplied by the ratio of the specimen area: hot plate area $q_{small}= (A_{sample}/A_{hot\ plate}) * q_{top}$. The obtained value is the energy in watts per hour required to heat the small sample. Table 3.6 illustrates an Excel file calculation of the thermal conductivity of sample no. 134 of mix KS40 stabilized with 40% straw by volume (small samples), while Figure 3.13 illustrates the temperature curve for the same sample. The hot plate has an area of 0.0122 m^2, about twice the small specimen's area. Hence more than half of the energy is required to heat the sample (energy q_{small} = 0.85 watts). The thermal equilibrium state is reached after 54 minutes when the bottom temperature T_1=27.4ºC and top

temperature T_2=21.5ºC. The temperature difference is calculated as 5.9ºC. A thermal conductivity value of 0.46 W/mK is obtained.

Table 3.6 Calculating thermal conductivity of samples smaller than hot plate

Sample number	**Measured data**							**Derived data**		
134	Size *(cm^2)*	Energy q_{total} *(wh)*	Energy q_{top} *(wh)*	Energy q_{small} *(wh)*	Thickness *(m)*	dT *(ºC)*	dt *(hrs)*	Area sample *(m^2)*	Area hot plate *(m^2)*	λ *(W/mK)*
	8.4x8.4 x3.4	3.0	1.5	0.85	0.034	5.9	0.9	0.007	0.012	**0.46**

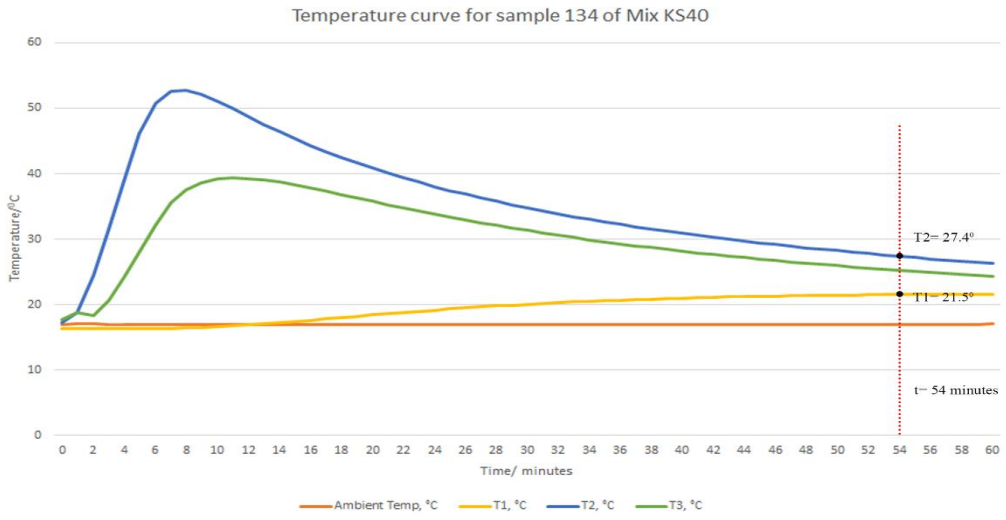

Figure 3.13 Temperature variation between the top, bottom and beneath the hot plate for sample no. 134 of mix KS40 (small samples)

CHAPTER 4

RESULTS AND DISCUSSION

This part of the study focused on the results obtained from the simplified experimental setup. As earlier mentioned in Chapter 3, the samples used in the research were divided into three categories; fibers, sand and fiber, and cow dung. The thermal conductivity values were analyzed according to the specimen composition, and comparisons were made with data from the literature review. Moreover, factors that affected the thermal conductivity of the earth samples, such as density, type and length of the fibers, were also discussed.

4.1 Thermal conductivity values of earthen samples

Thermal conductivity ranged from 0.39 W/mK to 0.58 W/mK in samples stabilized solely with short straws and from 0.41 W/mK to 0.60 W/mK in specimens stabilized with straw, river sand, and siliceous sand. Finally, thermal conductivity values ranged from 0.43 W/mK to 1.19 W/mK for cow dung stabilized samples.

4.1.1 Effect of fiber incorporation on the thermal conductivity of mud samples

Table 4.1 and Figure 4.1 show the thermal conductivity values for specimens stabilized with short straws. The lowest value of 0.39 W/mK was obtained by sample no. 139 of mix KS30, which contained 2.2% short straw incorporation by weight. On the other hand, sample no. 7 of mix KS05 with 0.3% by weight short straw produced the highest thermal conductivity of 0.58 W/mK. Generally, the values decreased as the percentage content of short straw increased; since straw has a low density and a low thermal conductivity, an increase in fiber content leads to a

decrease in the specimens' density. The same trend was observed in the literature, Calatan et al.,(2016) studied the use of hemp fibers and straw in the stabilization of adobe bricks. The authors utilized 3-15% by volume hemp fiber and 10- 60% by volume straw contents. The thermal conductivity of the samples decreased with the incorporation of straw.

Table 4.1 Samples stabilized with short straw fibers

Sample number	**Mix code**	**Additives**		**Density** *(kg/m^3)*	**Thermal conductivity** *(W/m^{2}K)*
		% Weight straw	% Volume straw		
7	KS05	0.3	5	2028.4	0.58
6	KS10	0.6	10	1760.9	0.57
19	KS20	1.7	20	1635.0	0.47
139	KS30	2.2	30	971.2	0.39
134	KS40	3.8	40	1383.7	0.46

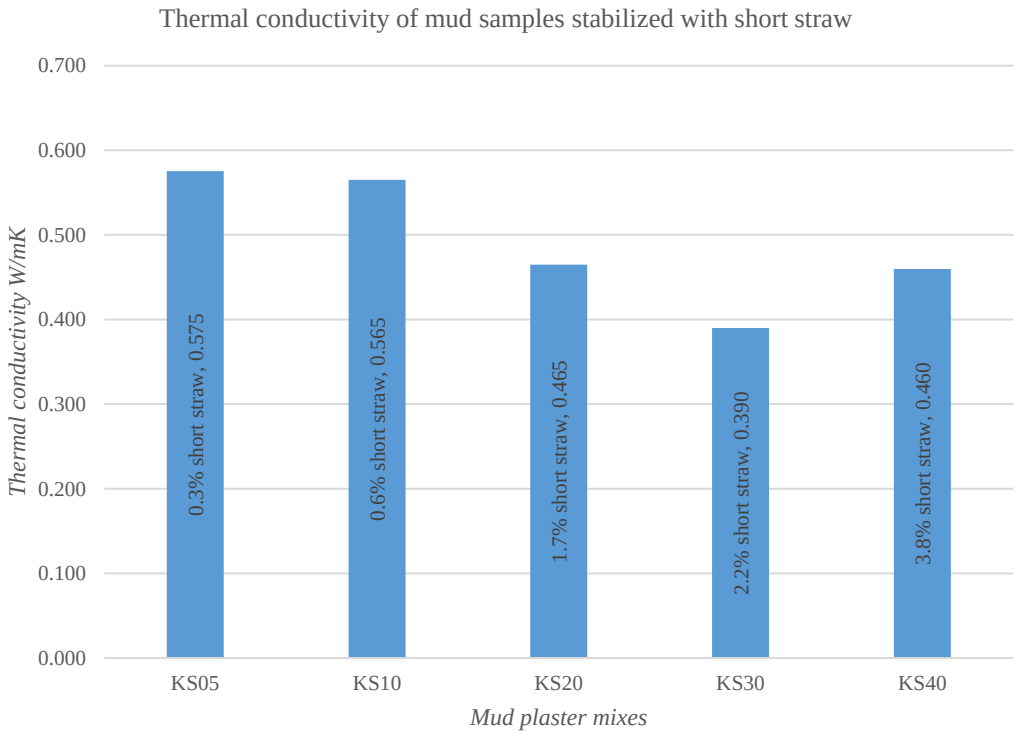

Figure 4.1 Thermal conductivity of earthen samples stabilized with fibers

Kossi et al. (2016) added nere pods in adobe bricks at different content percentages. The thermal conductivity of the specimens decreased as the plant content increased. Ouedraogo et al. (2019) noted a 67% decrease in the thermal conductivity for 1% straw content by weight. The presence of fonio straw led to an increase in closed porosity, thereby decreasing the thermal conductivity. Minguela (2017) noted a clear correlation between thermal conductivity and density; as the density increased, thermal conductivity also increased. Hemp fibers have a low bulk density; consequently, as the hemp content increased, the specimen reduced in density. However, Suarez-Dominguez, (2017) reported an increase in thermal conductivity in the samples stabilized with ixtle fiber. The sample without the fiber showed a lower thermal conductivity and a higher heat capacity.

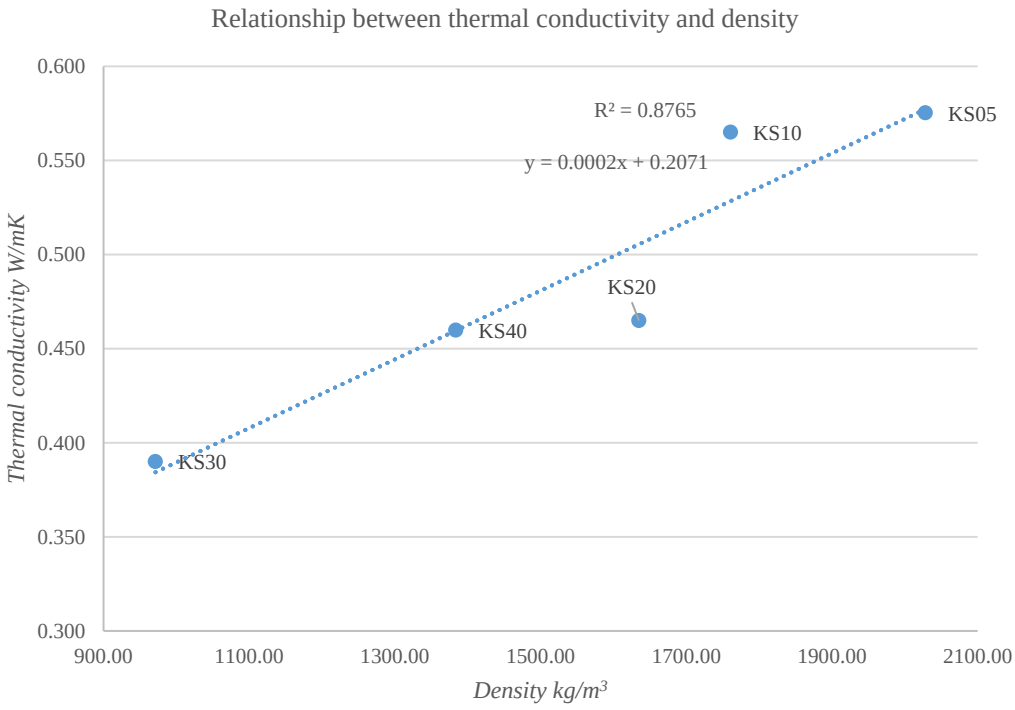

Figure 4.2 Relationship between thermal conductivity and density for samples stabilized with straw

However, not all of the samples in this study followed the same pattern; Figures 4.1 and 4.2 illustrate the thermal conductivity values of samples stabilized with short straw; in general, the thermal conductivity decreases as density and percentage of short straw increases. On the other hand, the value decreases and rises for samples no. 139 and no. 134 of mixtures KS30 and KS40, respectively. This behavior may be attributed to experimental error and difference in physical parameter such as thickness. Furthermore, factors such as the ambient temperature should be considered. Figure 4.3 shows the effect of ambient temperature on the thermal conductivity of sample no. 134, composed of KS40 mix, which was stabilized with 3.8% short straw by weight. Two experiments were carried out on the same sample in different seasons, allowing the hot plate to reach a predetermined temperature of 70º. The first experiment was performed in summer when the relative humidity was 35.36% and the ambient temperature was 30.9ºC. The bottom temperature 134B2 (recorded by thermocouple T3 in summer) increased steadily up to a peak temperature of 90º C and exponentially decreased when the energy supply to the laboratory stove was cut. The difference between the bottom temperature 134B2 and the top temperature 134T2 (recorded by thermocouple T2 in summer) was reported as Δ_2=10.9ºC.

The second experiment was carried out in autumn when the relative humidity was 43.21%, and the ambient temperature was 16.7ºC. In the second experiment, the bottom temperature 134B1 (recorded by thermocouple T3 in autumn) gradually increased to a maximum temperature of 74.8ºC and decreased sharply when the hot plate was disconnected. The difference between the top and bottom temperatures was noted as Δ_1=9.7ºC. The irregularity in the temperatures significantly affected the thermal conductivity values; 0.65 W/mK was obtained during the experiment in autumn, and a value of 0.85 W/mK was noted for the one in summer. A higher thermal conductivity was observed when the relative humidity was low and the temperature was high.

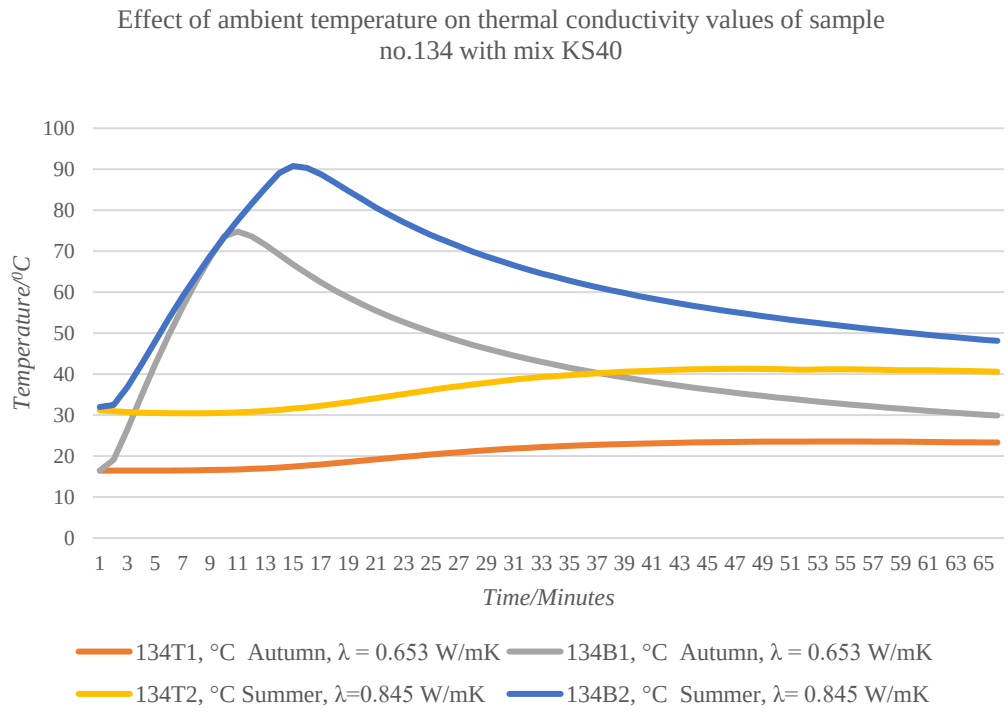

Figure 4.3 Effect of ambient temperature on the thermal conductivity of sample no.134 at relative humidity 43.2 and 35.4% for summer and fall experiments respectively.

Table 4.2 Effect of ambient temperature and relative humidity on thermal conductivity

Sample number	**Mix code**	**dT** *(⁰C)*	**Ambient temp** *(⁰C)*	**RH** *(%)*	**λ***(W/mK)*
122	KRS40	10.043	15.819	41.156	0.485
		6.529	28.518	40.731	0.742
134	KS40	9.742	16.77	43.21	0.653
		10.878	30.93	35.36	0.845

The same trend was noted in the experiments carried out on sample no. 122 with mix KRS40. According to the National Weather Service (2015), relative humidity is the measure of exact amount of moisture in the air to the total amount of moisture that it can hold at a specific time. Absolute humidity, on the other hand, measures the

exact amount of moisture in the air regardless of temperature. The relative humidity decreases with the increase in temperature if the system has a constant moisture content due to the fact that higher temperatures can hold more moisture (Singh, 2007). It is essential to note that relative humidity is not necessarily affected by changes in absolute temperature, but rather by the maximum amount of moisture the air can hold at that temperature. Nonetheless, high temperatures and humidity in the summer have a greater impact on thermal conductivity values than in the autumn. Moreover, since thermal conductivity is directly related to moisture content, an increase in one parameter causes an increment in the other. This observation is consistent with the one obtained in the literature. Araya-Letelier et al. (2021) studied the effect of incorporating jute fibers on adobe mixtures' physical and mechanical performance. The authors incorporated 0.5 and 2.0% by weight of jute fibers with varying lengths of 7, 15, and 30mm. The experiment showed a decrease in thermal conductivity as the moisture content decreased and the curing time increased. The same trend was observed by Ngaram, (2020) and Ekwue et al., (2006) when they studied the effect of moisture content on the thermal conductivity. Ekwue et al., (2006) attributed this behavior to the physical properties of water such as the thickness and the geometric formation of water layers in the soil matrix. Furthermore Singh et al. (2019) associated the behavior to the fact that water has a thermal conductivity of 0.6106 to 0.6372 W/mK which is higher than that of air (0.0272 W/mK) at 26.5ºC to 45ºC.

4.1.2 Effect of fiber and sand incorporation on the thermal conductivity of mud samples

Table 4.3 and Figure 4.4 show the thermal conductivity, and the densities of the samples stabilized with straw fibers and different sand aggregates. Sample no. 174 of mix KRS00 which contained 25% Kerkenes white earth and 75% river sand by volume, was used as a reference specimen since it was not stabilized with any fibers. The sample had a thermal conductivity value of 0.60 W/mK. The remaining samples

were stabilized with short straw. The effect of sand inclusion on thermal conductivity of mud samples is discussed in detail in subsequent subsections.

Table 4.3 Samples stabilized with sand and short straw fibers

Sample number	Mix code	Additives		Density *(kg/m³)*	λ *(W/mK)*
		% Weight	% Volume		
174	KRS00	0% straw	0% staw	1748.18	0.60
124	KRSiS4020	1.1 % straw 59% siliceous sand	20% straw 40% siliceous sand	1637.10	0.56
121	KRS25	1.4% straw	25% straw	1312.77	0.41
166	KRS33	2.4% straw	33% straw	1604.56	0.44
122	KRS40	3.1% straw	40% straw	1556.67	0.41

Sample no. 121 of mix KRS25, which was stabilized with 1.4% short straw by weight, and no. 122 of mix KRS40, which was reinforced with 3.1% short straw by weight, had the lowest thermal conductivity value of 0.41 W/mK, while sample no. 174 of mix KRS00 had the highest thermal conductivity value of 0.60 W/mK. Tables 4.3 and 4.5 revealed that, experimental samples had a lower thermal conductivity value than the control sample KRS00, which is consistent with the trends observed in the literature.

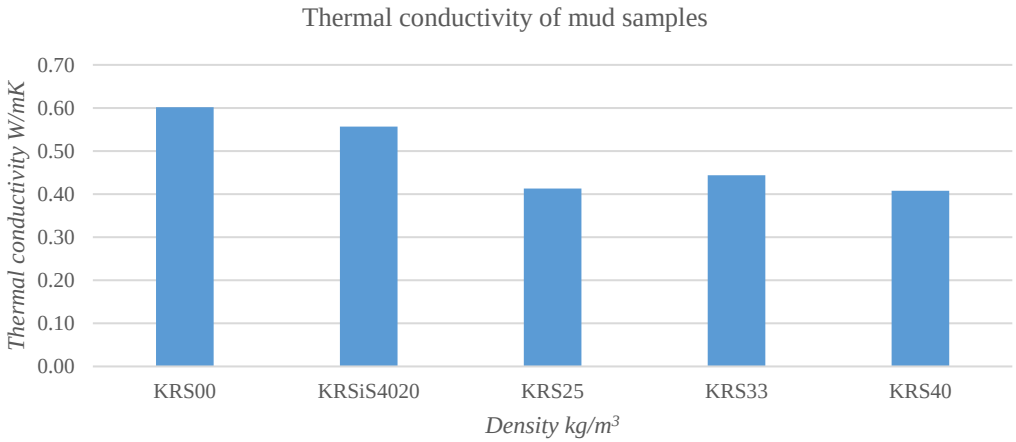

Figure 4.4 Thermal conductivity of samples stabilized by short straw fibers and sand

Figure 4.5 shows the relationship between the thermal conductivity and the density of samples stabilized with fibers and sand. Pearson correlation coefficient R=0.76, implying that the relationship between thermal conductivity values obtained and density is fairly strong but not perfect. Nonetheless, errors are expected owing to the simplified nature of the experimental setup and due to the fact that other factors, such as ambient temperature and relative humidity, are not kept constant. Furthermore, some of the samples used in this experiment may have been baked during the calibration process, as they were heated to temperatures greater than 90°C. Nonetheless, it can be deduced that thermal conductivity increases with an increment in density and decreases with a reduction in density.

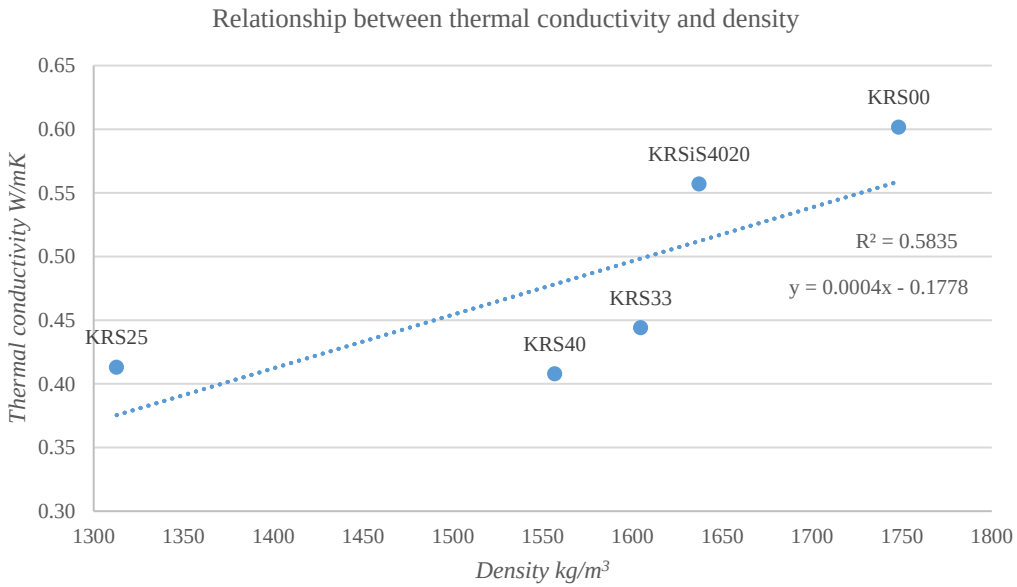

Figure 4.5 Relationship between thermal conductivity and density for samples stabilized with fiber and sand

As discussed earlier, the addition of fibers generally decreases the thermal conductivity of the samples due to their low bulk density. The incorporation of fibers leads to a decrease in the composition's density, directly affecting the thermal conductivity value. This trend is consistent with the work from other authors. Nasla

et al. (2021) compared the effect of pine needles and straw fibers on the mechanical and thermal properties and concluded that straw fibers were better at improving the thermal performance of mud samples than pine needles. Furthermore, the thermal conductivity decreased with addition of straw fibers and pine needle. Moreover, a thermal conductivity value of 0.667 W/mK was obtained by incorporating 2% by weight of straw, compared to 0.44 W/mK obtained by incorporating 2.4% by weight, as noted in this study. At the same time, Pedergnana & Elias-Ozkan (2021) obtained a value of 0.55 W/mK with 1.9% pine needle incorporation by weight and 0.70 W/mK with 1.9% by straw inclusion weight. On the other hand, a study by Olacia et al. (2020) revealed a value of 0.75 W/mK with 1.5% straw incorporation by weight. The variation in thermal conductivity values was expected, given the use of soils with distinct characteristics. Furthermore, the method of measurement was different.

Sample no. 124 of mix KRSiS4020 had a higher thermal conductivity than samples no. 121 of mix KRS25, no. 166 of mix KRS33, and no. 122 of mix KRS40 due to the presence of greater amounts of straw in the latter samples. However, the difference in values may also be attributed to the existence of silicate sand in the first sample. The results reveal that incorporating silicate sand increases thermal conductivity value, which is consistent with the trends observed by other studies. Singh et al. (2019) investigated the effect of adding sand (quartz) into the soil matrix in different adobe sand ratios and revealed that including 10% by volume of sand to 90% by volume of adobe decreased the thermal conductivity of the composition. The study also indicated that 80:20 and 85:15 clay to sand ratios increased the thermal conductivity of the overall composition. On the other hand, Bassoud et al. (2021) compared the effect of two kinds of sand in the soil matrix incorporated in various ratios. The study revealed that inclusion led to a decrease in the thermal conductivity value at different adobe to sand ratios regardless of the type of sand. Clay has a lower thermal conductivity coefficient than sand.

4.1.3 Effect of cow dung incorporation on the thermal conductivity of mud samples

The thermal conductivities and densities of samples stabilized with cow dung and straw are displayed in Tables 4.5 and Figure 4.6. These specimens also contained varying amounts of sand in their soil matrix.

Sample no. 18 of mix KRSC2020, which contained 0.9% straw and 11.1% cow dung by weight, had the lowest thermal conductivity of 0.43 W/mK, whereas the highest value of 1.19 W/mK was reported for sample no. 47 of mix KRSC1511, which consisted of 1.6% straw and 8% cow dung by weight. Generally, increasing the percentage content of cow dung has varying effects on the thermal conductivity of mud samples. Mahamat et al. (2015), who investigated the thermophysical behaviors of cow dung observed a decrease in thermal conductivity with an increase in cow dung. The authors reported that including cow dung in the soil matrix reduced the composition's closed porosity and decreased its bulk density. Furthermore, Millogo et al. (2016) reported that the cow dung fibers inhibit the formation of cracks in the samples, thereby reducing closed porosity. Kaolinite and fine quartz in clay and sand, respectively, react with cow dung to form insoluble amine silicate (Si (OH)4, 4NH3) which influences the porosity of the composition (Bamogo et al., 2020). Besides according to Kulshreshtha et al. (2022), the clay-sized negatively microbial aggregates influence soil characteristics such as water absorption which also affects the porosity of the samples. The porosity, in turn, influences bulk density, affecting thermal conductivity, as discussed earlier. Furthermore, Bamogo et al.(2020) also reported that the non-digested fibers in cow dung contain cellulose which has thermal insulating properties.

On the other hand, including cow dung into the soil matrix also increases the thermal conductivity of the sample; Bahobail (2012) incorporated 5%, 10%, and 15% cow dung by mass into adobe mud containing 40% clay and 60% by mass. The study reported a thermal conductivity value of 0.9006 W/mK for 5% cow dung, 0.9327 W/mK for 10%, and 0.9405 W/mK for 15%. It is essential to note, although not

scientifically proven, that the cow's diet may affect cow dung's properties; dry feeds such as hay produce cow dung that, when incorporated into the soil matrix, decreases thermal conductivity. Oil-rich foods, on the other hand, increase thermal conductivity when used to stabilize mud samples.

Table 4.4 Samples stabilized with cow dung and processed cow dung

Sample number	**Mix code**	**Additives**		**Density** *(kg/m³)*	**λ** *(W/m²K)*
		% Weight	% Volume		
47	KRSC1511	0.7 % straw 6% cow dung	11 % straw 11% cow dung	1748.9	1.19
198	KRSC2015	0.9 % straw 6% cow dung	20% straw 15% cow dung	1637.1	0.95
17	KRSC2010	1.6 % straw 6% cow dung	20 % straw 10% cow dung	1312.8	0.77
44	KSC2010	1.6 % straw 8% cow dung	20 % straw 10% cow dung	1604.7	0.79
18	KRSC2020	0.9 % straw 11% cow dung	20 % straw 20% cow dung	1556.7	0.43

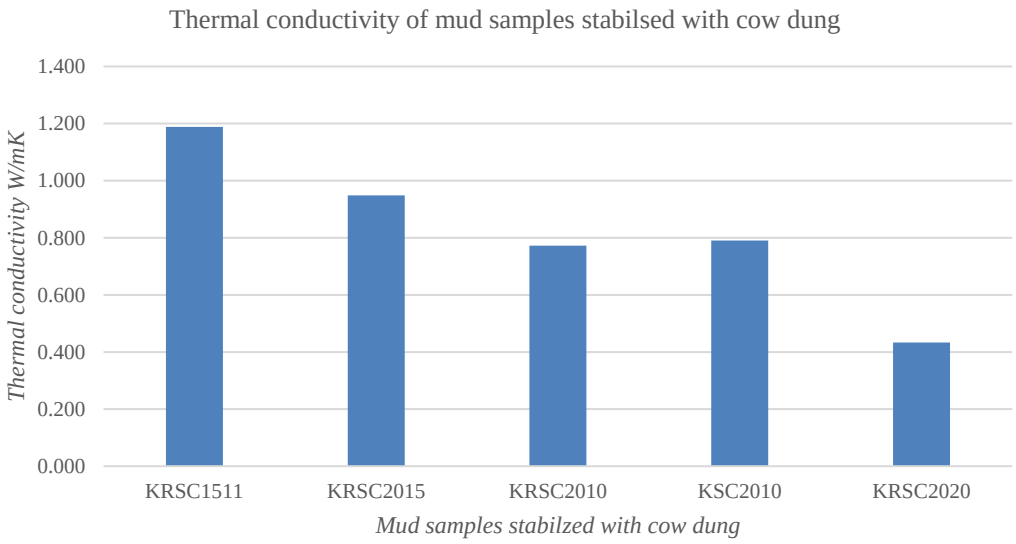

Figure 4.6 Thermal conductivity of mud samples stabilized with cow dung

Samples in this category have varying proportions of cow dung, short straw and river sand hence it is essential to determine the variation of these additives on the thermal conductivity of the composition. Sample no. 47 of mix KRSC1511, no. 189 of mix KRSC2015 and no. 17 of mix KRSC2010 have the same percentage weight of cow dung while the proportion of straw varies from 0.7 to 1.6% by weight straw. The thermal conductivity of the samples decreases with increase in fiber proportion which is consistent with literature review. For sample no. 44 of mix KSC2010 and no. 18 of mix KRSC2020, the proportions of straw and cow dung vary; a higher thermal conductivity of 0.79 W/mK was reported for KSC2010 while a value of 0.43 W/mK was noted for KRSC2020. For the samples listed above, an increase in cow dung decreases the thermal conductivity of mud plaster samples.

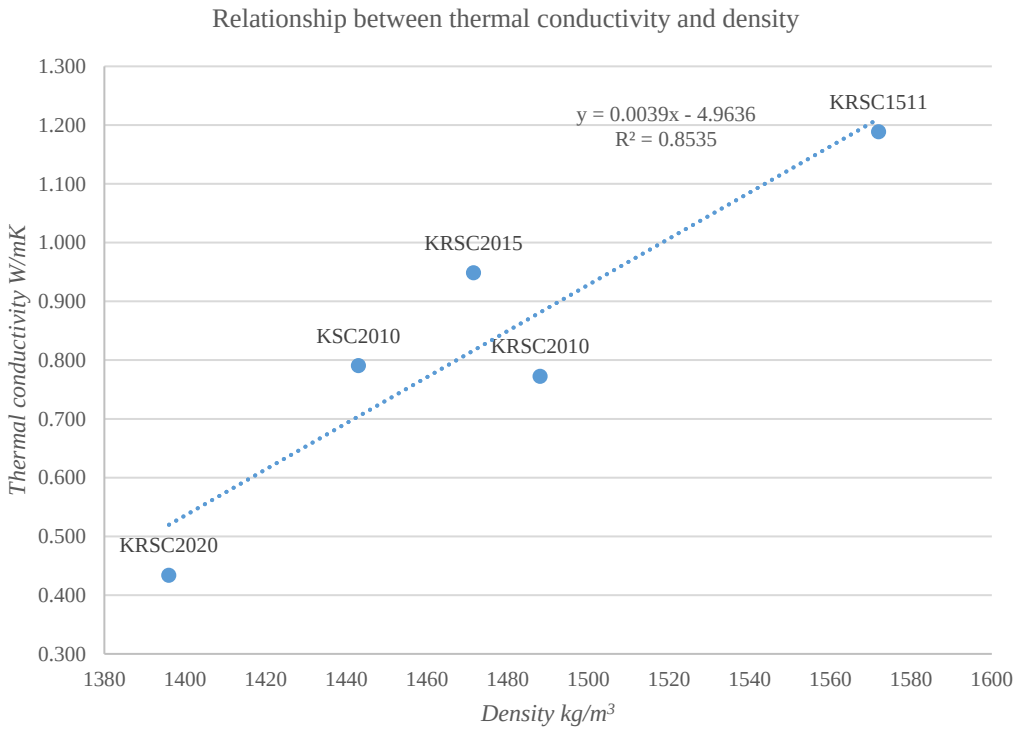

Figure 4.7 Relation between thermal conductivity and density for samples stabilized with cow dung and processed cow dung

The relationship between density and thermal conductivity is depicted in Figure 4.7. The Pearson correlation coefficient R is very close to 1 (R= 0.924), indicating a strong positive correlation between density and thermal conductivity; as the density of the sample stabilized with straw, sand, and cow dung increases, so does the thermal conductivity.

Bamogo et al. (2020) experimented with enhancing properties of adobe bricks, such as thermal conductivity, by incorporating 2, 4, and 6% by weight of cow dung, obtaining 0.84 w/mK for reference sample with 0% cow dung and 0.81, 0.79, and 0.75 w/mK for samples with 2, 4, and 6% by weight of cow dung, respectively. Furthermore, the thermal conductivity of the samples decreased with an increase in cow dung. By comparison, values of 1.19, 0.95 and 0.77 W/mK were obtained by 6% by weight cow dung and varying proportions of straw for this experiment. On the other hand, Mahamat et al. (2015) reported 0.80 W/mK for control sample and 0.50, 0.45, 0.39, and 0.34 W/mK, respectively, for 1, 2, 3, and 4% by weight cow dung inclusion.

4.2 Comparing the results obtained using two different methods of measuring thermal conductivity

Figure 4.8 displays the thermal conductivity of four sets of samples stabilized with straw, pine needles, short sheep wool, and silicate river sand. The green bars belong to the experiment conducted by Pedergnana & Elias-Ozkan (2021), while the blue ones represent values obtained from this study. Since the same mixes were utilized in both studies, comparing the thermal conductivity values of the two studies would therefore shed light on the accuracy of the simplified method employed in this experiment. The samples were also chosen based on the volumetric percentage of the principal additives; for purposes of comparison, the four sets of samples contained 20% of straw, pine needles, short sheep wool, and silicate river sand by volume. However, the physical parameters of the samples varied significantly, with the largest sample (sample no. 19 of mix KS20) measuring 21.5x16.5x3.5cm^3 and

the smallest sample (sample no. 194 of mix KRSw20) measuring 11.6x11.5x4.0cm^3. Furthermore, sample no. 27 of mix KPn20, no. 124 of mix KRSi4020, and no. 194 of mix KRSw20 had a thickness of 4.0cm, whereas sample no. 19 of mix KS20 had a thickness of 3.5cm.

Pedergnana & Elias-Ozkan (2021) employed a KEM QTM500 hot wire method apparatus to determine the thermal conductivity of samples measuring 10x10x4cm^3 under controlled laboratory conditions of 25ºC and 50% relative humidity (RH). The equipment measures thermal conductivity in the transient state, requiring a minimum surface of 60mm in diameter and a height of 15mm. On the other hand, the results of the thermal conductivity of experiments used for comparison were conducted in the summer at an average ambient temperature of 28ºC and relative humidity between 30 and 45% RH using a simplified hot plate method that measured the values at the state of thermal equilibrium.

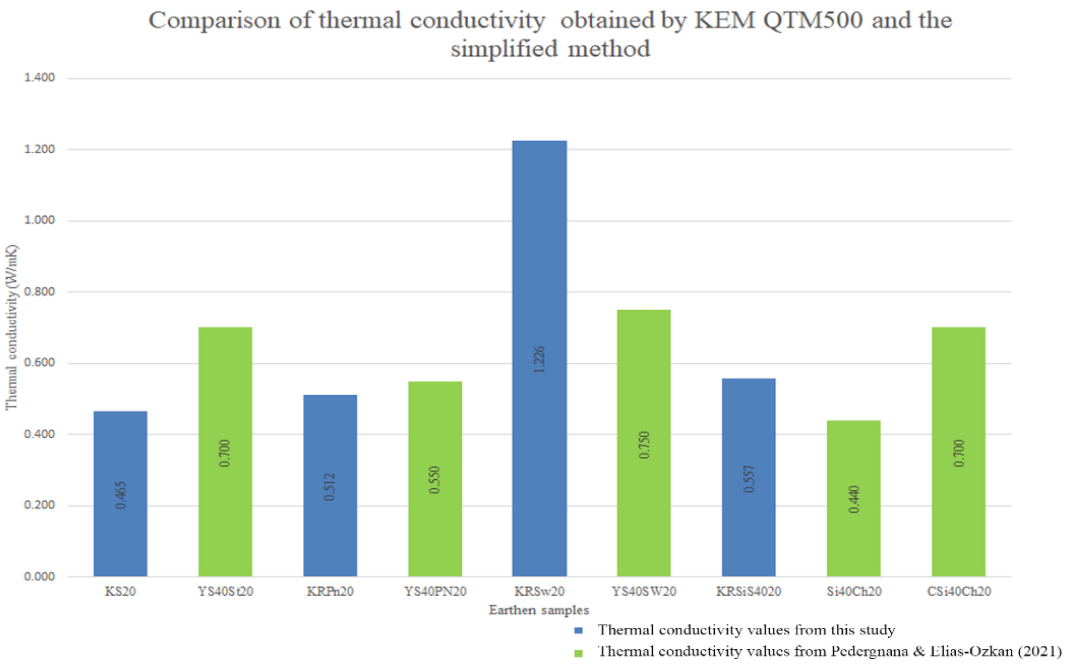

Figure 4.8 Comparing thermal conductivity values obtained using KEM QTM500 and the simplified method.

The first group consists of sample no. 19 of mix KS20, and YS40St20 stabilized with 20% by volume of short straw, resulting in thermal conductivities of 0.465 and 0.700 W/mK, respectively. The observed discrepancy in values could potentially be attributed to the varying laboratory conditions in which the two experiments were conducted. Furthermore, the ambient temperature and relative humidity were not kept constant while using the simplified setup. Furthermore, the physical parameters of the two samples differ; sample 19 has a surface area of 21.5x16.5cm and a thickness of 3.5cm, whereas YS40St20 has a surface area of 10x10 and a thickness of 4.0cm. The subsequent group consisted of sample no. 27 of mix KRPn20 and YS40PN20 with 20% pine needle inclusion and thermal conductivity values of 0.512 and 0.550 W/mK, respectively; thus, relatively close values. It is important to note that, despite having different surface areas, the two samples have the same thickness.

The values for sample no. 194 of mix KRSw20 and YS40SW20 reinforced with 20% short straw by volume were 1.226 and 0.750 W/mK, respectively. The significant difference in thermal conductivity values can be attributed to the fact that sample 194 was subjected to higher temperatures, which affected the accuracy of the results. Similar to the other samples, the experimental conditions and procedures for the two setups were distinct. As previously stated, sample no. 27 of mix KRPn20 and no. 194 of mix KRSw20 were not included in the analysis of the effect of additive incorporation; their inclusion in this section of the study is to solely determine the accuracy of the method used to measure thermal conductivity values.

The last category was made up of three different samples. The first sample, no. 124 of mix KRSi4020, was stabilized with 20% volume of short straw, silicate river sand, and river sand. The second specimen, Si40Ch20, was stabilized with 40% silicate and 20% chaff by volume. The final sample, CSi40Ch20, consisted of 40% coarse sand and 20% chaff. The thermal conductivity of the three samples was respectively 0.557, 0.440, and 0.700 W/mK. The sample CSi40Ch20 had a higher thermal conductivity value due to the presence of different soil type. On the other hand, Si40Ch20 and sample no. 124 of mix KRSi4020 had relatively similar values, which may be attributed to their similar sand composition.

4.2.1 Factors affecting the accuracy of the results

The results of this experiment were obtained using a simple experimental setup; consequently, errors were anticipated, as demonstrated in the sections that follow. According to ISO 8302:1991 (2019) factors such as type and thickness of material, moisture content and change in time and temperature influence the heat flow thereby affecting the accuracy of thermal conductivity results. Other factors to consider include sample surfaces, density and thickness, boundary effect, sample homogeneity, and environmental conditions (Yüksel, 2013). Consequently, the study investigated how temperature, relative humidity, and sample surface areas, among other variables, affected the accuracy of the results. The temperature was discussed in terms of ambient temperature and the predetermined value that the hot plate was allowed to reach.

4.2.1.1 Ambient temperature and relative humidity

As shown in Figure 4.8, the thermal conductivities determined by the KEM QTM500 hot wire method are similar to the values obtained in the current study for some samples. However, some samples had values that were greater than those noted in the literature review. The ambient temperature must be considered to explain the inconsistency of the results; the majority of the experiments were conducted in the summer at temperatures as high as 31ºC. The remaining experiments were done in the fall when average temperature was 17ºC. However, some experiments were repeated in winter with an ambient temperature of 15ºC and relative humidity of 42.8% and these were reported in the first sections of Chapter 3.

Figure 4.9 depicts the thermal conductivity values of samples during the summer and fall. The nomenclature is based on the season; for instance, sample 122S was conducted in the summer, while sample 122F was conducted in the autumn or fall; therefore, the blue bars represent fall values, and the green bars represent summer values. Summertime experiments generally yielded higher thermal conductivity

values than fall time experiments. In the fall, sample 122 produced a value of 0.485 W/mK, while the same specimen had a value of 0.742 W/mK in the summer; significant disparity that cannot be ignored. The same situation was observed with samples 134 and 18.

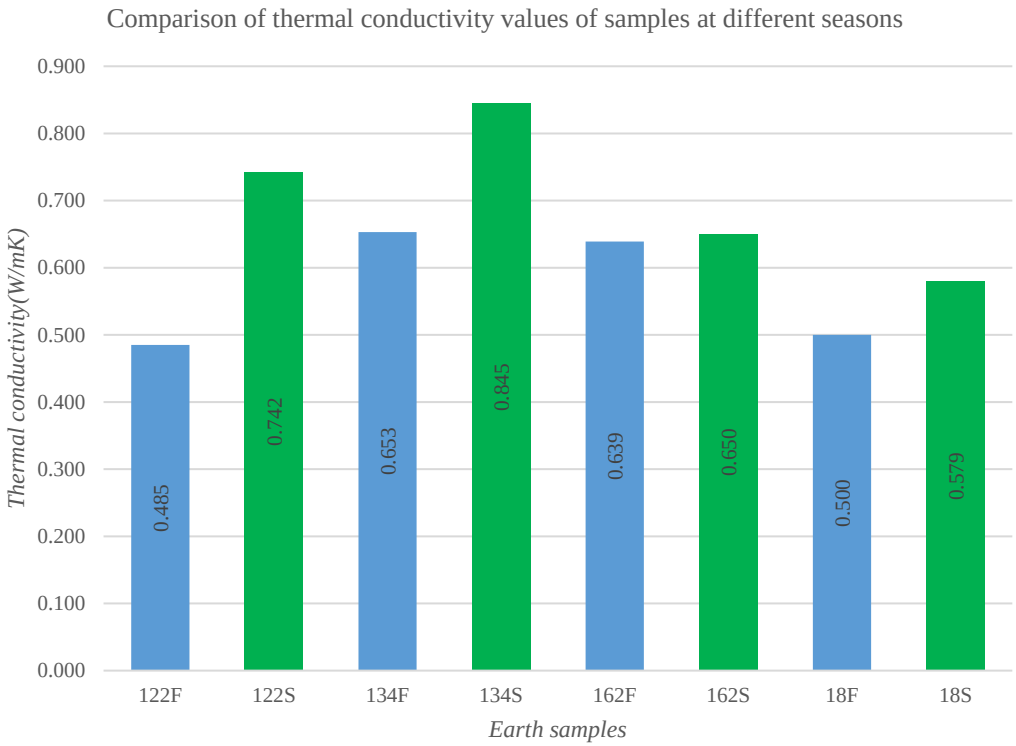

Figure 4.9 Comparison of thermal conductivity values of sample no. 122 of mix KRS40, no. 134 of mix KS40 and no. 18 of mix KRSC2020 in summer and autumn

Figure 4.10 illustrates the effect of ambient temperature on sample no. 162 of mix KRS40's thermal conductivity. T1 and T2 represent the temperature at the top measured by thermocouple T1 during autumn and summer respectively. While B1 and B2 display the temperature at the bottom measured by the thermal couple T2 respectively. Therefore, 162T1 and 162B1 represent the top and bottom temperatures recorded during the autumn experiment. Whereas 162T2 and 162B2 represent the summer experiments' temperatures both heated to predetermined temperature of 70ºC. As depicted in the graph, it took the sample 162 longer time to reach 70º C in

the fall than in the summer, indicating that more energy was consumed in the fall. In fact, 4.5 watts of energy were measured during the autumn experiment, compared to 3.5 watts during the summer. The temperature gradient between the top and bottom, on the other hand, is 8.1ºC *(T = 162B1 - 162T1)*. The experiment conducted in the summer reached the desired temperature of 70 degrees Celsius faster than the one conducted in the autumn. T = 7.5ºC was noted as the temperature gradient. Figure 4.10 shows a thermal conductivity value of 0.639 W/mK for the fall experiment and 0.650 W/mK for the summer experiment.

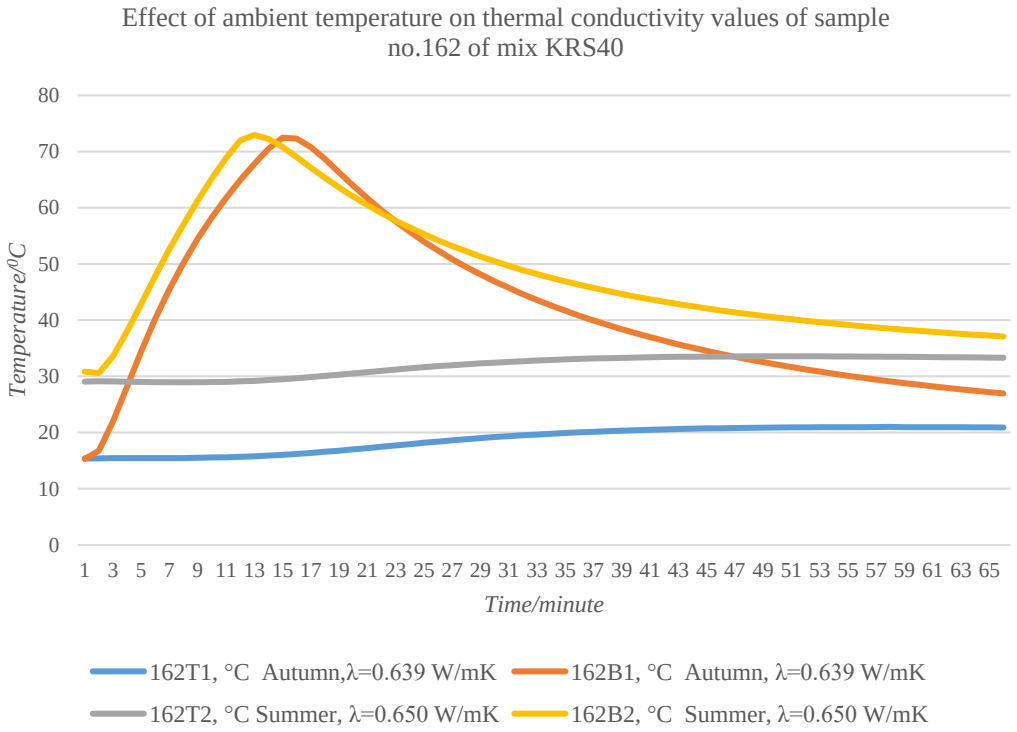

Figure 4.10 Thermal conductivity values of sample 162 of mix KRS40 at ambient temperature of 15.6ºC and 29.5ºC in autumn and summer respectively.

Figure 4.11 illustrates the influence of ambient temperature on the thermal conductivity values of sample no.18 of mix KRSC2020 stabilized with 0.9% short straw obtained by heating the sample to 70ºC. Unlike sample no. 162 of mix KRS40,

the experiment conducted on sample no. 18 took nearly the same amount of time to reach the predetermined temperature of 70ºC, indicating that both cases required nearly the same amount of energy. During the fall experiment, 3.5 watts of energy were used to heat the sample, whereas the summer experiment required only 3.0 watts because the sample was warmer.

On the other hand, for sample no. 18 of mix KRSC2020, temperature had more influence than the energy utilized in the experiment. Indeed, the temperature gradient for the summer experiment is recorded at 7.6ºC whereas a value of 10.3ºC was noted in the fall experiment. As seen from Figure 4.11 a thermal conductivity value of 0.500 W/mK was recorded for fall experiment and 0.579 W/mK was noted for summer experiment.

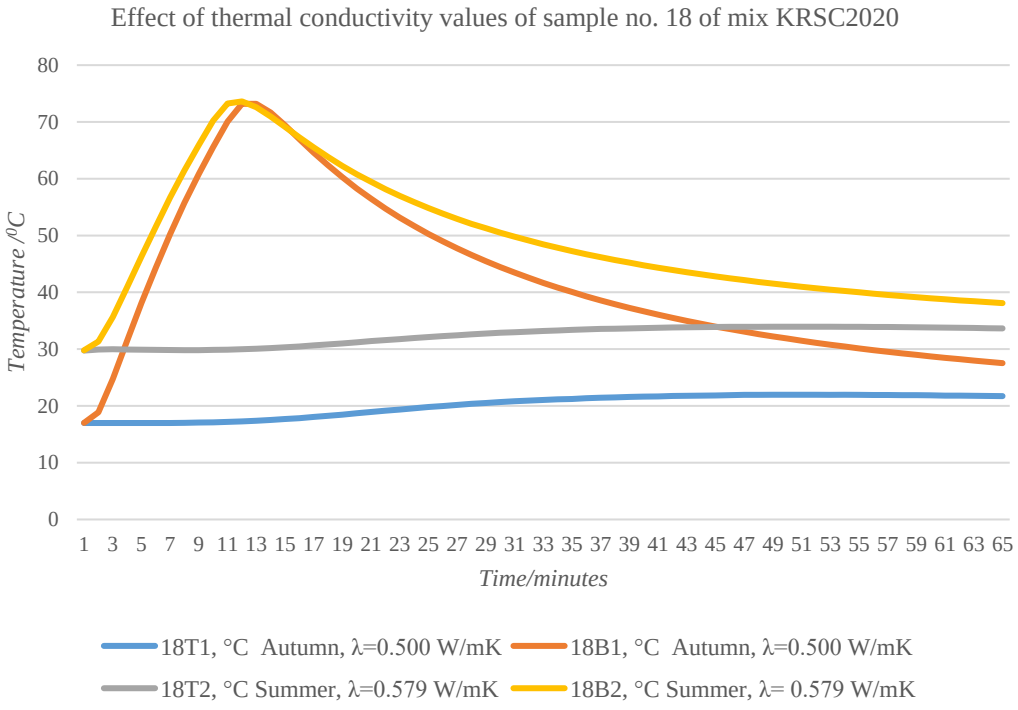

Figure 4.11 Thermal conductivity values of sample no. 18 of mix KRSC2020 at the ambient temperature of 17.5 and 29.8ºC in autumn and summer respectively.

4.2.1.2 Hotplate temperature

The energy supply to the laboratory stove was cut off when the temperature on the thermocouple T2 reached a predetermined value of 40 and 70ºC to determine the effect of hot plate temperature on thermal conductivity values. Figure 4.12 and Table 4.5 show the temperature variation and the thermal conductivity, respectively, when the hot plate is allowed to reach a predetermined temperature of 70ºC for sample no. 17 of mix KRSC2010 which contains 20 and 10% short straw by volume and cow dung, respectively. The experiment was conducted at a temperature of 26.5ºC and a relative humidity of 36%. The hot plate was gradually heated for 15 minutes and a maximum temperature of 73ºC was recorded. Furthermore, 5.5 watts of energy were required to reach this value; the temperature difference between thermocouple T2 and T3 was 10.689ºC. A thermal conductivity value of 0.99 W/mK was reported; however, a different value was reported for the same sample when the hot plate reached 40ºC.

Table 4.5 Calculation of the thermal conductivity of sample no. 17 of mix KRSC2010 when hot plate reaches 70ºC

Sample number	**Measured data**						**Derived data**		
17	Size *(cm^2)*	Energy q_{total} *(wh)*	Energy q_{top} *(wh)*	Thickness *(m)*	dT *(ºC)*	dt *(hrs)*	Area sample *(m^2)*	Area hot plate *(m^2)*	λ *(W/mK)*
	15.5x15.5x 4.0	11	5.5	0.04	10.7	0.87	0.024	0.012	**0.99**

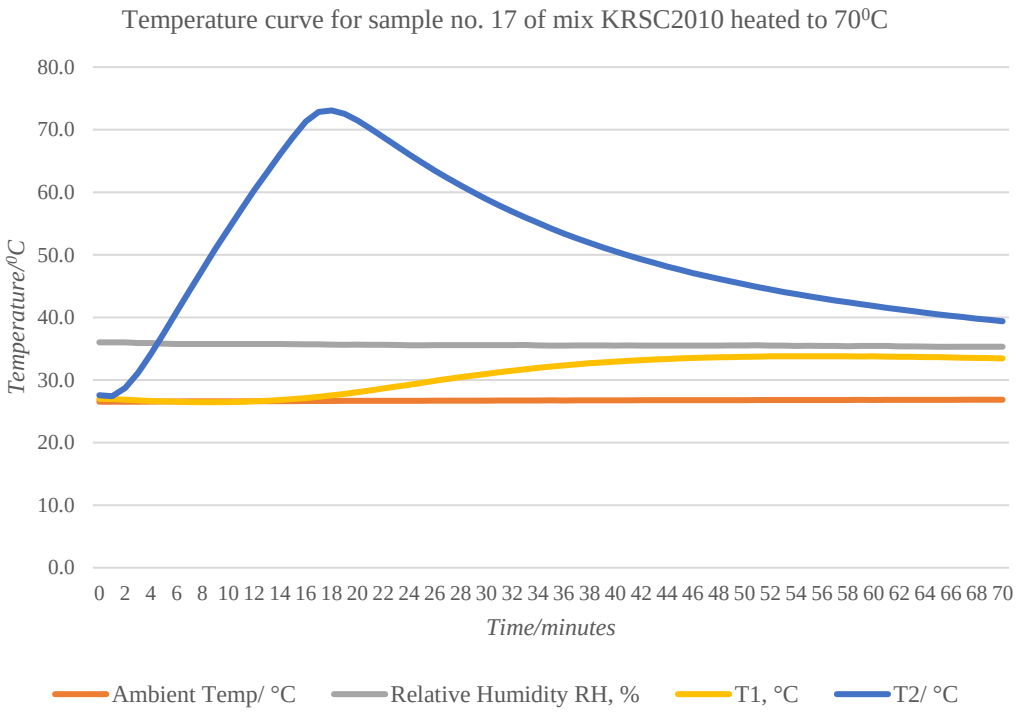

Figure 4.12 Temperature variation for sample no. 17 of mix KRSC2010 when hot plate reaches 70ºC

Figure 4.13 and Table 4.6 depict the temperature variation and thermal conductivity, respectively, for sample no .17 of mix KRSC2010 when the hot plate is allowed to reach a predetermined temperature of 40ºC. The experiment was conducted at 17.1°C and 44% relative humidity. In this case, the hot plate was gradually heated for four minutes, and the highest temperature reached was 47.8°C. Furthermore, 1.5 watts of energy were required to achieve this value; the difference in temperature between thermocouples T2 and T3 was 4.042 degrees Celsius. A thermal conductivity value of 0.77 W/mK was obtained for the same sample. Aside from the difference in laboratory ambient conditions, the temperature of the hot plate had a significant impact on the thermal condition results seen in these two experiments.

Table 4.6 Calculation of the thermal conductivity of sample no. 17 of KRSC2010 when hot plate reaches 40ºC

Sample number	**Measured data**						**Derived data**		
17	Size *(cm^2)*	Energy q_{total} *(wh)*	Energy q_{top} *(wh)*	Thickness *(m)*	dT *(ºC)*	dt *(hrs)*	Area sample *(m^2)*	Area hot plate *(m^2)*	λ *(W/mK)*
	15.5x15.5x 4.0	3.0	1.5	0.04	4.0	0.80	0.024	0.012	**0.77**

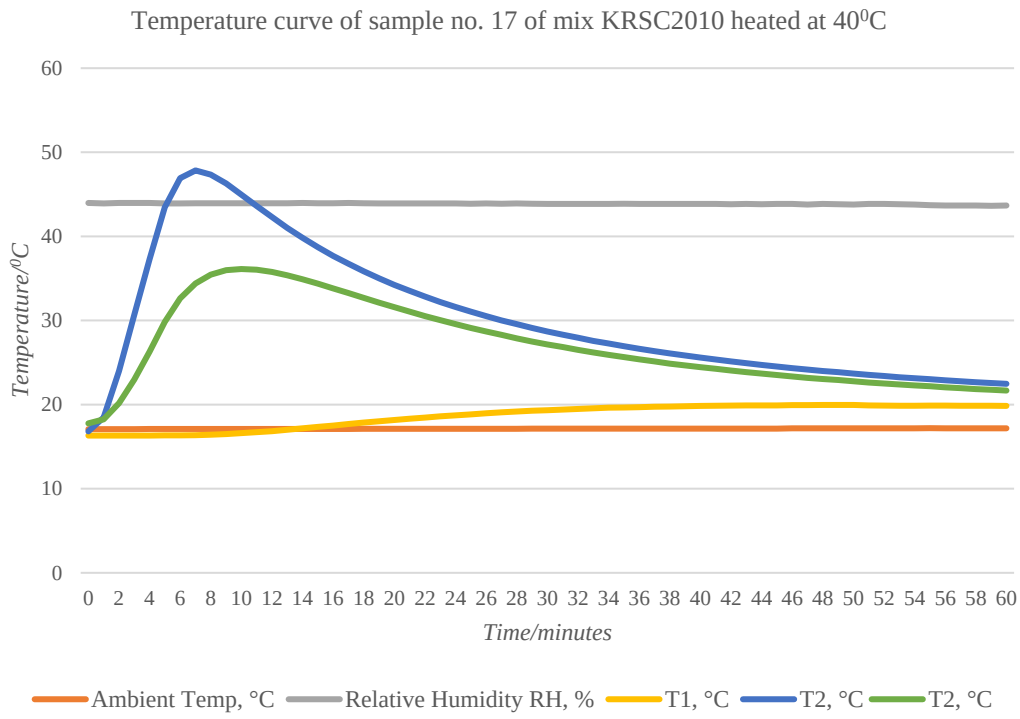

Figure 4.13 Temperature variation for sample no. 17 of mix KRSC2010 when hot plate reaches 40ºC

4.2.1.3 Sample surface area

The area of the samples was another factor that contributed to the accuracy of the findings. It was discovered that samples that were approximately the same size as the hot plate had a higher thermal conductivity value than those that were smaller. However, the thermal conductivity values were significantly lower when the hot plate was heated to 40ºC instead of 70ºC. For example, when the hot plate reached 70ºC, sample 17 of mix KRSC2010 had a value of 1.26 W/mK and a value of 0.97 W/mK when it reached 40ºC.

4.2.1.4 Cooling period

The cooling period is the time it takes for the hot plate to cool down following an experiment. The experiments were generally conducted for 1 hour, after which the hot plate was cooled for 30 minutes. It was observed that the second and third experiments required less time than the first to reach the predetermined temperature of 70ºC. In the second and third experiments, the temperature difference between the upper and lower portions of the apparatus was greater than in the first. Consequently, the results obtained for the first experiment of the day were considered in most cases. However, this was not the case for experiments carried out in winter; the same time and energy was required to heat the sample after which the hot plate was left to cool. The results improved when the hot plate was heated to 40°C; therefore, a lower temperature is recommended.

Other factors, such as the inconsistent contact between the thermocouple and the samples, must also be taken into account. In our investigation, three thermocouples were placed in three distinct locations: beneath the hot plate, on the hot plate in contact with the sample, and above the sample. A change in thermocouples brought about the observed changes in temperature.

Besides, we anticipated that some of the heat would escape through the sides of the apparatus. Six XPS 2-to-3-centimeter-thick layers were utilized to minimize heat

loss through the sides. The layers were not firmly attached because they had to be removed when the hot plate was cooled. Furthermore, there was always a small gap of 1 to 5mm between the hole made to hold the specimen and the sample itself.

4.2.2 Recommendation for improving the accuracy of the results

This experimental setup measured the thermal conductivity of mud plaster samples stabilized with fiber, sand, and fiber, and cow dung. Even though the majority of results obtained using this method were close to those found in the literature, the methodology had several limitations. The following suggestions are provided for enhancing the experimental design;

- The experiment can be conducted using a constant heat source that maintains a temperature of 40ºC. The heat used in this study was inconsistent; it was turned off when the temperature reached 40 and 70ºC. However best results were obtained when the hot plate was allowed to reach 40ºC; high temperatures resulted in high thermal conductivity values.
- It should be conducted with the laboratory temperature between 23 and 25ºC (room temperature) and the relative humidity (RH) between 30 and 50%. Otherwise, high thermal conductivity values will be attained if the experiment is conducted at high temperatures.
- Obtaining the necessary results requires a considerable amount of time; additional research should be conducted to shorten the duration of the experiment.
- Samples whose thermal conductivity is to be determined should have uniform physical parameters such as thickness, length and width. The density will vary according to material type and composition.
- The method is best suited for homogenous dry samples; this experiment cannot determine specimens with high moisture content since it relies on heat flow rate.

CHAPTER 5

CONCLUSION

This study examined the thermal properties of mud plaster samples stabilized with fiber, sand and fiber, and cow dung. The thermal conductivity of the samples was measured using a simple experimental setup based on the adapted equation of Fourier's law of heat transfer. The following conclusions were made from the study;

- Samples stabilized with fibers had the lowest thermal conductivity values ranging from 0.39 W/mK for KS30 to 0.58 W/mK for the KS05. Generally, the incorporation of short straw into the soil matrix decreases the thermal conductivity values since it reduces the bulk density of the composition. However, it is essential to note that factors such as thermal properties, and physical properties such as diameter and length of fibers significantly impact the composition's thermal conductivity.
- Samples with sand and fiber inclusion had a thermal conductivity value that ranged from 0.41 W/mK for KRS25 to 0.60 W/mK for KRS00. The study revealed that reinforcing mud plaster samples decreases thermal conductivity, whereas the addition of sand may increase the value; therefore, a suitable ratio of clay to sand is crucial. This research obtained a low thermal conductivity value of 0.41 W/mK for sample KRS40 with equal volumes of clay and sand, and 3.1% short straw, by weight.
- Generally, samples stabilized with cow dung exhibited the highest thermal conductivity values. The thermal conductivity of samples ranged from 0.43 W/mK for KRSC2020 with 11% by weight cow dung and 0.9% by weight straw to 1.19 W/mK for KRSC1511 with 6% cow dung by weight and 0.7% straw by weight. The effect of cow dung inclusion on thermal conductivity varies depending on factors such as soil composition, microbial activities and fibers. In

this study, incorporating cow dung generally decreased the thermal conductivity of mud plasters.

- Based on this research, mud plasters stabilized with only short straws had a better thermal performance of the three groups; however, other properties, such as compressive strength and tensile strength, should be considered to determine the suitable composition. The details about the physical and mechanical properties of the samples can be found in a study by Pedergnana (2022) since the same mixes were used.
- The research also revealed that factors such as temperature and humidity affected the thermal conductivity of mud plasters. For instance, experiments carried out in the summer produced higher thermal conductivity values. On the other hand, those conducted in the autumn had relatively low values. However, some samples had almost the same values regardless of the temperature and season. Furthermore, the best results were obtained when the hot plate was allowed to reach 40ºC instead of 70ºC.
- Consequently, the investigation demonstrated that a simple setup based on Fourier's law of thermal conductivity would yield relatively accurate results. It is essential to develop affordable methods for conducting research, especially in third-world nations with limited resources; the simplified setup can offer a variable alternative if its accuracy is improved.
- Almost 30% of the world’s population lives in dwellings made of mud; the number is high in East Asia and Africa. The walls of these dwellings are susceptible to erosion by torrential rain, and regular maintenance is required. However, stabilizing these materials improves their water resistance and thermal performance, which is essential for the hot climate in Africa. This research has revealed that reinforcing mud plaster samples with short straw and cow dung reduces their thermal conductivity; however, more studies are needed to standardize the practice, as is the case for modern construction materials.

REFERENCES

Abbas, A. G. N., Aziz, F. N. A. A., Abdan, K., Nasir, N. A. M., & Norizan, M. N. (2022). Kenaf Fibre Reinforced Cementitious Composites. *Fibers*, *10*(1), 1–24. https://doi.org/10.3390/fib10010003

Abdul Khalil, H. P. S., Bhat, I. U. H., Jawaid, M., Zaidon, A., Hermawan, D., & Hadi, Y. S. (2012). Bamboo fibre reinforced biocomposites: A review. *Materials and Design*, *42*, 353–368. https://doi.org/10.1016/j.matdes.2012.06.015

Aghimien, D. O., Makanjuola, S., & Fadeke, A. T. (2016). *Drivers and Barriers of Compressed Stabilized Interlocking Earth Blocks for Building Construction in Nigeria Drivers and Barriers of Compressed Stabilized Interlocking Earth Blocks for Building Construction in Nigeria*. *March 2019*. https://www.researchgate.net/publication/331828685

Ajouguim, S., Talibi, S., Djelal-Dantec, C., Hajjou, H., Waqif, M., Stefanidou, M., & Saadi, L. (2019). Effect of Alfa fibers on the mechanical and thermal properties of compacted earth bricks. *Materials Today: Proceedings*, *37*, 4049–4057. https://doi.org/10.1016/j.matpr.2020.07.539

Alawar, A., Hamed, A. M., & Al-Kaabi, K. (2009). Characterization of treated date palm tree fiber as composite reinforcement. *Composites Part B: Engineering*, *40*(7), 601–606. https://doi.org/10.1016/j.compositesb.2009.04.018

Alexander Asal. (2018). Building with Earth - Sustainable Stabilization and Additive Manufacturing for Rammed Earth Construction. *Bitkom Research*, *63*(2), 1–3. http://forschungsunion.de/pdf/industrie_4_0_umsetzungsempfehlungen.pdf%0Ahttps://www.dfki.de/fileadmin/user_upload/import/9744_171012-KI-Gipfelpapier-online.pdf%0Ahttps://www.bitkom.org/ sites/default/files/ pdf/Presse/Anhaenge-an-PIs/ 2018/180607 -Bitkom

Almeida, J., Ribeiro, A. B., Silva, A. S., & Faria, P. (2020). Overview of mining residues incorporation in construction materials and barriers for full-scale application. *Journal of Building Engineering*, *29*(October 2019), 101215. https://doi.org/10.1016/j.jobe.2020.101215

Almusaed, A., & Almssad, A. (2015). Building materials in eco-energy houses from Iraq and Iran. *Case Studies in Construction Materials*, *2*, 42–54. https://doi.org/10.1016/j.cscm.2015.02.001

Araya-Letelier, G., Antico, F. C., Burbano-Garcia, C., Concha-Riedel, J., Norambuena-Contreras, J., Concha, J., & Saavedra Flores, E. I. (2021). Experimental evaluation of adobe mixtures reinforced with jute fibers. *Construction and Building Materials*, *276*, 122127. https://doi.org/10.1016/j.conbuildmat.2020.122127

Ashour, T., Wieland, H., Georg, H., Bockisch, F. J., & Wu, W. (2010a). The influence of natural reinforcement fibres on insulation values of earth plaster for straw bale buildings. *Materials and Design*, *31*(10), 4676–4685. https://doi.org/10.1016/j.matdes.2010.05.026

Ashour, T., Wieland, H., Georg, H., Bockisch, F. J., & Wu, W. (2010b). The influence of natural reinforcement fibres on insulation values of earth plaster for straw bale buildings. *Materials and Design*, *31*(10), 4676–4685. https://doi.org/10.1016/j.matdes.2010.05.026

ASTM C 177. (2010). ASTM C 177 - Standard Test Method for Steady-State Heat Flux Measurements and Thermal Transmission Properties by Means of the Guarded-Hot-Plate Apparatus. *Annual Book of ASTM Standards*, *C*, 1–23. https://doi.org/10.1520/C0177-10.2

Babé, C., Kidmo, D. K., Tom, A., Mvondo, R. R. N., Boum, R. B. E., & Djongyang, N. (2020). Thermomechanical characterization and durability of adobes reinforced with millet waste fibers (sorghum bicolor). *Case Studies in Construction Materials*, *13*. https://doi.org/10.1016/j.cscm.2020.e00422

Bahobail, M. A. (2012a). the Mud Additives and Their Effect on Thermal

Conductivity of Adobe Bricks. *JES. Journal of Engineering Sciences*, *40*(1), 21–34. https://doi.org/10.21608/jesaun.2012.112711

Bahobail, M. A. (2012b). the Mud Additives and Their Effect on Thermal Conductivity of Adobe Bricks. *JES. Journal of Engineering Sciences*, *40*(1), 21–34. https://doi.org/10.21608/jesaun.2012.112711

Bamogo, H., Ouedraogo, M., Sanou, I., Aubert, J. E., & Millogo, Y. (2022). Physical, Hydric, Thermal and Mechanical Properties of Earth Renders Amended with Dolomitic Lime. *Materials*, *15*(11), 1–15. https://doi.org/10.3390/ma15114014

Bamogo, H., Ouedraogo, M., Sanou, I., Ouedraogo, K. A. J., Dao, K., Aubert, J. E., & Millogo, Y. (2020). Improvement of water resistance and thermal comfort of earth renders by cow dung: an ancestral practice of Burkina Faso. *Journal of Cultural Heritage*, *46*, 42–51. https://doi.org/10.1016/j.culher.2020.04.009

Barnaure, M., Bonnet, S., & Poullain, P. (2021). Earth buildings with local materials: Assessing the variability of properties measured using non-destructive methods. *Construction and Building Materials*, *281*, 122613. https://doi.org/10.1016/j.conbuildmat.2021.122613

Bassoud, A., Khelafi, H., Mokhtari, A. M., & Bada, A. (2021). Effectivenessof salty sand in improving the adobe's thermomechanical properties: Adrar case study (south Algeria). *Trends in Sciences*, *18*(19). https://doi.org/10.48048/tis.2021.6

Beas, M. I. G. (1991). *Traditional architectural renders on earthen surfaces*. 261.

Ben, I. U. (2016). Traditional Building Materials as a Sustainable Resource and Material for Low Cost Housing in Nigeria: Advantages, Challenges and the Way Forward. *International Journal of Research in Chemical, Metallurgical and Civil Engineering*, *3*(2). https://doi.org/10.15242/ijrcmce.u0716311

Bhattacharyya, D., Subasinghe, A., & Kim, N. K. (2015). Natural fibers: Their composites and flammability characterizations. In *Multifunctionality of*

Polymer Composites: Challenges and New Solutions. Elsevier Inc. https://doi.org/10.1016/B978-0-323-26434-1.00004-0

Bosman, G., & Salzmann-McDonald, K. (2015). Contemporary soil-cement and rammed earth in South Africa. *Rammed Earth Construction - Proceedings of the 1st International Conference on Rammed Earth Construction, ICREC 2015*, 47–50. https://doi.org/10.1201/b18046-10

Brouard, Y., Belayachi, N., Hoxha, D., Ranganathan, N., & Méo, S. (2018). Mechanical and hygrothermal behavior of clay – Sunflower (Helianthus annuus) and rape straw (Brassica napus) plaster bio-composites for building insulation. *Construction and Building Materials*, *161*(December), 196–207. https://doi.org/10.1016/j.conbuildmat.2017.11.140

Calatan, G., Hegyi, A., Dico, C., & Mircea, C. (2016). Determining the Optimum Addition of Vegetable Materials in Adobe Bricks. *Procedia Technology*, *22*(October 2015), 259–265. https://doi.org/10.1016/j.protcy.2016.01.077

Charai, M., Sghiouri, H., Mezrhab, A., & Karkri, M. (2021). Thermal insulation potential of non-industrial hemp (Moroccan cannabis sativa L.) fibers for green plaster-based building materials. *Journal of Cleaner Production*, *292*, 126064. https://doi.org/10.1016/j.jclepro.2021.126064

Charai, M., Sghiouri, H., Mezrhab, A., Karkri, M., Elhammouti, K., & Nasri, H. (2020). Thermal performance and characterization of a sawdust-clay composite material. *Procedia Manufacturing*, *46*(2019), 690–697. https://doi.org/10.1016/j.promfg.2020.03.098

Chen, R. (2020). Mechanical and Thermal Behaviors of Cement Stabilized Compressed Earth Bricks. *IOP Conference Series: Earth and Environmental Science*, *474*(7), 3–11. https://doi.org/10.1088/1755-1315/474/7/072090

Da Silva, T. T., Mendonça Da Silveira, P. H. P., Ribeiro, M. P., Lemos, M. F., Da Silva, A. P., Monteiro, S. N., & Cassiano Nascimento, L. F. (2021). Thermal and chemical characterization of kenaf fiber (Hibiscus cannabinus) reinforced epoxy matrix composites. *Polymers*, *13*(12), 1–15.

https://doi.org/10.3390/polym13122016

Dao, K., Ouedraogo, M., Millogo, Y., Aubert, J. E., & Gomina, M. (2018). Thermal, hydric and mechanical behaviours of adobes stabilized with cement. *Construction and Building Materials*, *158*, 84–96. https://doi.org/10.1016/j.conbuildmat.2017.10.001

David Salmon. (2001). Thermal conductivity of insulations using guarded hot plates, including recent developments and sources of reference materials. *Measurement Science and Technology*, *89*. http://iopscience.iop.org/0957-0233/12/12/201

Decagon Devices, I. (2016). *KD2 Pro Thermal Properties Analyzer*. 1–71. http://link.springer.com/10.1007/978-3-642-10841-9_18

Dieye, Y., Sambou, V., Faye, M., Thiam, A., Adj, M., & Azilinon, D. (2017). Thermo-mechanical characterization of a building material based on Typha Australis. *Journal of Building Engineering*, *9*(December 2016), 142–146. https://doi.org/10.1016/j.jobe.2016.12.007

Drexel, A., & Aigner, P. (2018). *Lawinenschutzbauten Walmendinger Horn* -.

Dündar, T., Kurt, Ş., As, N., & Uysal, B. (2012). Nondestructive evaluation of wood strength using thermal conductivity. *BioResources*, *7*(3), 3306–3316. https://doi.org/10.15376/biores.7.3.3306-3316

Egenti, C., Khatib, J., & Oloke, D. (2013). A Pilot Study of Low Utilisation of Earth for Housing Development in Urban Environment in Nigeria. *International Workshop on Earthquake and Sustainable Materials (IWESM)*, *1*.

Ekwue, E. I., Stone, R. J., & Bhagwat, D. (2006). Thermal Conductivity of Some Compacted Trinidadian Soils as affected by Peat Content. *Biosystems Engineering*, *94*(3), 461–469. https://doi.org/10.1016/j.biosystemseng.2006.03.002

Fabbri, A., Morel, J.-C., & Gallipoli, D. (2018). Assessing the performance of earth

building materials: a review of recent developments. *RILEM Technical Letters*, *3*, 46–58. https://doi.org/10.21809/rilemtechlett.2018.71

Faizi, M. K., Shahriman, A. B., Majid, M. S. A., Shamsul, B. M. T., Ng, Y. G., Basah, S. N., Cheng, E. M., Afendi, M., Zuradzman, M. R., Wan, K., & Hazry, D. (2016). An overview of the Oil Palm Empty Fruit Bunch (OPEFB) potential as reinforcing fibre in polymer composite for energy absorption applications. *MATEC Web of Conferences*, *90*. https://doi.org/10.1051/matecconf/20179001064

Fay, D. L. (1967). Fundamentals of Heat and mass transfer. In *Angewandte Chemie International Edition, 6(11), 951–952.*

Fraser, D. (1962). African Architecture. *African Studies Review*, *5*(02), 47–49. https://doi.org/10.1017/s0002020600040506

Gandia, R. M., Corrêa, A. A. R., Gomes, F. C., Marin, D. B., & Santana, L. S. (2018). *PHYSICAL , MECHANICAL AND THERMAL BEHAVIOR OF ADOBE STABILIZED WITH " SYNTHETIC TERMITE SALIVA " Adobe is an efficient construction material for several reasons , such as its thermal comfort , sustainability , and lower energy cost , as well as the simpli*. *39*(2), 139–149.

Gandia, R. M., Corrêa, A. A. R., Gomes, F. C., Marin, D. B., & Santana, L. S. (2019). Physical, mechanical and thermal behavior of adobe stabilized with “synthetic termite saliva.” *Engenharia Agricola*, *39*(2), 139–149. https://doi.org/10.1590/1809-4430-Eng.Agric.v39n2p139-149/2019

Gandia, R. M., Gomes, F. C., Corrêa, A. A. R., Rodrigues, M. C., & Mendes, R. F. (2019). Physical, mechanical and thermal behavior of adobe stabilized with glass fiber reinforced polymer waste. *Construction and Building Materials*, *222*, 168–182. https://doi.org/10.1016/j.conbuildmat.2019.06.107

Giroudon, M., Laborel-Préneron, A., Aubert, J. E., & Magniont, C. (2019). Comparison of barley and lavender straws as bioaggregates in earth bricks. *Construction and Building Materials*, *202*, 254–265.

https://doi.org/10.1016/j.conbuildmat.2018.12.126

Hadji, F., Ihaddadene, N., Ihaddadene, R., Betga, A., Charick, A., & Logerais, P. O. (2020). Thermal conductivity of two kinds of earthen building materials formerly used in Algeria. *Journal of Building Engineering*, *32*(September), 101823. https://doi.org/10.1016/j.jobe.2020.101823

Hao, L. C., Sapuan, S. M., Hassan, M. R., Sheltami, R. M., & Sheltami, R. M. (2018). Natural fiber reinforced vinyl polymer composites. In *Natural Fiber Reinforced Vinyl Ester and Vinyl Polymer Composites: Development, Characterization and Applications*. Elsevier Ltd. https://doi.org/10.1016/B978-0-08-102160-6.00002-0

Haywood, L. (2021). *Legislative preventing the recycling of mining waste* (Issue August).

Houben, H., & Hubert, G. (1994). *Earth Construction_A comprehensive guide*.

Ige, O., & Danso, H. (2021). Physico-mechanical and thermal gravimetric analysis of adobe masonry units reinforced with plantain pseudo-stem fibres for sustainable construction. *Construction and Building Materials*, *273*, 121686. https://doi.org/10.1016/j.conbuildmat.2020.121686

ISO 8302:1991. (2019). Thermal insulation — Determination of steady-state thermal resistance and related properties — Guarded hot plate apparatus. *International Organization for Standardization*.

Ispir, A. C., Dikeç, E., & Onbaşioğlu, S. U. (2016). Solution of Leakage Problem in a Guarded Hot Plate Device. *Procedia Engineering*, *157*, 488–495. https://doi.org/10.1016/j.proeng.2016.08.393

Jannot, Y., Felix, V., & Degiovanni, A. (2010). A centered hot plate method for measurement of thermal properties of thin insulating materials. *Measurement Science and Technology*, *21*(3). https://doi.org/10.1088/0957-0233/21/3/035106

Jové-Sandoval, F., Barbero-Barrera, M. M., & Flores Medina, N. (2018).

Assessment of the mechanical performance of three varieties of pine needles as natural reinforcement of adobe. *Construction and Building Materials*, *187*, 205–213. https://doi.org/10.1016/j.conbuildmat.2018.07.187

Khelifi, H., Lecompte, T., Perrot, A., & Ausias, G. (2016). Mechanical enhancement of cement-stabilized soil by flax fibre reinforcement and extrusion processing. *Materials and Structures/Materiaux et Constructions*, *49*(4), 1143–1156. https://doi.org/10.1617/s11527-015-0564-z

Kossi, I., Florent, K., Vincent, S., Emmanuel, O., Daniel, G., & Moussa, T. (2016). Study of the Thermal and Mechanical Performance of Laterite Blocks Mixed with Néré Pod for the Thermal Insulation of Buildings. *Physical Science International Journal*, *11*(2), 1–10. https://doi.org/10.9734/psij/2016/25610

Kostic, M., & Simham, K. C. (2009). Computerized , Transient Hot-Wire Thermal Conductivity (HWTC) Apparatus for Nanofluids. *Design(WSEAS HMT09)*, 71–78. http://www.wseas.us/e-library/conferences/2009/ningbo/CD-HMT/HMT10.pdf

Kouta, N., Saliba, J., & Saiyouri, N. (2020). Effect of flax fibers on early age shrinkage and cracking of earth concrete. *Construction and Building Materials*, *254*, 0–32. https://doi.org/10.1016/j.conbuildmat.2020.119315

Kulshreshtha, Y., Vardon, P. J., Meesters, G., van Loosdrecht, M. C. M., Mota, N. J. A., & Jonkers, H. M. (2022). What Makes Cow-Dung Stabilised Earthen Block Water-Resistant. *Bio-Based Building Materials*, *1*, 540–548. https://doi.org/10.4028/www.scientific.net/cta.1.540

Kyoto Electronics. (2009). *Quick Thermal Conductivity Meter, QTM-500, Operation Manual* (p. 70).

Laaroussi, N., Lauriat, G., Garoum, M., Cherki, A., & Jannot, Y. (2014). Measurement of thermal properties of brick materials based on clay mixtures. *Construction and Building Materials*, *70*, 351–361. https://doi.org/10.1016/j.conbuildmat.2014.07.104

Laborel-Préneron, A., Aubert, J. E., Magniont, C., & Bertron, A. (2015). Influence of straw content on the mechanical and thermal properties of bio-based earth composites. *First International Conference on Bio-Based Building Materials*, *33*(November), 517–522.

Laborel-Préneron, A., Aubert, J. E., Magniont, C., Tribout, C., & Bertron, A. (2016). Plant aggregates and fibers in earth construction materials: A review. *Construction and Building Materials*, *111*, 719–734. https://doi.org/10.1016/j.conbuildmat.2016.02.119

Laborel-Préneron, A., Magniont, C., & Aubert, J. E. (2018). Hygrothermal properties of unfired earth bricks: Effect of barley straw, hemp shiv and corn cob addition. *Energy and Buildings*, *178*, 265–278. https://doi.org/10.1016/j.enbuild.2018.08.021

Lamrani, M., Laaroussi, N., Khabbazi, A., Khalfaoui, M., Garoum, M., & Feiz, A. (2017a). Experimental study of thermal properties of a new ecological building material based on peanut shells and plaster. *Case Studies in Construction Materials*, *7*(July), 294–304. https://doi.org/10.1016/j.cscm.2017.09.006

Lamrani, M., Laaroussi, N., Khabbazi, A., Khalfaoui, M., Garoum, M., & Feiz, A. (2017b). Experimental study of thermal properties of a new ecological building material based on peanut shells and plaster. *Case Studies in Construction Materials*, *7*(October), 294–304. https://doi.org/10.1016/j.cscm.2017.09.006

Lekshmi, M. S., Vishnudas, S., & Nair, D. G. (2020). Strength, sorptivity and shrinkage characteristics of cow dung stabilized mud mortar. *Materials Today: Proceedings*, *32*(xxxx), 782–787. https://doi.org/10.1016/j.matpr.2020.03.715

Lertwattanaruk, P., & Choksiriwanna, J. (2011). The physical and thermal properties of adobe brick containing bagasse for earth construction. *Built*, *1*(1), 53–62.

http://scholar.google.com/scholar?hl=en&btnG=Search&q=intitle:The+Physical+and+Thermal+Properties+of+Adobe+Brick+Containing+Bagasse+for+Earth+Construction#0

Lima, J., & Faria, P. (2016). Eco-efficient earthen plasters: The influence of the addition of natural fibers. *RILEM Bookseries*, *12*(February), 315–327. https://doi.org/10.1007/978-94-017-7515-1_24

Lima, J., Faria, P., & Silva, A. S. (2016). Earthen plasters based on illitic soils from barrocal region of algarve: Contributions for building performance and sustainability. *Key Engineering Materials*, *678*, 64–77. https://doi.org/10.4028/www.scientific.net/KEM.678.64

Magar, J. (2020). Application of Industrial and Agricultural Waste for Sustainable Construction. *International Journal for Research in Applied Science and Engineering Technology*, *8*(7), 1869–1875. https://doi.org/10.22214/ijraset.2020.30699

Mahamat, A. D., Hamid, O. I., Soultan, M., Khayal, M. Y., Elhamdouni, Y., Garoum, M., & Gaye, S. (2015). Effect of cow's dung on thermophysical characteristics of building materials based on clay. *Research Journal of Applied Sciences, Engineering and Technology*, *10*(4), 464–470. https://doi.org/10.19026/rjaset.10.2512

Maheri, M. R., Maheri, A., Pourfallah, S., Azarm, R., & Hadjipour, A. (2011). Improving the durability of straw-reinforced clay plaster cladding for earthen buildings. *International Journal of Architectural Heritage*, *5*(3), 349–366. https://doi.org/10.1080/15583051003663859

Mallick, P. K. (2007). *Fiber-reinforced composite*.

Mansingh, B. B., Binoj, J. S., Manikandan, N., Sai, N. P., Siengchin, S., Mavinkere Rangappa, S., Bharath, K. N., & Indran, S. (2022). Kenaf fibers, their composites and applications. *Plant Fibers, Their Composites, and Applications*, 283–304. https://doi.org/10.1016/B978-0-12-824528-6.00011-4

Manu, D. (2013). *Strength and Durability Properties of Cow Dung Stabilised Earth*. *3*(13), 117–126.

Mbereyaho, L., Irafasha, D., Habumugisha, E., & Musabirema, J. (2020). Assessment of Cohesive Soil - Cow Dung Mortar Properties as Replacement of Cement Mortar for Simple Plastering Works. *Rwanda Journal of Engineering, Science, Technology and Environment*, *3*(2). https://doi.org/10.4314/rjeste.v3i2.6

Millogo, Y., Aubert, J. E., Séré, A. D., Fabbri, A., & Morel, J. C. (2016). Earth blocks stabilized by cow-dung. *Materials and Structures/Materiaux et Constructions*, *49*(11), 4583–4594. https://doi.org/10.1617/s11527-016-0808-6

Millogo, Y., Morel, J. C., Aubert, J. E., & Ghavami, K. (2014). Experimental analysis of Pressed Adobe Blocks reinforced with Hibiscus cannabinus fibers. *Construction and Building Materials*, *52*, 71–78. https://doi.org/10.1016/j.conbuildmat.2013.10.094

Minguela, A. F. (2017). Bio-Composites to Tackle UK Built Environment Carbon Emissions: Comparative Analysis on Load-Bearing Capacity, Hygroscopic and Thermal Performance of Compressed Earth Blocks with Addition of Industrial Hemp Waste. *The Open Construction and Building Technology Journal*, *11*(1), 395–412. https://doi.org/10.2174/1874836801711010395

Minke, G. (2006). *Building with Earth*. https://www.ptonline.com/articles/how-to-get-better-mfi-results

Mishra, S., Mohanty, A. K., Drzal, L. T., Misra, M., & Hinrichsen, G. (2004). A review on pineapple leaf fibers, sisal fibers and their biocomposites. *Macromolecular Materials and Engineering*, *289*(11), 955–974. https://doi.org/10.1002/mame.200400132

Montana, G., Randazzo, L., & Sabbadini, S. (2014). Geomaterials in green building practices: Comparative characterization of commercially available clay-based plasters. *Environmental Earth Sciences*, *71*(2), 931–945.

https://doi.org/10.1007/s12665-013-2499-4

Mostafa, M., & Uddin, N. (2015). Effect of banana fibers on the compressive and flexural strength of compressed earth blocks. *Buildings*, *5*(1), 282–296. https://doi.org/10.3390/buildings5010282

Mukhopadhyay, S., Fangueiro, R., Arpaç, Y., & Şentürk, Ü. (2008). Banana Fibers – Variability and Fracture Behaviour. *Journal of Engineered Fibers and Fabrics*, *3*(2), 155892500800300. https://doi.org/10.1177/155892500800300207

Muñoz, P., Letelier, V., Muñoz, L., & Bustamante, M. A. (2020). Adobe bricks reinforced with paper & pulp wastes improving thermal and mechanical properties. *Construction and Building Materials*, *254*. https://doi.org/10.1016/j.conbuildmat.2020.119314

Muñoz, P., Letelier, V., Muñoz, L., & Zamora, D. (2021). Assessment of technological performance of extruded earth block by adding bottom biomass ashes. *Journal of Building Engineering*, *39*(February). https://doi.org/10.1016/j.jobe.2021.102278

Namboonruang, W., Rawangkul, R., Yodsudjai, W., & Suphadon, N. (2012). Thermal conductivity and strength properties of soil-based lime adobe stabilized with pottery burnt hull ash. *Advanced Materials Research*, *535–537*, 1950–1954. https://doi.org/10.4028/www.scientific.net/AMR.535-537.1950

Nasla, S., Gueraoui, K., Cherraj, M., Samaouali, A., Nchiti, E., Jamil, Y., Arab, O., & Bougtaib, K. (2021). An experimental study of the effect of pine needles and straw fibers on the mechanical behavior and thermal conductivity of adobe earth blocks with chemical analysis. *JP Journal of Heat and Mass Transfer*, *23*(1), 35–56. https://doi.org/10.17654/HM023010035

National Weather Service. (2015). *Discussion on Humidity*. National Weather Service. https://www.weather.gov/lmk/humidity

Ngaram, S. M. (2020). Effects of Moisture Content on Thermal Properties of

Adobe Bricks as a Sustainable Building Material. *American Journal of Applied Sciences*, *17*(1), 50–55. https://doi.org/10.3844/ajassp.2020.50.55

Ngowi, A. B. (1997). Improving the traditional earth construction: A case study of Botswana. *Construction and Building Materials*, *11*(1), 1–7. https://doi.org/10.1016/S0950-0618(97)00006-8

Nitcheu, M., Meukam, P., Damfeu, J. C., & Njomo, D. (2018). Thermomechanical Characterisation of Compressed Clay Bricks Reinforced by Thatch Fibres for the Optimal Use in Building. *Materials Sciences and Applications*, *09*(12), 913–935. https://doi.org/10.4236/msa.2019.912066

Nunes, L. (2017). Nonwood bio-based materials. *Performance of Bio-Based Building Materials*, 97–186. https://doi.org/10.1016/B978-0-08-100982-6.00003-3

Obonyo, E., Tate, D., Sika, V., & Tia, M. (2010). Advancing the structural use of earth-based bricks: Addressing key challenges in the East African context. *Sustainability*, *2*(11), 3561–3571. https://doi.org/10.3390/su2113561

Odeyale, T. O., & Adekunle, T. O. (2008). Innovative and sustainable local material in traditional African architecture - Socio cultural dimension. *Structural Analysis of Historic Construction: Preserving Safety and Significance - Proceedings of the 6th International Conference on Structural Analysis of Historic Construction, SAHC08*, *2*, 991–998. https://doi.org/10.1201/9781439828229.ch113

OECD-FAO. (2021). *Agriculture in Africa 2021* (Issue April).

Olacia, E., Pisello, A. L., Chiodo, V., Maisano, S., Frazzica, A., & Cabeza, L. F. (2020). Sustainable adobe bricks with seagrass fibres. Mechanical and thermal properties characterization. *Construction and Building Materials*, *239*, 117669. https://doi.org/10.1016/j.conbuildmat.2019.117669

Omer, A. (2018). Soil thermal properties: Effects of density, moisture, salt concentration and organic matter. *Advances in Science, Technology and*

Innovation, 113–114. https://doi.org/10.1007/978-3-319-70548-4_39

Oshike, E. E. (2015). Building with earth in Nigeria: A review of the past and present efforts to enhance future housing developments. *International Journal of Science, Environment and Technology*, *4*(1), 646–660.

Ouakarrouch, M., El Azhary, K., Mansour, M., Laaroussi, N., & Garoum, M. (2020). Thermal study of clay bricks reinforced by sisal-fibers used in construction in south of Morocco. *Energy Reports*, *6*, 81–88. https://doi.org/10.1016/j.egyr.2019.11.045

Ouedraogo, M., Dao, K., Millogo, Y., Aubert, J. E., Messan, A., Seynou, M., Zerbo, L., & Gomina, M. (2019). Physical, thermal and mechanical properties of adobes stabilized with fonio (Digitaria exilis) straw. *Journal of Building Engineering*, *23*(February), 250–258. https://doi.org/10.1016/j.jobe.2019.02.005

Pachamama, R. A. V. C. N., Marco, P., Penido, A., & Faria, P. D. P. (2020). *ECO-EFFICIENT EARTH PLASTERS : EFFECT OF COW DUNG AND AIR LIME ON A KAOLINITIC CLAYISH EARTH*. *10*, 39323–39328.

Palumbo, M., McGregor, F., Heath, A., & Walker, P. (2016). The influence of two crop by-products on the hygrothermal properties of earth plasters. *Building and Environment*, *105*, 245–252. https://doi.org/10.1016/j.buildenv.2016.06.004

Patil Durvesh Gunvant, Yattinmani Ganesh Mallesh, Chinchole Pradip Vasant, & Bhagwat Rushikesh Anil. (2022). Feasibility of Cowdung Bricks as Insulator in Cavity Wall. *International Journal of Advanced Research in Science, Communication and Technology*, *2*(8), 416–436. https://doi.org/10.48175/ijarsct-4518

Pedergnana, M., & Elias-Ozkan, S. T. (2021a). Hygro-Thermal, Hydric, and Mechanical Properties of Fibre and Aggregate-Reinforced Earth Plasters. *International Journal of Digital Innovation in the Built Environment*, *10*(2), 29–45. https://doi.org/10.4018/ijdibe.2021070103

Pedergnana, M., & Elias-Ozkan, S. T. (2021b). Impact of various sands and fibres on the physical and mechanical properties of earth mortars for plasters and renders. *Construction and Building Materials*, *308*(37), 125013. https://doi.org/10.1016/j.conbuildmat.2021.125013

Pedergnana, M., & Elias-Ozkan, S. T. (2022). *Impact of natural additives on the properties of earth plasters*. Middle East Technical University.

Pekdoğan, T., & Tahsin, B. (2016). *PARAMETRIC TRANSIENT ANALYSIS OF THERMAL INSULATING PLASTER FOR EXTERIOR WALL*. *September*.

Pekmezci, B. Y., Kafesçioğlu, R., & Agahzadeh, E. (2012). Improved performance of earth structures by lime and gypsum addition. *Metu Journal of the Faculty of Architecture*, *29*(2), 205–221. https://doi.org/10.4305/METU.JFA.2012.2.9

Pinas, J. M., Lira, L., Horn, M., Solis, J. L., & Gómez, M. M. (2020). Influence of Stipa ichu on the thermal and mechanical properties of adobe as a biocomposite material. *Journal of Physics: Conference Series*, *1433*(1). https://doi.org/10.1088/1742-6596/1433/1/012003

Pollock, S. (1999). *Ancient Mesopotamia: The Eden That Never Was*. *65*(4), 763–764.

Qiu, L., Liu, Y., Du, Y., & Li, F. (2022). Microwire, fiber, nanotube, and nanowire. In *Micro and Nano Thermal Transport: Characterization, Measurement, and Mechanism*. https://doi.org/10.1016/B978-0-12-823539-3.00010-6

Rame. (2018). Oil Palm Empty Fruit Bunches (OPEFB): Existing Utilization and Current Trends Bio Refinery in Indonesia. *E3S Web of Conferences*, *31*, 1–5. https://doi.org/10.1051/e3sconf/20183103014

Randazzo, L., Montana, G., Hein, A., Castiglia, A., Rodonò, G., & Donato, D. I. (2016). Moisture absorption, thermal conductivity and noise mitigation of clay based plasters: The influence of mineralogical and textural characteristics. *Applied Clay Science*, *132–133*, 498–507. https://doi.org/10.1016/j.clay.2016.07.021

Reddy, N., & Yang, Y. (2015). *Innovative Bio bers from Renewable Resources*.

Rivera-Gómez, C., Galán-Marín, C., López-Cabeza, V. P., & Diz-Mellado, E. (2021). Sample key features affecting mechanical, acoustic and thermal properties of a natural-stabilised earthen material. *Construction and Building Materials*, *271*. https://doi.org/10.1016/j.conbuildmat.2020.121569

Robert, U. W., Etuk, S. E., Agbasi, O. E., Okorie, S., Ekpenyong, N. E., & Anonaba, A. U. (2022). *On the Modification of Lee – Charlton ' s Disc Apparatus Technique for Thermal Conductivity Determination*. 1–17.

Sánchez-Calderón, I., Merillas, B., Bernardo, V., & Rodríguez-Pérez, M. Á. (2022). Methodology for measuring the thermal conductivity of insulating samples with small dimensions by heat flow meter technique. *Journal of Thermal Analysis and Calorimetry*, *147*(22), 12523–12533. https://doi.org/10.1007/s10973-022-11457-7

Santos, T., Nunes, L., & Faria, P. (2017). Production of eco-efficient earth-based plasters: Influence of composition on physical performance and bio-susceptibility. *Journal of Cleaner Production*, *167*, 55–67. https://doi.org/10.1016/j.jclepro.2017.08.131

Schmidt, W., Commeh, M., Olonade, K., Schiewer, G. L., Dodoo-Arhin, D., Dauda, R., Fataei, S., Tawiah, A. T., Mohamed, F., Thiedeitz, M., Radebe, N. W., & Rogge, A. (2021). Sustainable circular value chains: From rural waste to feasible urban construction materials solutions. *Developments in the Built Environment*, *6*(August 2020), 100047. https://doi.org/10.1016/j.dibe.2021.100047

Segetin, M., Jayaraman, K., & Xu, X. (2007). Harakeke reinforcement of soil-cement building materials: Manufacturability and properties. *Building and Environment*, *42*(8), 3066–3079. https://doi.org/10.1016/j.buildenv.2006.07.033

Silva, F. de A., Filho, R. D. T., Filho, J. de A. M., & Fairbairn, E. de M. R. (2010). Physical and mechanical properties of durable sisal fiber-cement composites.

Construction and Building Materials, *24*(5), 777–785. https://doi.org/10.1016/j.conbuildmat.2009.10.030

Singh, M., Mamania, D., & Shinde, V. (2018). The scope of hemp (Cannabis sativa L.) use in historical conservation in india. *Indian Journal of Traditional Knowledge*, *17*(2), 314–321.

Singh, P. (2007). *Relative Humidity Calculator*. National Oceanic and Atmospheric Administration. https://www.omnicalculator.com/physics/relative-humidity

Singh, S. K., S. M., N., & H. P., W. (2019). Determination of Thermal Conductivity for Adobe (Clay Soil) Mixed With Different Proportions of Quartz (Sharp Sand). *International Journal of Research -GRANTHAALAYAH*, *7*(3), 335–345. https://doi.org/10.29121/granthaalayah.v7.i3.2019.979

Singh, S. K., Wante, H. P., & Ngaram, S. M. (2019). Using Adobe (Clay Soil) Mixed With Quartz (Sharp Sand) To Determine the Thermal Comfort of Residential Building in North-Mubi L. G, Adamawa State, Nigeria. *International Journal of Research -GRANTHAALAYAH*, *7*(3), 274–281. https://doi.org/10.29121/granthaalayah.v7.i3.2019.973

Soldatova, L. N., Rocca-Serra, P., Dumontier, M., & Shah, N. H. (2014). World Health Organization Guidelines for indoor air quality: dampness and mould. *Journal of Biomedical Semantics*, *5*. https://doi.org/10.1186/2041-1480-5-S1-I1

Suarez-dominguez, E. J. (2017). Behavior of the heat capacity and ultrasonic characterization for poured earth. *IOSR Journal of Mechanical and Civil Engineering (IOSR-JMCE), April 2018*. https://doi.org/0000-0002-5026-507X

Suwansaard, A., Kongpun, T., & Khemkhao, M. (2022). Properties of mortars mixed with polystyrene and hemp fiber wastes. *Applied Science and Engineering Progress*, *15*(1), 1–11. https://doi.org/10.14416/j.asep.2021.09.004

Taallah, B., & Guettala, A. (2016). The mechanical and physical properties of

compressed earth block stabilized with lime and filled with untreated and alkali-treated date palm fibers. *Construction and Building Materials*, *104*, 52–62. https://doi.org/10.1016/j.conbuildmat.2015.12.007

Taallah, B., Guettala, A., Guettala, S., & Kriker, A. (2014). Mechanical properties and hygroscopicity behavior of compressed earth block filled by date palm fibers. *Construction and Building Materials*, *59*, 161–168. https://doi.org/10.1016/j.conbuildmat.2014.02.058

Ul Abdin, Z., & Khitab, A. (2021). Effect of pine needle fibers on properties of cementitious mortars. *Proceedings of the Pakistan Academy of Sciences: Part A*, *57*(4), 33–46.

Yang, I., Kim, D., & Lee, S. (2018). Construction and preliminary testing of a guarded hot plate apparatus for thermal conductivity measurements at high temperatures. *International Journal of Heat and Mass Transfer*, *122*, 1343–1352. https://doi.org/10.1016/j.ijheatmasstransfer.2018.02.072

Yüksel, N. (2013). The review of commonly used methods and Techniques to measure the thermal conductivity of insulation materials. *Intech*, *32*(July), 137–144. http://www.intechopen.com/books/trends-in-telecommunications-technologies/gps-total-electron-content-tec- prediction-at-ionosphere-layer-over-the-equatorial-region%0AInTec%0Ahttp://www.asociatiamhc.ro/wp-content/uploads/2013/11/Guide-to-Hydropower.pdf

Zhao, D., Qian, X., Gu, X., Jajja, S. A., & Yang, R. (2016). Measurement techniques for thermal conductivity and interfacial thermal conductance of bulk and thin film materials. *Journal of Electronic Packaging, Transactions of the ASME*, *138*(4), 1–64. https://doi.org/10.1115/1.4034605

APPENDICES

A. A list showing type of solid waste, their sources and utilization

Table 5.1 A list showing type of solid wastes, their sources and utilization (Magar, 2020)

Type of solid waste	Source details	Recycling and utilization
Mineral waste	Mining waste tailing from gold, Zinc, copper, iron, and aluminum industries	Fine and course light weight aggregates, bricks, tiles
Hazardous waste	Galvanizing waste, tannery waste, contaminated blasting materials, metallurgical residues, sludge from waster and water treatment plant	Cement, tiles, boards, bricks, ceramics
Non-hazardous waste	Lime stone waste, kiln dust, lime sludge, waste gypsum, broken glass and ceramics, marbles processing residues	Hydraulic binder, bricks, blocks, cement cylinder, fibrous gypsum boards, super-sulfated cement, gypsum plaster.
Inorganic industrial waste	Steel slag, construction debris, coal combustion residues, bauxite red mud	Fine and coarse aggregate, concrete, bricks, tiles, paints, blocks, cements, wood substitute products.
Organic agro- waste	Saw mill waste, cotton stalk, vegetable residues, jute sisal, groundnut shell, baggasse, rice, wheat straw, husk	Root sheets, bricks, reinforced composite, polymers composite, acid proof cement boards, particle boards, insulation boards

B. Minimum thermal conductivity values from literature review

Table 5.2 Thermal conductivity values and thermal conductivity measure methods from literature review

References	Min. Thermal conductivity $(W\ m^{-1}K^{-1})$	Method for measuring thermal conductivity
Muñoz et al. (2020)	0.60	Transient Plane Source (TPS)
Giroudon et al. (2019)	0.16	EP500 Guarded hot plate apparatus
Calatan et al. (2016)	0.35	Thermofluxmetric method
Barnaure et al. (2021)	0.55	Hot Disk method
Araya-Letelier et al. (2021)	1.00	KD2- Pro thermal analyzer
Laborel-Préneron et al. (2018)	0.14	EP500 Guarded hot plate apparatus
Pekmezci et al. (2012)	0.22	Heat flow method
Pinas et al. (2020)	0.35	Guarded hot plate (ACG- 305)
Laborel-Préneron et al. (2015)	0.14	EP500 Guarded hot plate apparatus
Gandia et al. (2018)	0.82	Thermal box
Gandia et al. (2019)	0.68	Thermal box
Gandia, Corrêa, et al. (2019)	0.85	Thermal box
Dao et al. (2018b)	0.30	TR-01 probe connected to thermal pro analyzer
Ige & Danso (2021)	Undefined	Thermal gravimetric analysis
Kossi et al. (2016)	0.43	Asymmetric hot plan
Olacia et al. (2020)	0.68	KD2- Pro thermal analyzer
Lertwattanaruk & Choksiriwanna, (2011)	0.45	Undefined
Namboonruang et al. (2012)	0.74	Undefined
Hadji et al. (2020)	0.38	Hot wire method
Charai et al. (2020)	0.63	Hot disk method
Nitcheu et al. (2018)	0.44	Hot plate method
Babé et al. (2020)	0.74	Transient asymmetrical hot plate
Dieye et al. (2017)	0.13	Transient hot plate method

C. Additives, density, soil types and thermal conductivity from literature review

Table 5.3 Additives, density, soil types and thermal conductivity of earthen samples from literature

References	**Soil, Sand and** Clay type	**Additives or Stabilizer**	**Optimum content (wt%, vol %)**	**Density (Kg/m3)**	λ **(W $m^{-1}K^{-1}$)**
Muñoz et al. (2020)	Clay, silt and sand	Paper pulp (PPR)	15%	1800	0.6
Giroudon et al. (2019)	FWAS (Quarry fines from washing aggregate sludge)	3% Barley straw	3% Barley straw	1170	0.16
Calatan et al. (2016)	Sandy clay and Sand	Hemp fiber	Hemp fiber 9-10%	1680	0.35
Barnaure et al. (2021)	Sandy loam (Clay, silt and sand)	hemp shives and reed	8% (7% hemp, 1% reed)	1439	0.55
Araya-Letelier et al. (2021)	Clayey soil ;(12% clay, 54% silt and 34% sand)	Jute fibers	2.0 wt% and 15mm fiber	Undefined	1.00
Laborel-Préneron et al. (2018)	FWAS (Quarry fines from washing aggregate washing processing)	Barley straw	6 wt% Barley straws	1100	0.14
Pekmezci et al. (2012)	Natural clay and sand	Gypsum and lime	10% Gypsum 5% Lime	Undefined	0.22
Pinas et al. (2020)	Clay (10-20%)	Stipa ichu (Plant fiber)	undefined	Undefined	0.35

Table 6.3 cont'd

Laborel-Préneron et al. (2015)	FWAS (Fines from washing Limestone aggregate sludge)	Barley straw	6% Barley straw	1400	0.14
Gandia et al. (2018)	41% clay, 2% silt and 57% sand	Synthetic termite saliva (STS)	0.8 % STS	Undefined	0.82
Rômulo Marçal Gandia et al. (2019)	41% clay, 2% silt and 57% sand	Glass fiber reinforced polymer (GFRP)	10% GFRP	1524	0.68
Rômulo M Gandia et al. (2019)	41% clay, 2% silt and 57% sand	Sludge from water treatment plants (WTPs)	3% Sludge	Undefined	0.85
M. Ouedraogo et al. (2019)	Clayey soil	Fonio straw (FS)	0.4% Fonio straw FS	Undefined	0.30
Ige & Danso (2021)	15% clay, 20% silt, 46% sand and 19% gravel	Plantain pseudo- stem fibre PPSF	0.5- 0.75%	1601	Undefined
Kossi et al. (2016)	Laterite soil	Nere pod	14- 16% Nere pod	1400	0.43
Olacia et al. (2020)	60% clay, 40% sand and 20% gravel	Sea plant fibre	1.5%	1918	0.68

Table 6.3 cont'd

Lertwattanaruk & Choksiriwanna (2011)	60% clay, 20% sand and 20% silt	Rice husk and Bagasse	6% Bagasse	Undefined	0.45
W. Namboonruang et al. (2012)	Natural soil	Lime and Burnt hull ash (BHA)	10% lime and 25% BHA	Undefined	0.74
Hadji et al. (2020)	Agri. soil (14 % silt, 15% clay, 71% sand) Hamada soil (20% silt, 10% clay, 70% sand	Wheat fiber	5% wheat fiber	Undefined	0.38
Charai et al. (2020)	6.5% sand, 34.5% silt and 59% clay	Saw dust	10% Saw dust	1648.51	0.63
Nitcheu et al. (2018)	Laterite soil (6.67% gravel, 34.34% sand, 23.02% limon and 38.85% clay)	Thatch fibre	4% Thatch fiber	Undefined	0.44
Babé et al. (2020)	Clayey soil (61% sand, 12.85% silt and 24.91% clay)	Millet fiber	2% millet fiber	1736	0.74

Table 6.3 cont'd

Dieye et al. (2017)	Clay soil	Binders (Clay + Typha Australis fiber)	77.13% binder	1000	0.13

D. Temperature variation curves for samples stabilized with fibers

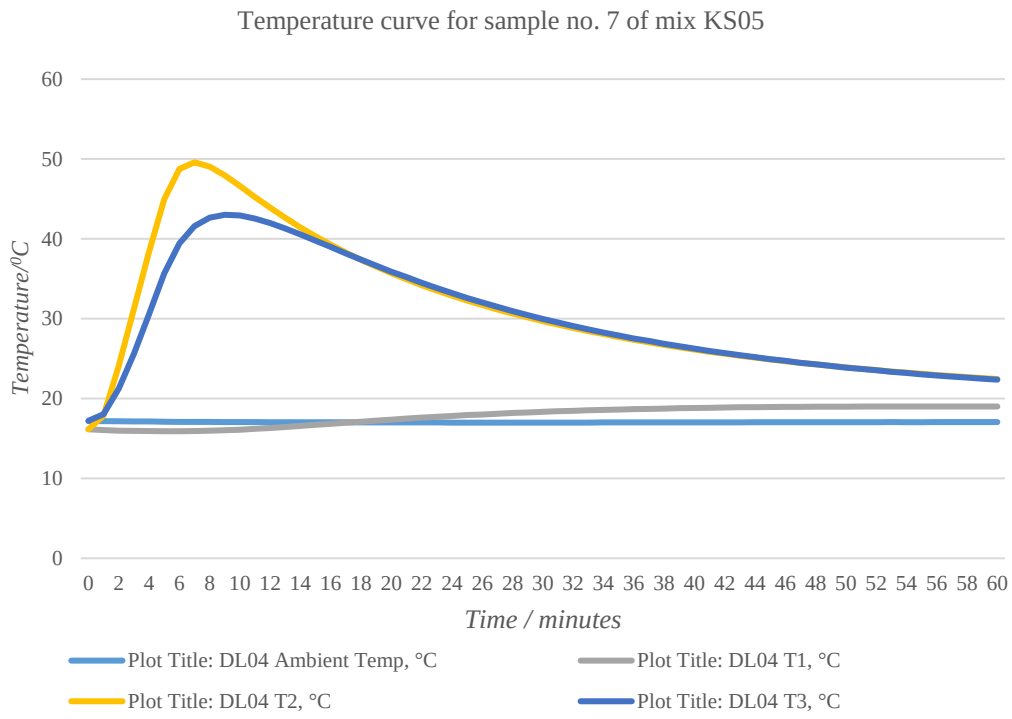

Figure 5.1 Temperature variation curves of sample 7 of mix KS05 containing 5% straw by volume

Table 5.4 Calculation of the thermal conductivity of sample no. 7 of mix KS05 stabilized by 5% straw by volume

Sample number	**Measured data**						**Derived data**		
7	Size *(cm^2)*	Energy total *(wh)*	Energy q_{top} *(wh)*	Thickness *(m)*	dT *(°C)*	dt *(hrs)*	Area sample *(m^2)*	Area hot plate *(m^2)*	λ *(W/mK)*
	17.5x14.5x 4.0	3.0	1.5	0.04	4.7	0.85	0.025	0.012	**0.58**

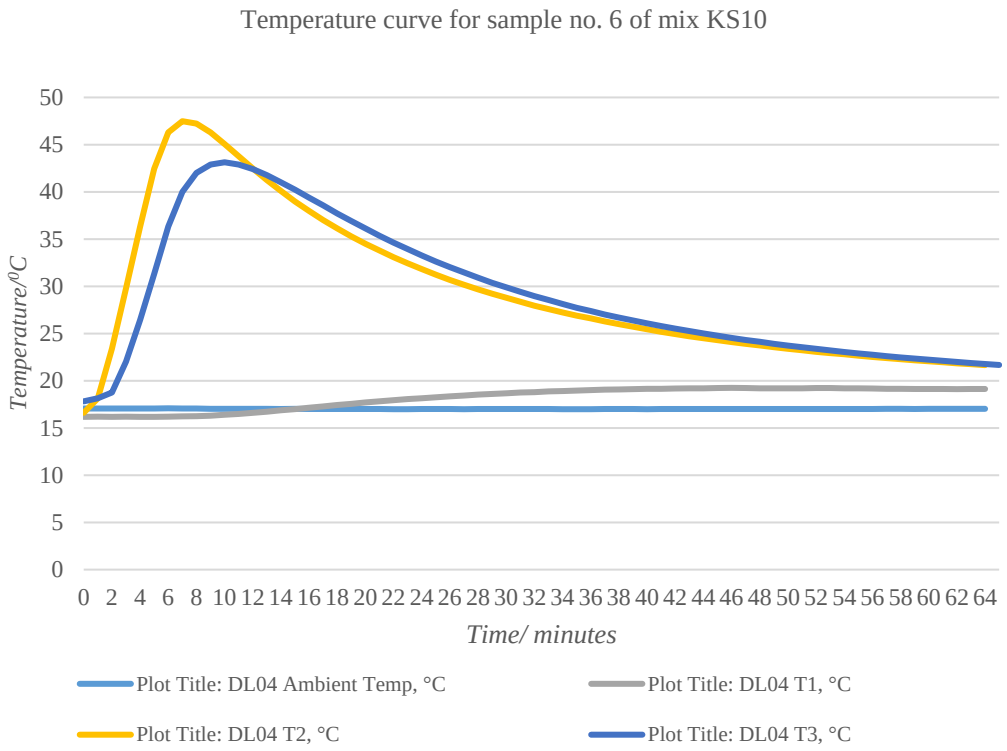

Figure 5.2 Temperature variation curves of sample no. 6 of mix KS10 containing 10% straw by volume

Table 5.5 Calculation of the thermal conductivity of sample no. 6 of mix KS010 stabilized by 10% short straw by volume

Sample number	**Measured data**						**Derived data**		
6	Size *(cm^2)*	Energy total *(wh)*	Energy q_{top} *(wh)*	Thickness *(m)*	dT *(ºC)*	dt *(hrs)*	Area sample *(m^2)*	Area hot plate *(m^2)*	λ *(W/mK)*
	16.5x16.0x 3.7	3.0	1.5	0.037	4.9	0.85	0.026	0.012	**0.57**

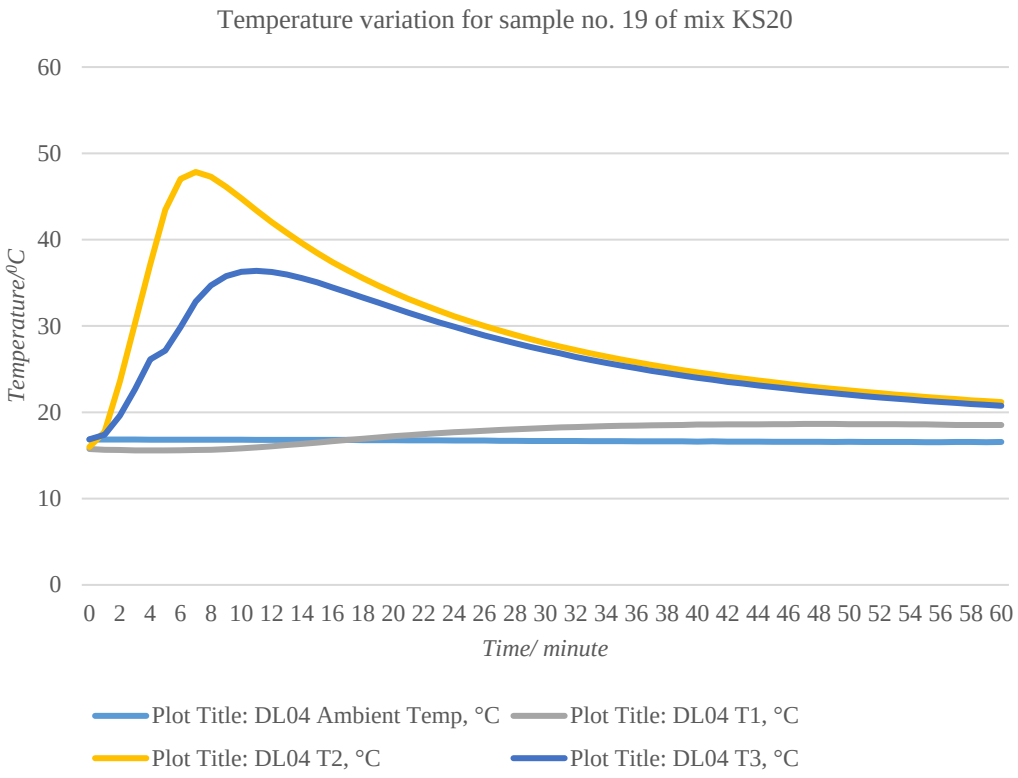

Figure 5.3 Temperature variation for sample no. 19 of mix KS20 stabilized with 20% short straw by volume

Table 5.6 Calculation of thermal conductivity of sample no. 19 of mix KS20 stabilized by 20% short straw by volume

Sample number	**Measured data**						**Derived data**		
19	Size *(cm^2)*	Energy total *(wh)*	Energy q_{top} *(wh)*	Thickness *(m)*	dT *(°C)*	dt *(hrs)*	Area sample *(m^2)*	Area hot plate *(m^2)*	λ *(W/mK)*
	21.5x16.5x 3.8	3.0	1.5	0.038	4.4	0.78	0.035	0.012	**0.47**

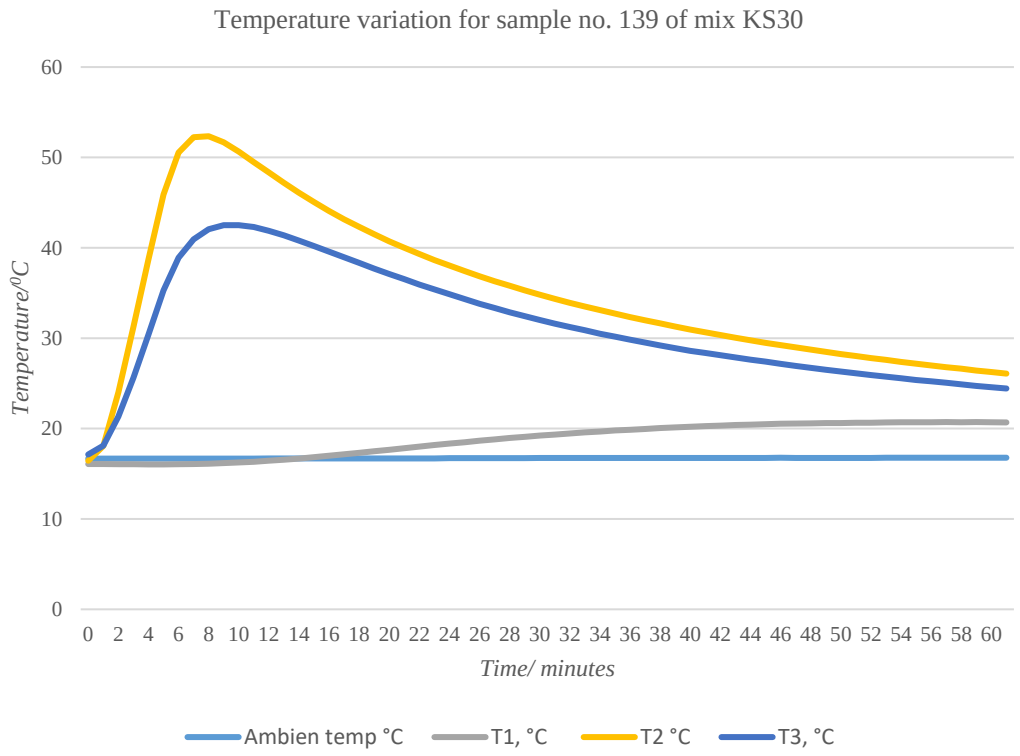

Figure 5.4 Temperature variation curve for sample no. 139 of mix KS30 stabilized with 30% straw by volume

Table 5.7 Calculation of thermal conductivity of sample no.139 stabilized with 30% straw by volume

Sample number	**Measured data**							**Derived data**		
139	Size *(cm^2)*	Energy total *(wh)*	Energy q_{top} *(wh)*	Energy q_{small} *(wh)*	Thickness *(m)*	dT *(°C)*	dt *(hrs)*	Area sample *(m^2)*	Area hot plate *(m^2)*	λ *(W/mK)*
	8.0x8.0 x3.4	3.0	1.5	0.85	0.034	5.9	0.95	0.0064	0.012	**0.39**

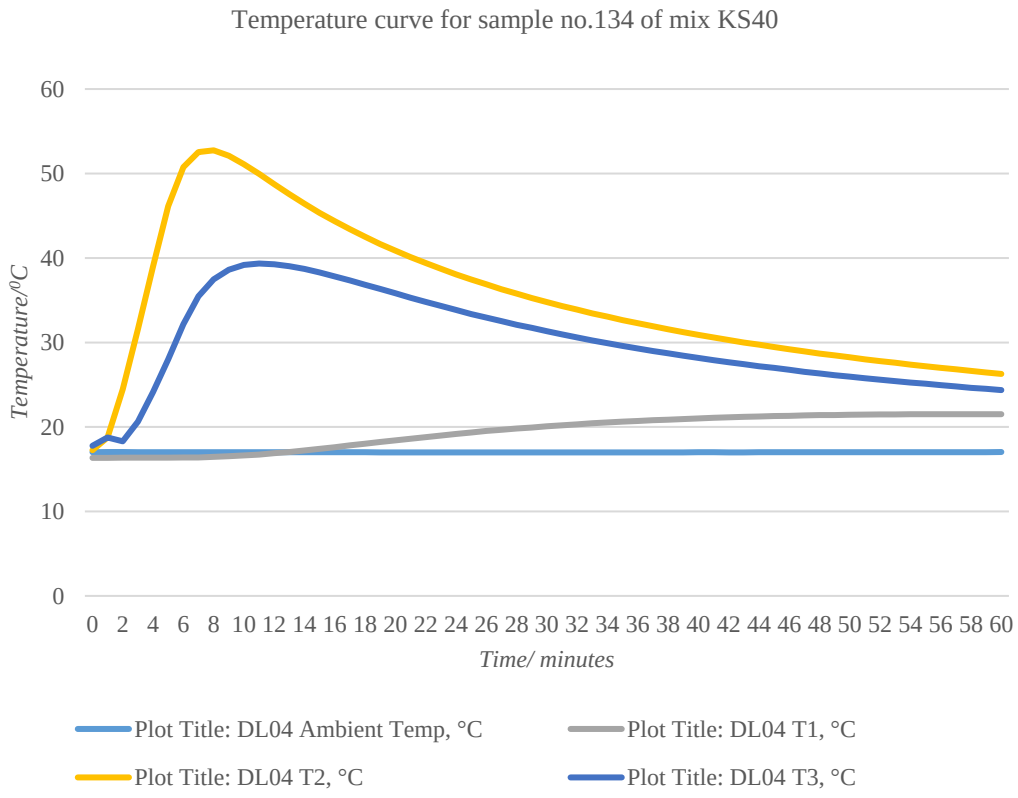

Figure 5.5 Temperature curve for sample no. 134 of mix KS40 stabilized by 40% short straw by volume

Table 5.8 Calculation of thermal conductivity of sample no. 134 of mix KS40 stabilized by 40% short straw by volume

Sample number	**Measured data**							**Derived data**		
134	Size *(cm^2)*	Energy total *(wh)*	Energy q_{top} *(wh)*	Energy q_{small} *(wh)*	Thickness *(m)*	dT *(ºC)*	dt *(hrs)*	Area sample *(m^2)*	Area hot plate *(m^2)*	λ *(W/mK)*
	8.4x8.3 x3.4	3.0	1.5	0.85	0.034	5.9	0.9	0.007	0.012	**0.46**

E. Temperature variation curves for samples stabilized with sand and fibers

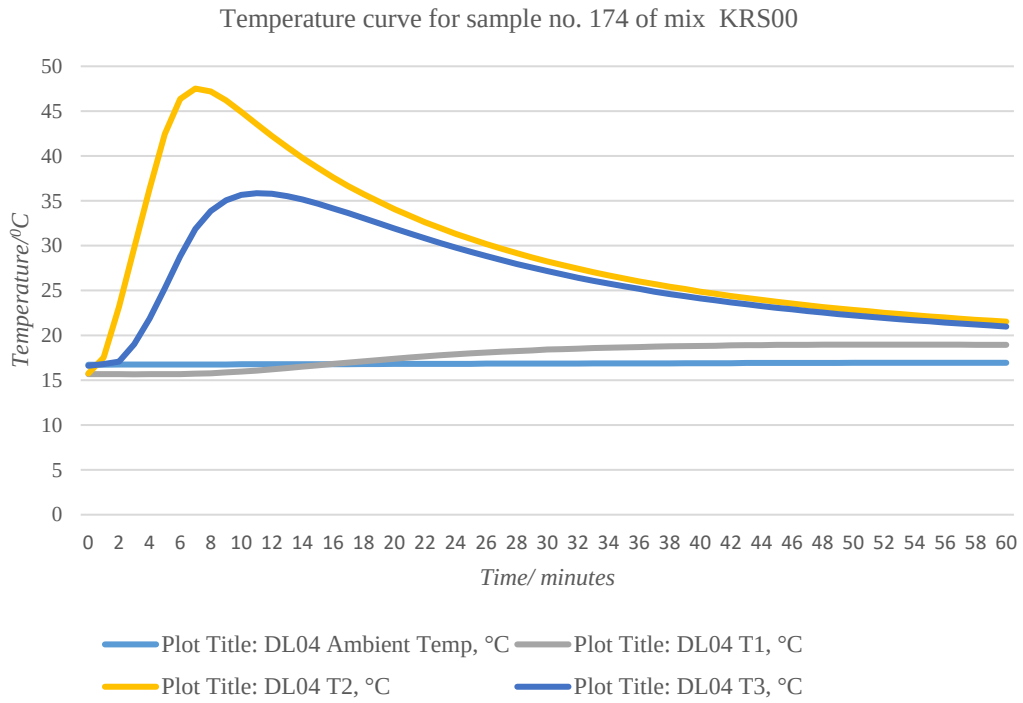

Figure 5.6 Temperature curve for sample no. 174 of mix KRS00 (reference sample)

Table 5.9 Calculation of the thermal conductivity of sample no. 174 of mix KRS00

Sample number	**Measured data**						**Derived data**		
174	Size *(cm^2)*	Energy total *(wh)*	Energy q_{top} *(wh)*	Thickness *(m)*	dT *(ºC)*	dt *(hrs)*	Area sample *(m^2)*	Area hot plate *(m^2)*	λ *(W/mK)*
	17.2x16.4x 3.8	3.0	1.5	0.038	4.2	0.80	0.028	0.012	**0.60**

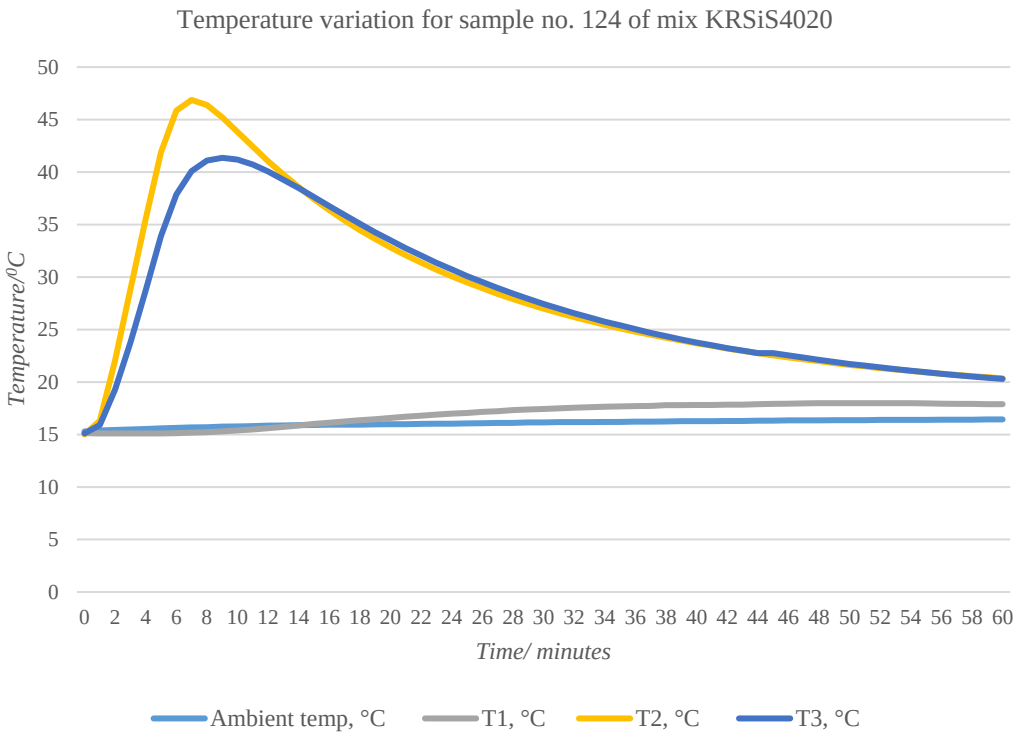

Figure 5.7 Temperature variation curve for sample no. 124 of mix KRSiS40 stabilized by 40% siliceous sand and 20% short straw by volume

Table 5.10 Calculation of thermal conductivity of sample no. 124 of mix KRSiS4020 stabilized by 40% Siliceous sand and 20% short straw by volume

Sample number	**Measured data**						**Derived data**		
174	Size *(cm^2)*	Energy total *(wh)*	Energy q_{top} *(wh)*	Thickness *(m)*	dT *(ºC)*	dt *(hrs)*	Area sample *(m^2)*	Area hot plate *(m^2)*	λ *(W/mK)*
	20.4x16.5x 4.0	3.0	1.5	0.04	4.0	0.80	0.033	0.012	**0.56**

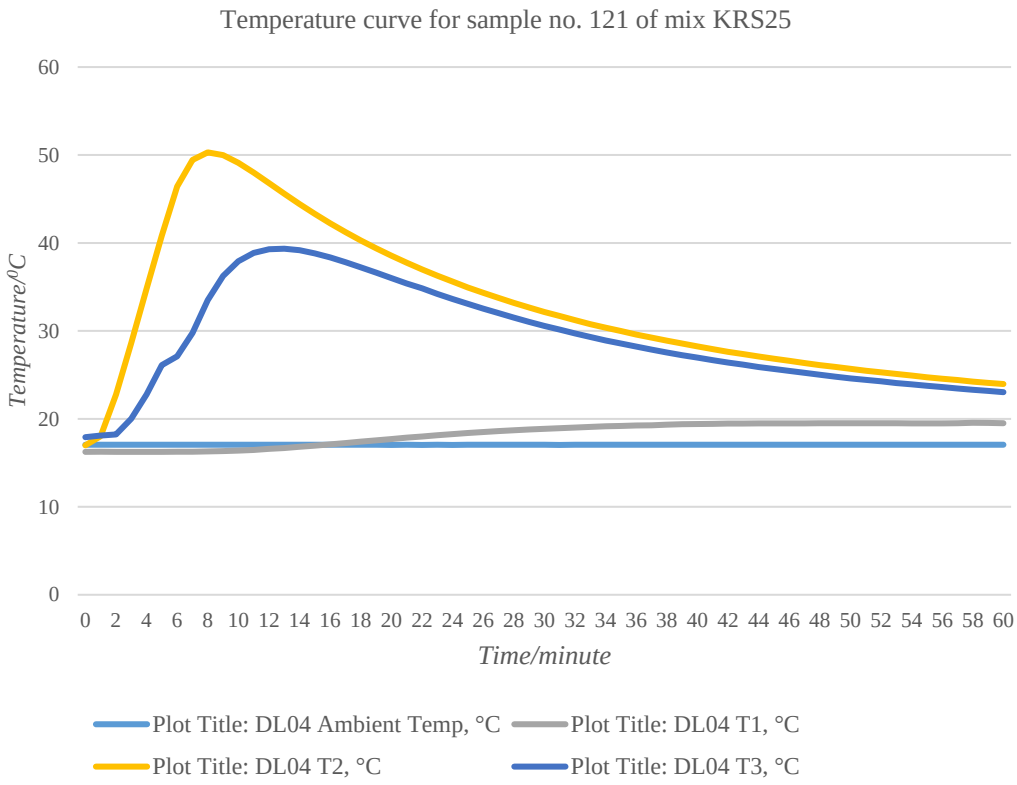

Figure 5.8 Temperature curve for sample no. 121 of mix KRS25 stabilized by 25% straw by volume

Table 5.11 Temperature variation curve for sample no. 121 of mix KRS25 stabilized by 25% straw by volume

Sample number	**Measured data**						**Derived data**		
121	Size *(cm^2)*	Energy total *(wh)*	Energy q_{top} *(wh)*	Thickness *(m)*	dT *(ºC)*	dt *(hrs)*	Area sample *(m^2)*	Area hot plate *(m^2)*	λ *(W/mK)*
	20.5x17.0x 3.8	3.0	1.5	0.038	6.6	0.80	0.033	0.012	**0.41**

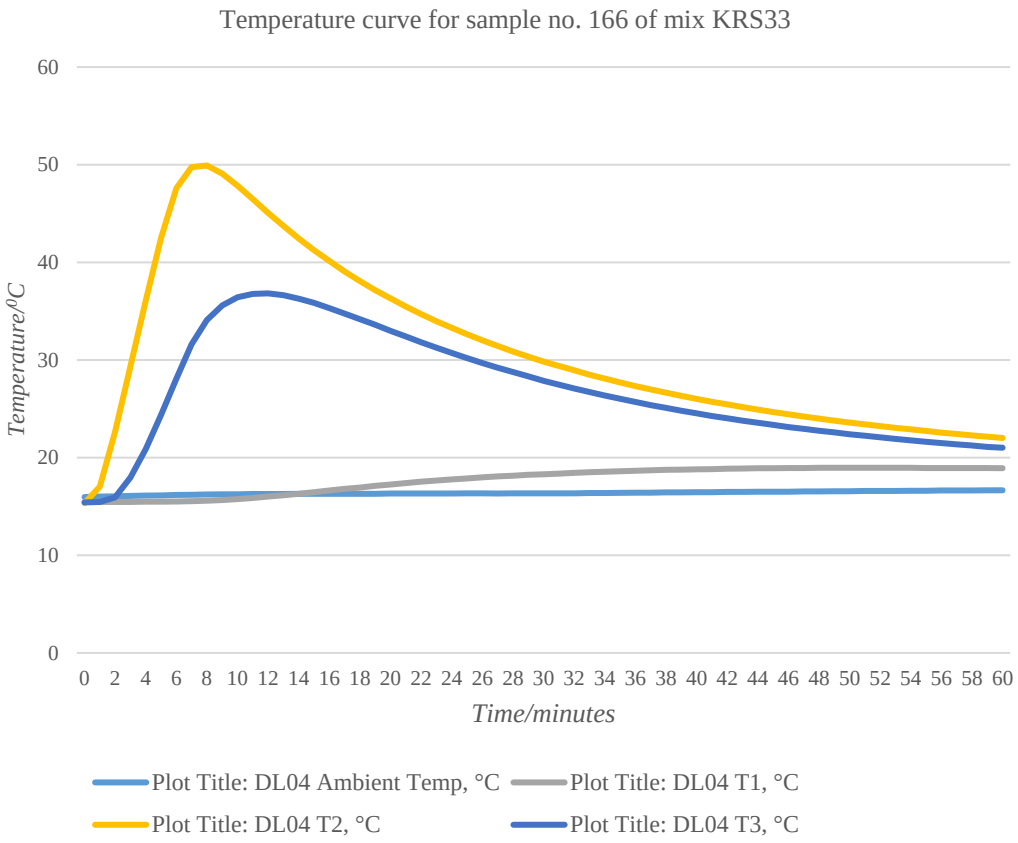

Figure 5.9 Temperature variation curve for sample no. 166 of mix KRS33 stabilized by 40% short straw by volume

Table 5.12 Calculation of thermal conductivity of sample no. 166 of mix KRS40 stabilized by 40% short straw by volume

Sample number	**Measured data**						**Derived data**		
166	Size *(cm^2)*	Energy total *(wh)*	Energy q_{top} *(wh)*	Thickness *(m)*	dT *(°C)*	dt *(hrs)*	Area sample *(m^2)*	Area hot plate *(m^2)*	λ *(W/mK)*
	19.9x16.0x 3.8	3.0	1.5	0.038	5.0	0.80	0.031	0.012	**0.44**

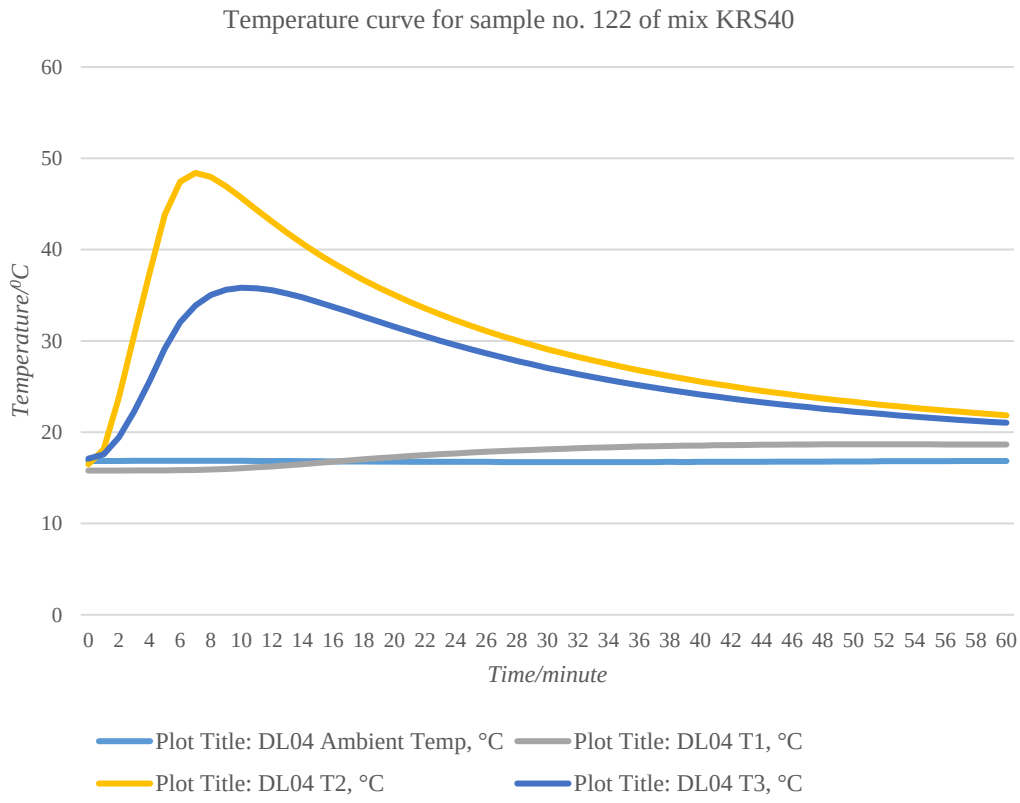

Figure 5.10 Temperature variation curve for sample no. 122 of mix KRS40 stabilized by 40% short straw by volume

Table 5.13 Calculation of thermal conductivity of sample no. 122 of mix KRS40 stabilized by 40% short straw by volume

Sample number	**Measured data**						**Derived data**		
122	Size *(cm^2)*	Energy total *(wh)*	Energy q_{top} *(wh)*	Thickness *(m)*	dT *(ºC)*	dt *(hrs)*	Area sample *(m^2)*	Area hot plate *(m^2)*	λ *(W/mK)*
	20.5x17.0x 3.8	3.0	1.5	0.038	5.0	0.80	0.035	0.012	**0.41**

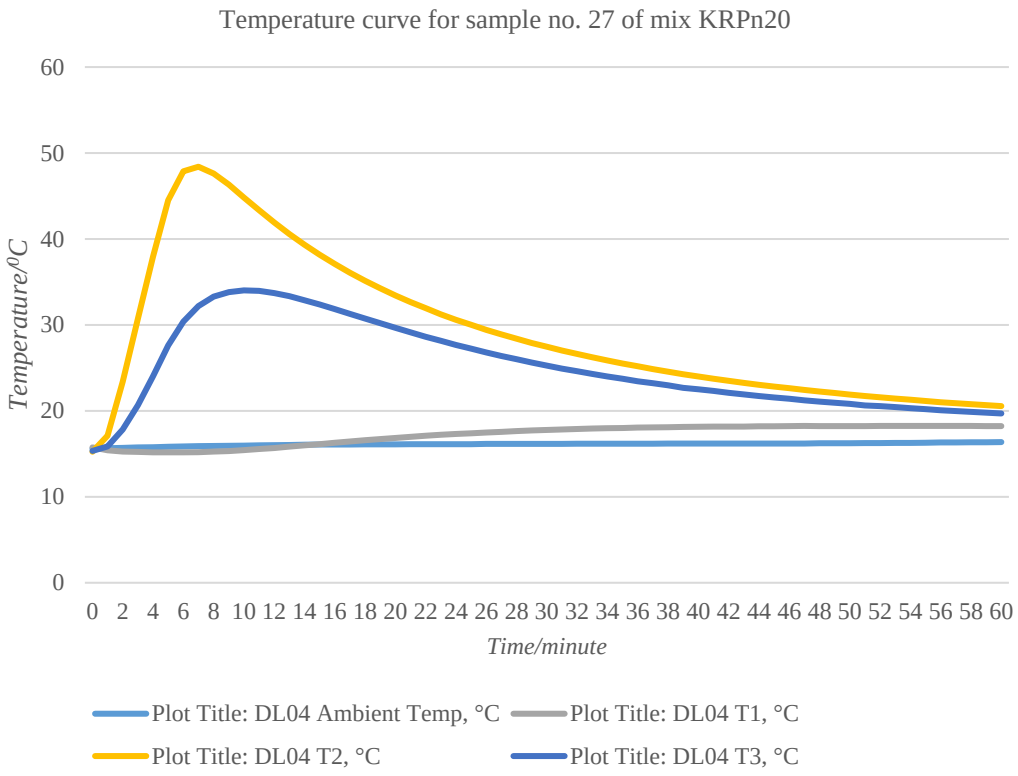

Figure 5.11 Temperature variation curve for sample no. 27 of mix KRPn20 stabilized by 20% pine needle by volume

Table 5.14 Calculation of thermal conductivity of sample no. 27 of KRPn20 stabilized by 20% pine needle by volume

Sample number	**Measured data**						**Derived data**		
27	Size *(cm^2)*	Energy total *(wh)*	Energy q_{top} *(wh)*	Thickness *(m)*	dT *(°C)*	dt *(hrs)*	Area sample *(m^2)*	Area hot plate *(m^2)*	λ *(W/mK)*
	21.0x17.0x 4.0	3.0	1.5	0.04	5.0	0.78	0.036	0.012	**0.51**

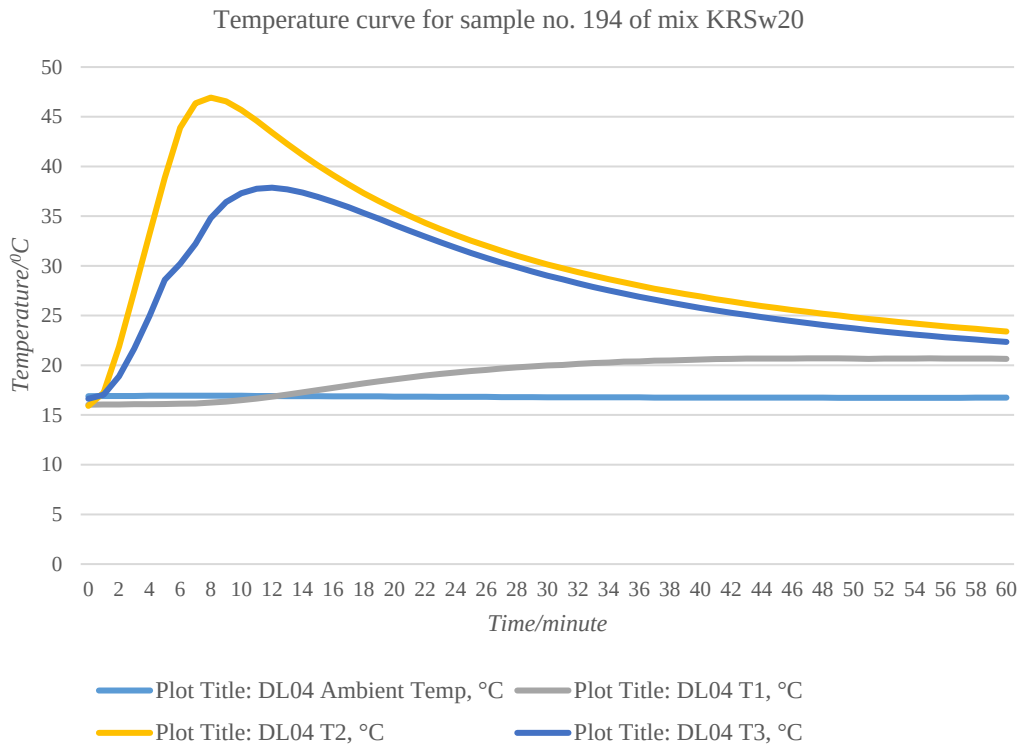

Figure 5.12 Temperature variation curve for sample no. 194 of mix KRSw20 stabilized by 20% by short sheep wool by volume

Table 5.15 Calculation of thermal conductivity of sample no. 194 of mix KRSw20 stabilized by 20% short sheep wool by volume

Sample number	**Measured data**						**Derived data**		
194	Size *(cm^2)*	Energy total *(wh)*	Energy q_{top} *(wh)*	Thickness *(m)*	dT *(ºC)*	dt *(hrs)*	Area sample *(m^2)*	Area hot plate *(m^2)*	λ *(W/mK)*
	11.6x11.5x 4.0	3.0	1.5	0.04	4.7	0.78	0.013	0.012	**1.23**

F. Temperature variation curves for samples stabilized with cow dung and processed cow dung

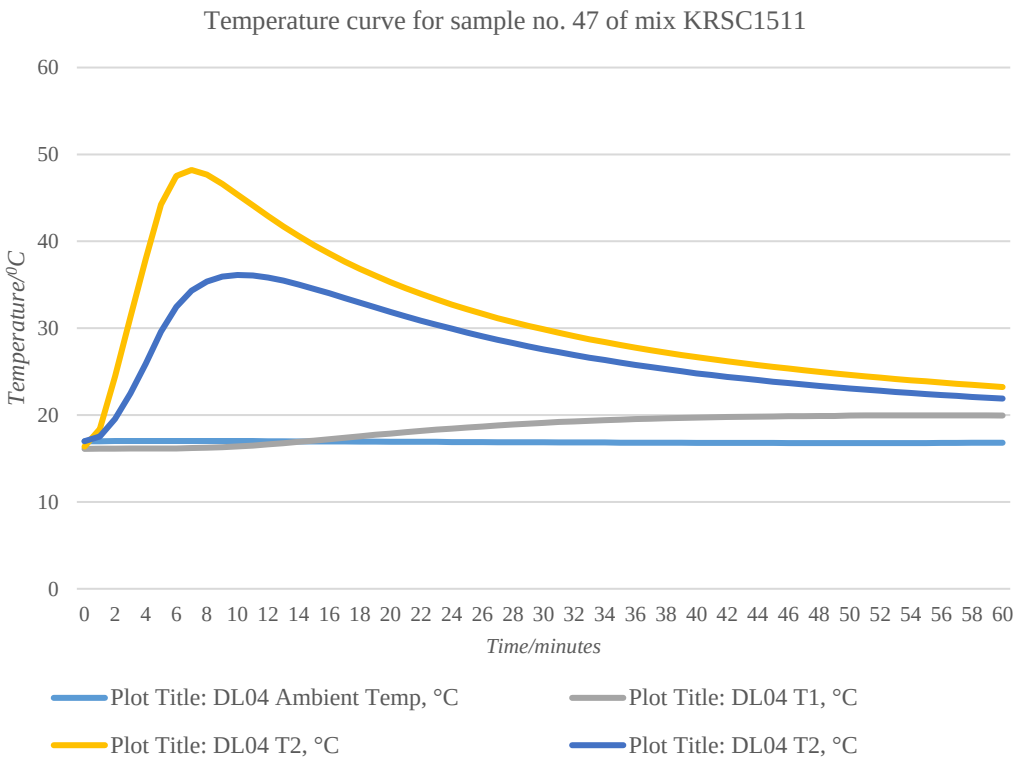

Figure 5.13 Temperature variation curve of sample no. 47 of mix KRSC1511 stabilized with 15% straw and 11% cow dung by volume

Table 5.16 Calculation of thermal conductivity of sample no. 47 of mix KRSC1511 stabilized by 15% short straw and 11% cow dung by volume

Sample number	**Measured data**						**Derived data**		
194	Size *(cm^2)*	Energy total *(wh)*	Energy q_{top} *(wh)*	Thickness *(m)*	dT *(°C)*	dt *(hrs)*	Area sample *(m^2)*	Area hot plate *(m^2)*	λ *(W/mK)*
	12.0x11.0x 4.0	3.0	1.5	0.04	4.5	0.85	0.013	0.012	**1.19**

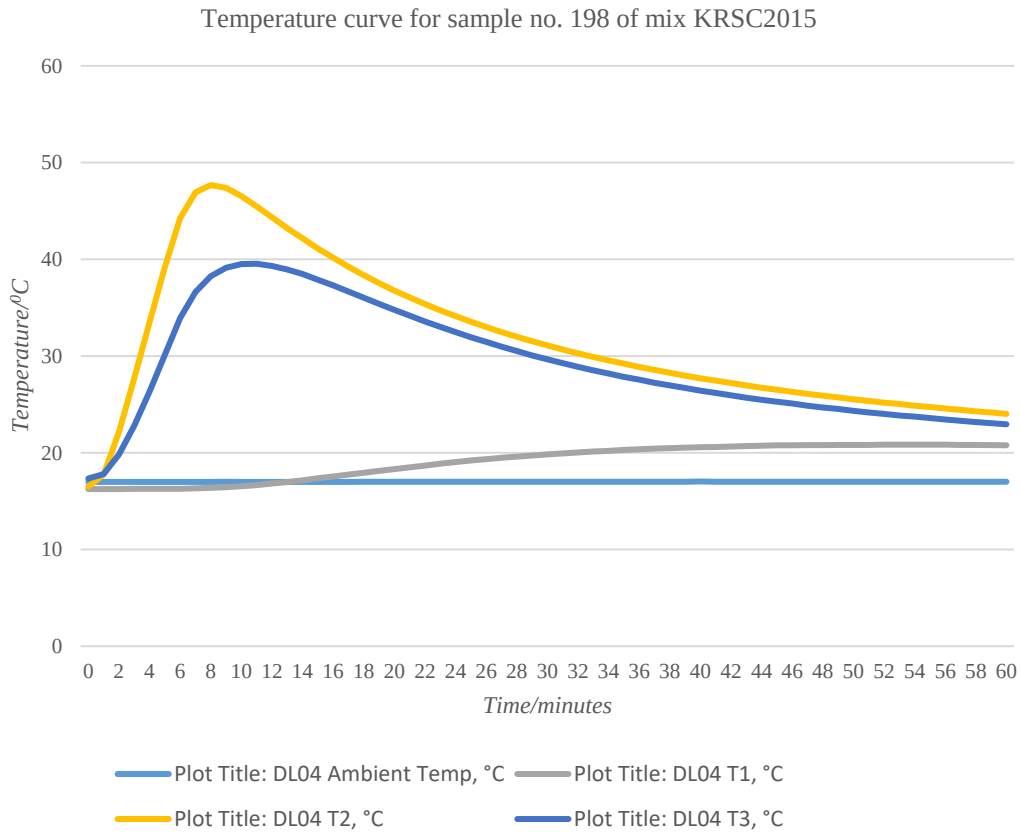

Figure 5.14 Temperature variation curve for sample no. 198 of mix KRSC2015 stabilized by 20% short straw and 15% cow dung by volume

Table 5.17 Calculation of thermal conductivity of sample no. 198 of mix KRSC2015 stabilized by 20% short straw and 15% cow dung by volume

Sample number	**Measured data**						**Derived data**		
198	Size *(cm^2)*	Energy total *(wh)*	Energy q_{top} *(wh)*	Thickness *(m)*	dT *(^oC)*	dt *(hrs)*	Area sample *(m^2)*	Area hot plate *(m^2)*	λ *(W/mK)*
	12.6x12.0x 3.6	3.0	1.5	0.036	4.3	0.87	0.015	0.012	**0.95**

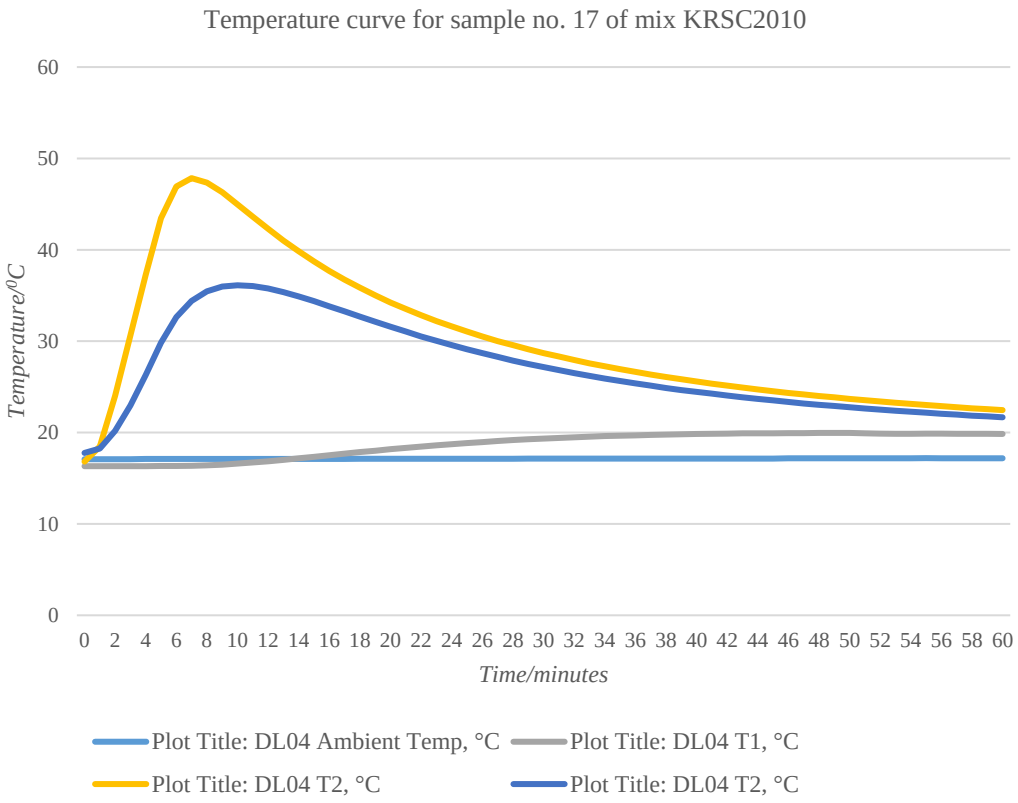

Figure 5.15 Temperature variation curve for sample no. 17 of mix KRSC2010 stabilized by 20% short straw and 10% cow dung by volume

Table 5.18 Calculation of sample no. 17 of mix KRSC2010 stabilized by 20% by short straw and 10% cow dung by volume

Sample number	**Measured data**						**Derived data**		
17	Size *(cm^2)*	Energy total *(wh)*	Energy q_{top} *(wh)*	Thickness *(m)*	dT *(ºC)*	dt *(hrs)*	Area sample *(m^2)*	Area hot plate *(m^2)*	λ *(W/mK)*
	15.5x15.5x 3.6	3.0	1.5	0.036	4.0	0.80	0.024	0.012	**0.77**

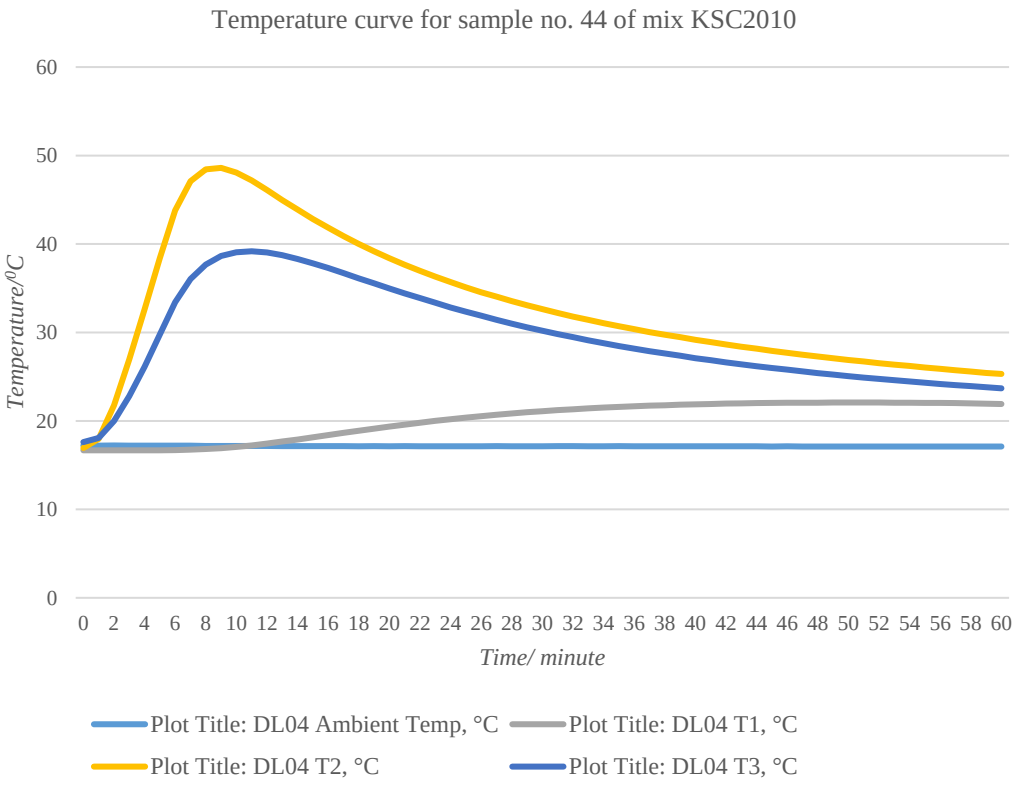

Figure 5.16 Temperature variation curve for sample no. 44 of mix KSC2010 stabilized by 20% by short straw and 10% cow dung by volume

Table 5.19 Calculation of thermal conductivity of sample no. 44 of mix KSC2010 stabilized by 20% short straw and 10% cow dung by volume

Sample number	**Measured data**							**Derived data**		
44	Size *(cm^2)*	Energy total *(wh)*	Energy q_{top} *(wh)*	Energy q_{small} *(wh)*	Thickness *(m)*	dT *(°C)*	dt *(hrs)*	Area sample *(m^2)*	Area hot plate *(m^2)*	λ *(W/mK)*
	11.0x9.8x3.5	3.0	1.5	1.318	0.035	5.0	0.95	0.011	0.012	**0.79**

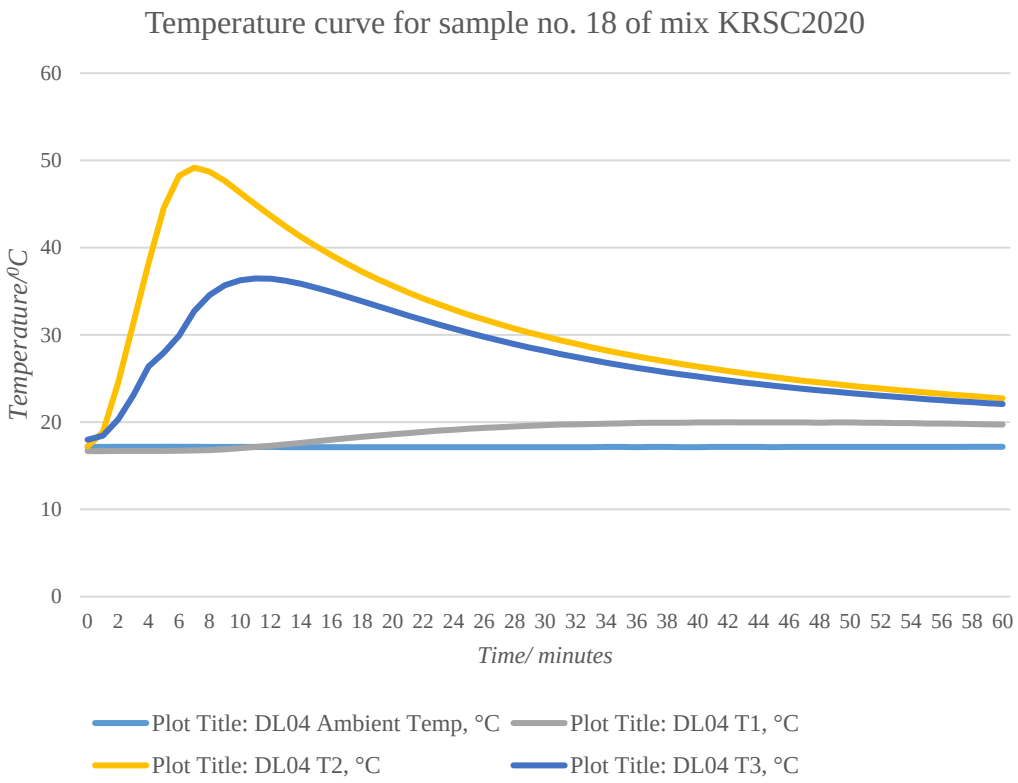

Figure 5.17 Temperature variation curve for sample no. 18 of mix KRSC2020 stabilized by 20% short straw and cow dung by volume

Table 5.20 Calculation of thermal conductivity of sample no. 18 of KRSC2020 stabilized by 20% short straw and cow dung by volume

Sample number	**Measured data**						**Derived data**		
18	Size *(cm^2)*	Energy total *(wh)*	Energy q_{top} *(wh)*	Thickness *(m)*	dT *(ºC)*	dt *(hrs)*	Area sample *(m^2)*	Area hot plate *(m^2)*	λ *(W/mK)*
	20.5x16.2x 3.6	3.0	1.5	0.036	5.7	0.71	0.034	0.012	**0.43**